

IURI SIDNEY BESSA

Laboratory and field study of fatigue cracking prediction in asphalt pavements

**São Paulo
2017**

IURI SIDNEY BESSA

Laboratory and field study of fatigue cracking prediction in asphalt pavements

Dissertation presented to the *Escola Politécnica* of the *Universidade de São Paulo* to obtain the degree of Doctor of Science

**São Paulo
2017**

IURI SIDNEY BESSA

Laboratory and field study of fatigue cracking prediction in asphalt pavements

Dissertation presented to the *Escola Politécnica* of the *Universidade de São Paulo* to obtain the degree of Doctor of Science

Research area:
Transportation Engineering

Advisor: Prof. D.Sc. Liedi Legi Bariani
Bernucci
Co-advisor: Prof. Verônica Teixeira Franco
Castelo Branco, Ph.D.

**São Paulo
2017**

Este exemplar foi revisado e corrigido em relação à versão original, sob responsabilidade única do autor e com a anuência de seu orientador.

São Paulo, _____ de _____ de _____

Assinatura do autor: _____

Assinatura do orientador: _____

Catálogo-na-publicação

Bessa, Iuri Sidney

Laboratory and field study of fatigue cracking prediction in asphalt pavements / I. S. Bessa -- versão corr. -- São Paulo, 2017.
138 p.

Tese (Doutorado) - Escola Politécnica da Universidade de São Paulo. Departamento de Engenharia de Transportes.

1.Pavimentação asfáltica 2.Asfalto [desempenho] 3.Defeito [previsão]
4.Fadiga dos materiais 5.Reologia I.Universidade de São Paulo. Escola Politécnica. Departamento de Engenharia de Transportes II.t.

ACKNOWLEDGEMENTS

I would like to express my enormous gratitude to my advisor, Professor Liedi Bernucci, for being so generous throughout the past four years. Her generosity can be translated into scientific contribution, professional cooperation and personnel help whenever I needed the most. The experience that I have had working with her has changed my life in a way that I will never be able to express properly. I also thank my co-advisor, Professor Verônica Castelo Branco, for all this time working together, for always pushing me and taking the best out of me since day one. Thank you for being the most passionate and most inspiring teacher I have ever had. I also acknowledge Professor Kamilla Vasconcelos, for being such a special human being, and such a courageous and competent professional. Her teaching, guidance and partnership are some of the best things that ever happened to me.

I would also like to acknowledge my colleagues and friends at USP, especially Professor Rosângela Motta, Diomária, Edson, Robson, Vand, Manu, Patrícia, Matheus, Kazuo, Lucas, Zila, André, Talita, Márcia, Paulo, Ingrid, Laura, Gui, Fernanda and João. You all have contributed for the completion of this dissertation. Special thanks go to Erasmo for putting so much effort in the laboratory. Thanks to Bruno for helping develop the research. I also thank Guilherme, Hugo and Igor at CDT/Arteris for the help during the construction and monitoring of the experimental test site. I would like to thank Luis Nascimento at CENPES/Petrobras for helping with part of the tests presented in this dissertation. Thanks to CAPES for the scholarship.

I would also like to thank my friends and family for understanding the choices that I have made in my life during the past years, and for supporting me no matter what. Very special thanks go to Luiz for simply being there for me, for knowing exactly how to handle each difficult situation and for having the best advices I could ask for. I thank my dear friend Daniel for having me when I had nowhere to live and for the special moments we had. Thanks to my dearest friends Felipe and Camila, who have been there for me even now that we are all thousands of miles away from each other. The most special thanks goes to my parents and to my brother, for trusting me and for giving the most important thing that brought me here: the possibility of studying.

RESUMO

A previsão do desempenho de pavimentos asfálticos em relação aos seus principais defeitos tem sido proposta por diferentes pesquisadores, por meio da caracterização em laboratório e da avaliação de dados de campo. No que diz respeito ao trincamento por fadiga, não há um consenso universal sobre o tipo de ensaio a ser realizado, o critério de dano a ser considerado, e as condições de ensaio a serem adotadas (nível e frequência de carregamento, e temperatura), além da geometria das amostras testadas. Ensaio realizados em ligantes asfálticos e em misturas asfálticas são usados para estudar o comportamento em relação à fadiga e para prever a vida útil. A caracterização dos ligantes asfálticos é relevante, uma vez que o trincamento por fadiga é altamente dependente das características reológicas desses materiais. Nesta pesquisa, a obtenção dos parâmetros viscoelásticos lineares e a caracterização por meio de ensaios de varredura de tempo e de varredura de deformação foram realizados. Em relação à caracterização laboratorial das misturas asfálticas, ensaios baseados em compressão diametral, vigota de quatro pontos e em tração-compressão axial foram realizados. Dados de evolução do dano de campo obtidos em duas seções de pavimentos asfálticos foram coletados de um trecho experimental construído em uma rodovia de alto volume de tráfego. Três ligantes asfálticos (um ligante não modificado, um ligante modificado por polímero do tipo SBS e um ligante altamente modificado, HiMA), e uma mistura asfáltica do tipo concreto asfáltico constituída pelo ligante não modificado foram testados em laboratório. O trecho experimental era composto por dois segmentos, constituídos por diferentes tipos de camadas de base (brita graduada simples e brita graduada tratada com cimento) que forneciam diferentes respostas mecânicas à camada de revestimento asfáltico. Os dados de campo foram comparados com modelos de previsão de vida de fadiga que utilizam resultados empíricos obtidos em laboratórios e simulações computacionais. Correlações entre as diferentes escalas são discutidas nesta tese, com o objetivo de prever o desempenho de pavimentos asfálticos ao trincamento por fadiga.

Palavras-chave: Materiais asfálticos. Trincamento por fadiga. Caracterização laboratorial. Avaliação de dados de campo.

ABSTRACT

The prediction of asphalt pavements performance in relation to their main distresses has been proposed by different researchers, by means of laboratory characterization and field data evaluation. In relation to fatigue cracking, there is no universal consensus about the laboratory testing to be performed, the damage criterion to be considered, the testing condition to be set (level and frequency of loading, and temperature), and the specimen geometry to be used. Tests performed in asphalt binders and in asphalt mixes are used to study fatigue behavior and to predict fatigue life. The characterization of asphalt binders is relevant, since fatigue cracking is highly dependent on the rheological characteristics of these materials. In the present research, the linear viscoelastic characterization, time sweep tests, and amplitude sweep tests were done. In respect to the laboratorial characterization of asphalt mixes, tests based on indirect tensile, four point flexural bending beam, and tension-compression were performed. Field damage evolution data of two asphalt pavement sections were collected from an experimental test site in a very heavy traffic highway. Three asphalt binders (one neat binder, one SBS-modified binder and one highly modified binder, HiMA), and one asphalt concrete constituted by the neat binder were tested in laboratory. The experimental test site was composed by two segments, constituted by different base layers (unbound course and cement-treated crushed stone) that provided different mechanical responses in the asphalt wearing course. The field damage data were compared to fatigue life models that use empirical results obtained in the laboratory and computer simulations. Correlations among the asphalt materials scales were discussed in this dissertation, with the objective of predicting the fatigue cracking performance of asphalt pavements.

Keywords: Asphalt materials. Fatigue cracking. Laboratory characterization. Field data evaluation.

LIST OF FIGURES

| | |
|--|----|
| Figure 1.1 – Burmister’s solution for elastic layered system (Adapted from Balbo, 2007) | 19 |
| Figure 1.2 – Results from elastic and viscoelastic analyses: (a) deflections and (b) strains (Mejlun et al., 2017) | 20 |
| Figure 1.3 – Fatigue cracking stages (Bernucci et al., 2007)..... | 21 |
| Figure 1.4 – Components of asphalt concrete material response as a function of temperature/frequency (Little, Crockford and Gaddam, 1992) | 22 |
| Figure 1.5 – Fatigue performance for different gradations: (a) aggregate size distributions and (b) fatigue life (Hafeez, Kamal and Mirza, 2015) | 24 |
| Figure 1.6 – Fatigue performance for different types of asphalt binder: (a) neat binders and (b) modified binders (Sugandh et al., 2007)..... | 25 |
| Figure 1.7 – Types of asphalt pavements: (a) flexible and (b) semi rigid (Christopher, Schwartz and Boudreau, 2006) | 26 |
| Figure 1.8 – Location of critical tensile strain: (a) flexible and (b) semi rigid asphalt pavement (Flintsch, Diefenderfer and Nunez, 2008) | 27 |
| Figure 1.9 – 2002 AASHTO design guide overall procedure (NCHRP, 2004)..... | 29 |
| Figure 1.10 – Predicted damage versus percentage of cracked area (NCHRP, 2004) | 30 |
| Figure 1.11 – Comparison between observed and predicted cracked area: (a) based on $T_{0.35}$ and (b) based on R_{12-1} (Nascimento, 2015) | 36 |
| Figure 1.12 – Asphalt pavement design protocol: (a) typical pavement structure used in Brazil, (b) predicted cracked area versus traffic, (c) traffic accumulation versus layer thickness, and (d) designed asphalt layer (Nascimento, 2015) | 37 |
| Figure 1.13 – Comparison between observed and predicted cracked area (Adapted from Fritzen, 2016) | 40 |
| Figure 2.1 – Comparisons between fatigue cracking and Superpave parameter: (a) Petersen et al., 1994 and (b) Bahia et al., 2001 | 47 |
| Figure 2.2 – Time sweep tests results: (a) Martono and Bahia (2008), and Tabatabaee and Tabatabaee (2010) | 49 |
| Figure 2.3 – LAS test: (a) crack growth rate approach and (b) comparison between LAS test and TST (Hintz, 2012)..... | 51 |

| | |
|---|----|
| Figure 2.4 – Comparison between: (a) traditional Superpave parameter and LAS test results (Lyndgal, 2005) and (b) fatigue life of binder and fatigue life of mixes (Saboo and Kumar, 2016)..... | 55 |
| Figure 2.5 – Asphalt binder sample preparation: (a) heating, (b) molding, (c) placing in the DSR, and (d) final adjustments..... | 57 |
| Figure 2.6 – Master curves at 40°C for unaged binders: (a) dynamic shear modulus $ G^* $ and (b) phase angle δ | 58 |
| Figure 2.7 – Master curves at 40°C for aged binders: (a) dynamic shear modulus $ G^* $ and (b) phase angle | 59 |
| Figure 2.8 – Parameter $ G^* \times \sin\delta$ at different temperatures | 60 |
| Figure 2.9 – $ G^* $ values from strain sweep test..... | 61 |
| Figure 2.10 – Fatigue behavior of the asphalt binders at time sweep test..... | 62 |
| Figure 2.11 – TST test results: (a) evolution of normalized $ G^* $ and (b) comparison between $ G^* _{norm}$ and 50% reduction | 64 |
| Figure 2.12 – Evolution of $ G^* $ during the time sweep test (6% strain)..... | 64 |
| Figure 2.13 – Evolution of $ G^* $ during TST: (a) neat binder, (b) steric hardening on neat binder (2%), (c) SBS and (d) HiMA | 66 |
| Figure 2.14 – Superpave parameter <i>versus</i> TST results: (a) all the strain levels tested and (b) 6% strain..... | 67 |
| Figure 2.15 – DER values: (a) evolution during the time sweep test and (b) comparison with traditional fatigue life criterion..... | 68 |
| Figure 2.16 – Peak phase angle results: (a) evolution of phase angle during the test and (b) comparison with traditional fatigue life criterion (50% stiffness reduction) | 68 |
| Figure 2.17 – LAS test procedure: (a) frequency sweep and (b) current ramp amplitude sweep; (c) old stepwise amplitude sweep (Hintz et al., 2011) and (d) output data found using the old procedure (Hintz and Bahia, 2013) | 70 |
| Figure 2.18 – Stress-strain curves after LAS test..... | 71 |
| Figure 2.19 – Damage characteristic curves the three binders tested: (a) until failure and (b) entire curves | 72 |
| Figure 2.20 – Fatigue life curves obtained from LAS test..... | 73 |
| Figure 2.21 – Crack growth rate evolution from LAS test | 74 |
| Figure 2.22 – Comparison between LAS test approaches: (a) crack growth rate and (b) peak stress..... | 75 |

| | |
|--|-----|
| Figure 3.1 – Characteristics of the laboratory tests studied by Di Benedetto et al. (2004)..... | 77 |
| Figure 3.2 – Testing conditions influencing fatigue life: (a) different frequencies and temperatures (Al-Khateeb and Ghuzlan, 2014) and (b) stress- or strain-controlled modes (Boudabbous et al., 2013) | 79 |
| Figure 3.3 – Stiffness at failure versus initial stiffness in controlled-strain tests (Lundstrom et al., 2004) | 81 |
| Figure 3.4 – Indirect tensile test: (a) stresses during the test and (b) equipment commonly used | 83 |
| Figure 3.5 – Indirect tensile test: (a) influence of specimen size (Li, 2013) and failure criterion by Nguyen et al. (2013) | 84 |
| Figure 3.6 – Four point beam bending test: (a) loading pulse (ASTM D 7460, 2010) and (b) shear force and bending moment diagrams during the test | 84 |
| Figure 3.7 – Specimen prepared for tension-compression test (Nascimento et al., 2014) | 86 |
| Figure 3.8 – Trapezoidal fatigue test: (a) specimens used in the test (Barra, 2009) and (b) LCPC equipment (RDT-CONCEPA/ANTT, 2014) | 89 |
| Figure 3.9 – APA equipment (Loureiro, 2003) | 90 |
| Figure 3.10 – Size distributions: (a) aggregates and (b) asphalt mix composition..... | 91 |
| Figure 3.11 – Fatigue life according to ITT: (a) lab specimens and (b) field samples | 93 |
| Figure 3.12 – Four point beam bending test: (a) stiffness and normalized modulus evolution and (b) hysteresis loop (Ahmed, 2016) | 96 |
| Figure 3.13 – Evolution of ratio dissipated energy change (Shen and Carpenter, 2005) | 96 |
| Figure 3.14 – Fatigue life according to 4PBBT: (a) lab specimens and (b) field samples (40% of E^*); (c) lab specimens and (d) field samples (50% of E^*) | 97 |
| Figure 3.15 – Comparison between fatigue life: 50% of stiffness versus peak of normalized modulus | 99 |
| Figure 3.16 – Energy ratio evolution: (a) Pronk’s 1990 method and (b) Pronk’s 1997 method | 99 |
| Figure 3.17 – Energy ratio evolution: (a) Rowe and Bouldin method (2000) and (b) Ghuzlan and Carpenter method (2000)..... | 100 |

| | |
|--|-----|
| Figure 3.18 – Fatigue life according to Rowe and Bouldin method: (a) fatigue life and (b) comparison with 50% of E^* ; (c) field samples and (d) comparison with 50% of E^* | 101 |
| Figure 3.19 – Master curves of the asphalt mix: (a) dynamic modulus and (b) phase angle | 103 |
| Figure 3.20 – S-VECD results: (a) damage characteristics curve fittings and (b) G_r curve | 104 |
| Figure 3.21 – S-VECD simulation: fatigue life in different temperatures and (b) comparison with 50% of E^* method (20°C) | 105 |
| Figure 3.22 – Fatigue area factor: (a) calculation (Adapted from Nascimento, 2015) and (b) comparison between FAF_B and FAF_M | 106 |
| Figure 3.23 – Comparison between asphalt binder and asphalt mix fatigue lives ... | 107 |
| Figure 4.1 – Pavement sections structure | 110 |
| Figure 4.2 – Construction of the experimental test site: (a) milling of the old pavement structure, (b) compaction of the crushed stone base layer, (c) placing of the crushed stone with cement, and (d) placing of the asphalt mixture layer | 111 |
| Figure 4.3 – Traffic accumulation throughout the time (ESALs) | 112 |
| Figure 4.4 – Evolution of cracked area: (a) versus number of ESALs and (b) versus time, in months | 112 |
| Figure 4.5 – Horizontal stresses in the pavement layers: (a) segment 1 and (2) segment 2 | 114 |
| Figure 4.6 – Deflection basins of (a) segment 1 and (b) segment 2 | 115 |
| Figure 4.7 – Backcalculated moduli for (a) segment 1 and (b) segment 2 | 116 |
| Figure 4.8 – Results from the computer simulations: (a) damage accumulation and (b) predicted cracked area | 117 |
| Figure 4.9 – Comparison between observed and predicted cracked area: (a) segment 1 and (b) segment 2 | 118 |

LIST OF TABLES

| | |
|---|-----|
| Table 1.1 – Fitting coefficients of early fatigue prediction models | 31 |
| Table 1.2 – Fitting coefficients of AI and Shell Oil fatigue prediction models | 32 |
| Table 1.3 – Modified fitting coefficients of AI and Shell models (Rajbongshi, 2009).. | 33 |
| Table 1.4 – Fitting coefficients from Nascimento (2015) | 35 |
| Table 1.5 – Fitting coefficients from Fritzen (2016) | 39 |
| Table 2.1 – Empirical characterization of the asphalt binders | 56 |
| Table 2.2 – $ G^* $ values of unaged and aged binders at the reference temperature .. | 59 |
| Table 2.3 – Parameters of the fatigue curves for the time sweep test..... | 62 |
| Table 2.4 – Percentage of $ G^* $ at peak phase angle value | 69 |
| Table 2.5 – Parameters of fatigue curves for LAS test..... | 72 |
| Table 3.1 – Aggregates characterization..... | 90 |
| Table 3.2 – HMA design parameters..... | 91 |
| Table 3.3 – Fatigue curves parameters for 4PBBT | 98 |
| Table 3.4 – Results of the statistical parameters studied | 102 |
| Table 3.5 – S-VECD parameters..... | 104 |
| Table 4.1 – Fatigue life according to classical prediction models..... | 120 |

LIST OF ABBREVIATIONS

| | |
|--------|--|
| FAM | Fine aggregate mix |
| AASHTO | American Association of State Highway and Transportation Officials |
| LTPP | Long-Term Pavement Performance |
| MAPT | Mean annual pavement temperature |
| 4PBBT | Four-point bending beam test |
| ITT | Indirect tensile test |
| NMAS | Nominal maximum aggregate size |
| SMA | Stone matrix asphalt |
| AI | Asphalt Institute |
| HMA | Hot mix asphalt |
| ESAL | Equivalent single axle load |
| CBR | California bearing ratio |
| CA | Cracked area |
| MEPDG | Mechanistic-empirical pavement design guide |
| AC | Asphalt cement |
| LVECD | Layered viscoelastic continuum damage |
| S-VECD | Simplified viscoelastic continuum damage |
| USACE | United States Army Corps of Engineers |
| WIM | Weigh-in-motion |
| APT | Accelerated pavement testing |
| FWD | Falling weight deflectometer |
| SHRP | Strategic Highway Research Program |
| PG | Performance grade |
| LVE | Linear viscoelastic region |
| TST | Time sweep test |
| LAS | Linear amplitude sweep |
| DSR | Dynamic shear rheometer |
| SBS | Styrene-butadiene-styrene |
| HiMA | Highly modified binder |
| FHWA | Federal Highway Administration |
| VECD | Viscoelastic continuum damage |

| | |
|-------|--|
| RTFOT | Rolling thin film oven test |
| PAV | Pressure aging vessel |
| ASTM | American Society for Testing and Materials |
| TTS | Time-temperature superposition principle |
| CX | Cross-head |
| WTT | Wheel tracking test |
| APA | Asphalt pavement analyzer |
| MTS | Materials testing system |
| DE | Dissipated energy |
| RDEC | Ratio of dissipated energy change |
| MAE | Mean absolute error |
| AGD | Average geometric deviation |
| FAF | Fatigue area factor |
| RAP | Reclaimed asphalt pavement |
| FEM | Finite element method |

TABLE OF CONTENTS

| | | |
|----------|--|-----------|
| 1 | INTRODUCTION AND BACKGROUND..... | 14 |
| 1.1 | INTRODUCTION..... | 14 |
| 1.1.1 | Objectives | 16 |
| 1.1.2 | Dissertation outline..... | 16 |
| 1.2 | LITERATURE REVIEW..... | 17 |
| 1.2.1 | Stress and strain in asphalt pavements..... | 17 |
| 1.2.2 | Fatigue cracking..... | 20 |
| 1.2.3 | Variables influencing the fatigue cracking of asphalt pavements | 21 |
| 1.2.4 | Fatigue cracking in flexible and semi rigid asphalt pavements..... | 26 |
| 1.3 | INPUT OF FATIGUE CRACKING IN ASPHALT PAVEMENT DESIGN..... | 27 |
| 1.4 | FATIGUE CRACKING PREDICTION..... | 30 |
| 1.4.1 | Proposed methods for Brazilian asphalt pavement structures | 34 |
| 1.4.2 | Traffic input in fatigue cracking models | 40 |
| 1.5 | ACCELERATED TESTING FOR FATIGUE CRACKING PREDICTION | 43 |
| 2 | CHARACTERIZATION OF FATIGUE CRACKING RESISTANCE OF ASPHALT BINDERS USING DIFFERENT METHODS..... | 45 |
| 2.1 | INTRODUCTION..... | 45 |
| 2.2 | REVIEW OF LITERATURE | 46 |
| 2.3 | MATERIALS AND METHODS | 56 |
| 2.4 | RESULTS AND DISCUSSIONS | 59 |
| 2.4.1 | Superpave fatigue parameter..... | 59 |
| 2.4.2 | Time sweep test (TST)..... | 60 |
| 2.4.3 | Linear amplitude sweep (LAS) test | 69 |
| 2.5 | SUMMARY AND FINDINGS | 75 |
| 3 | DIFFERENT PROCEDURES TO EVALUATE FATIGUE CRACKING RESISTANCE OF ASPHALT MIXES | 76 |
| 3.1 | INTRODUCTION AND BACKGROUND..... | 76 |
| 3.2 | FATIGUE CHARACTERIZATION OF ASPHALT MIXES | 80 |
| 3.2.1 | Indirect tensile test | 82 |
| 3.2.2 | Four point beam bending test..... | 84 |
| 3.2.3 | Tension-compression test | 85 |

| | | |
|----------|--|------------|
| 3.2.4 | Other fatigue tests | 88 |
| 3.3 | ASPHALT MIXES DESIGN | 90 |
| 3.4 | RESULTS AND DISCUSSIONS | 92 |
| 3.5 | SUMMARY AND FINDINGS | 107 |
| 4 | INFLUENCE OF DIFFERENT TYPES OF BASE COURSE ON THE FATIGUE RESISTANCE OF ASPHALT WEARING COURSE | 108 |
| 4.1 | INTRODUCTION..... | 108 |
| 4.2 | PROJECT OF THE EXPERIMENTAL PAVEMENT TEST SECTION | 109 |
| 4.3 | MONITORING OF THE EXPERIMENTAL TEST SITE | 111 |
| 4.4 | NON-DESTRUCTIVE DEFLECTION TESTING..... | 114 |
| 4.5 | FATIGUE CRACKING PREDICTION..... | 116 |
| 4.6 | SUMMARY AND FINDINGS | 120 |
| 5 | CONCLUSIONS..... | 122 |
| 5.1 | FINAL CONSIDERATIONS..... | 122 |
| 5.2 | SUGGESTIONS FOR FUTURE WORK..... | 123 |
| | REFERENCES..... | 125 |

1 INTRODUCTION AND BACKGROUND

1.1 INTRODUCTION

Among the main forms of distresses found in asphalt pavement structures, two of them normally occur in most of Brazilian highways: rutting and cracking. There are several types of cracking, including block cracking, longitudinal cracking, reflective cracking, and the most common, fatigue cracking, which results from traffic loading repetitions associated with other factors. These factors include the materials' properties, the climate conditions, the structural design of the pavement and the subgrade bearing capacity.

Although repeated load applications increase pavement cracking progression, there are other mechanisms that lead to cracking in asphalt pavements, such as aging, fracture resistance of the asphalt surface layer, and thermal stresses (Huang and Di Benedetto, 2015). Cracking caused by fatigue tends to propagate from the asphalt layer and, then, accelerates the structural deterioration of the asphalt pavement, causing water infiltration and pumping of unbound materials (Priest and Timm, 2006). Traditionally, there used to be a consensus that cracking would initiate at the bottom of the asphalt layer due to the repeated loading and that it would be associated with tensile strains (Huang, 2003). Lately, many researchers have addressed top-down cracking as another major distress in asphalt pavements, but have reported difficulties in predicting pavement responses using the conventional pavement analysis models to explain the initiation and propagation of these cracks (Park and Kim, 2013; Zhao, Alae and Fu, 2017).

The prediction of fatigue-related performance of asphalt pavements has been the scope of study of many researchers in the past decades. Laboratory tests have been developed and improved to better assess the materials properties and damage responses in order to predict field performance by means of stress-strain analyses.

Asphalt mixes have been widely characterized in the laboratory in terms of their fatigue resistance, but other scales have also been studied: asphalt binder and fine aggregate mix (FAM), which is an intermediate phase. Different variables have provided many combinations to be considered in laboratory testing: specimen

geometry, mode of loads, stress/strain amplitude, and frequency and temperature parameters (Di Benedetto et al., 2004). The tests performed based on these several conditions are combined with field data collection and computational simulations to enhance the prediction of the fatigue life of asphalt mixtures and to propose fatigue models to be considered in the design of pavement structures.

Failure of asphalt pavements represents the occurrence of fracture in the material and characterizes the fatigue life, i.e., the asphalt pavement's ability to resist to fatigue cracking. Several approaches have been considered in the characterization of fatigue life of asphalt pavements (mostly phenomenological approaches and the fracture mechanics approach). Failure prediction is normally based on the cumulative damage concept proposed by Miner's law (Equation 1.1). Damage is calculated by the ratio between the number of traffic repetitions and the maximum allowable number of repetitions, which is based on a pre-established failure criterion. For field performance evolution, the percentage of cracked area is generally considered.

$$D = \sum_{i=1}^T \frac{n_i}{N_i} \quad (1.1)$$

Where: D is damage;
 T is the total number of periods;
 n_i is the actual traffic for period i ;
 N is the number of allowable load repetitions.

Different failure criteria have been proposed depending on which approach is considered. There have been several attempts to correlate the results obtained among these criteria. The decrease in the specimen stiffness (Rowe, 1993; Harvey et al., 1995; Witczak et al., 2002) and energy-based concepts (Ghuzlan and Carpenter, 2000) have been considered for strain-controlled tests; for stress-controlled tests, the total fracture of the specimen (Ghuzlan and Carpenter, 2003) or a rapid increase on the load displacement (Nguyen, Lee and Baek, 2013) are normally considered. In terms of fracture mechanics, the prediction of fatigue life involves an empirical crack growth model, Paris' law, shown in Equation 1.2 (Li, 1999). This model considers the stress state (by means of the stress intensity factor, K) at the tip of a crack and was

firstly introduced to modeling linear elastic materials but has been justified for viscoelastic materials, such as asphalt mixes, by Schapery (1973).

$$\frac{dc}{dN} = A(\Delta K)^n \quad (1.2)$$

Where: c is the crack length;
 N is the number of load applications;
 A, n are material constants;
 ΔK is the range of stress intensity factor.

Results obtained from laboratory tests are often used as input data for mechanistic-empiric design projects that include fatigue cracking performance models. Besides the laboratory tests performed in asphalt mixes, other data should be considered, e.g., traffic distribution and climate conditions. Among the main issues related to the use of such models, the calibration of these methods requires a wide number of pavement structures to be studied.

Fatigue cracking prediction models have been incorporated to design methods based on test road sections constructed and monitored throughout the pavement life. For example, the American Association of State Highway and Transportation Officials (AASHTO) Road Test and the Long-Term Pavement Performance (LTTP) test sections have been used to develop and calibrate such models (Priest, 2005). The failure criterion normally observed in test sections is obtained in terms of cracked area in the wheel path lane or in the entire pavement section.

1.1.1 Objectives

The main objective of this dissertation is to predict the fatigue cracking of asphalt pavements using different approaches and materials scales.

1.1.2 Dissertation outline

The present research approaches the study of fatigue cracking of different materials, which are based on the scales of asphalt materials that were characterized: asphalt

binder, asphalt mix and real asphalt pavement. The dissertation is divided into five chapters as described by the following:

- Chapter 1 (Introduction and Background): this chapter provides an overview on the concepts related to asphalt pavements fatigue cracking. Also, the research objectives are described.
- Chapter 2 (Fatigue Resistance of Asphalt Binders): firstly, this chapter presents a summarized literature review on the characterization of asphalt binders in relation to their fatigue resistance. Then, three different asphalt binders are studied by means of different testing methods, and their results are analyzed by different approaches.
- Chapter 3 (Fatigue Life of Asphalt Mixtures): an introduction to asphalt mix fatigue cracking characterization is provided. Then, one asphalt concrete mixture is evaluated using three different test methods, and various analyzes are performed.
- Chapter 4 (Field Evaluation): this chapter presents the construction of an experimental test site consisting of different structures in a high traffic highway in Brazil and its monitoring during 18 months, in terms of several distresses, especially fatigue cracking, which is computed in terms of cracked area. Then, different fatigue cracking performance models and on newly developed Brazilian empirical-mechanistic design method are used to predict the asphalt pavement performance in terms of fatigue cracking.
- Chapter 5 (Summary and Conclusions): this chapter provides a summary of the results obtained after the studies performed in the dissertation. Conclusions taken from the analyses in the three scales (asphalt binder, asphalt mix and field pavement section) are also done.

1.2 LITERATURE REVIEW

1.2.1 Stress and strain in asphalt pavements

Boussinesq's theory was developed to propose solutions to calculate the stresses, strains and displacements in homogeneous half-space medium (Medina and Motta, 2015). The generalized Hooke's law (Equations 1.3 to 1.8) can be used to calculate the strain values at any given point of the material in study, including asphalt

pavement structures. This theory considers the hypothesis of linear behavior among the strains responses to the stresses applied.

$$\varepsilon_x = \frac{1}{E} [\sigma_x - \nu \times (\sigma_y + \sigma_z)] \quad (1.3)$$

$$\varepsilon_y = \frac{1}{E} [\sigma_y - \nu \times (\sigma_x + \sigma_z)] \quad (1.4)$$

$$\varepsilon_z = \frac{1}{E} [\sigma_z - \nu \times (\sigma_x + \sigma_y)] \quad (1.5)$$

$$\gamma_{xy} = \frac{1}{G} \times \tau_{xy} \quad (1.6)$$

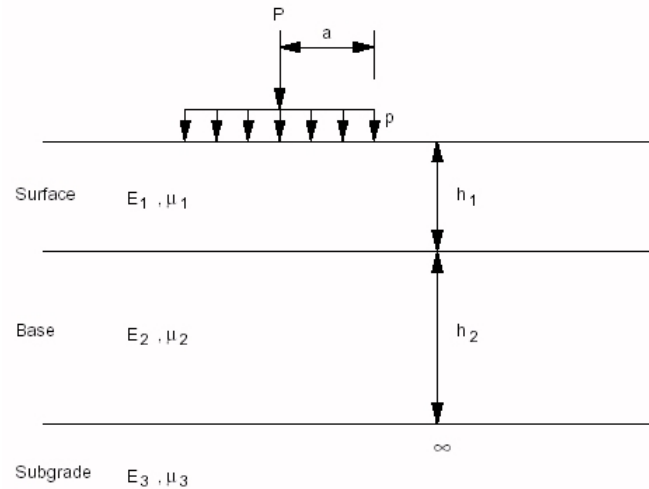
$$\gamma_{xz} = \frac{1}{G} \times \tau_{xz} \quad (1.7)$$

$$\gamma_{yz} = \frac{1}{G} \times \tau_{yz} \quad (1.8)$$

Where: ε is the axial strain in each direction (x, y and z);
 E is the medium's modulus of elasticity;
 σ is the normal stress in each direction (x, y and z);
 ν is the Poisson's ratio;
 γ is the shear strain in each direction (xy, xz and yz);
 G is the transversal modulus of elasticity;
 τ is the shear stress in each direction (xy, xz and yz).

Due to the one-layer system consideration, the Boussinesq's theory cannot properly provide the deflections that are in accordance to field measurements, especially when the asphalt layer is very thick or when there is a rigid layer on the pavement structure (Medina and Motta, 2015). This issue was addressed by Burmister by considering a two or three-layer system to calculate the strain and stress levels (Figure 1.1). Burmister's solutions for linear elastic layered systems is based on some boundary conditions: the materials are elastic, isotropic and homogeneous; Hooke's law is valid and the modulus of compressive stress is equal to the modulus of tensile stress; the layers are weightless and the inferior layer is semi-infinite; there are no shear stresses at the surface layer, and there are no stresses outside the loading application point at the surface layer (Balbo, 2007).

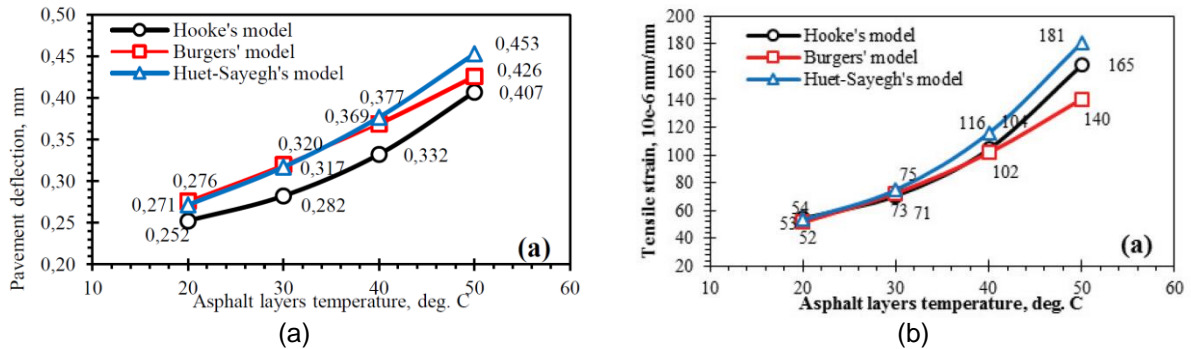
Figure 1.1 – Burmister's solution for elastic layered system (Adapted from Balbo, 2007)



Both Boussinesq's and Burmister's solutions consider the materials to be elastic, but it is well-known that asphalt mixtures are viscoelastic materials, meaning that they depend on the loading time and temperature. The application of the theory of viscoelasticity to analyze layered systems is done by means of the elastic-viscoelastic correspondence principle (Huang, 2003).

Mejlun, Judycki and Dolzycki (2017) did comparisons among two viscoelastic models and one elastic model to calculate an asphalt pavement's deflections and strains at the bottom of the asphalt surface layer, up to 50°C (Figure 1.2). A typical flexible pavement structure used in Poland was considered (200mm of asphalt courses and 200mm of unbound base course). Each asphalt layer was modeled as either elastic or viscoelastic materials, while the unbound base course and the subgrade material were only modeled as elastic materials. In general, the use of the viscoelastic models (Burgers' and Huet-Sayegh's) led to higher values of deflection in comparison to the use of the elastic model (Hooker's). The authors stated that the speed considered in the calculations and analyses was 60km/h, and lower speeds could lead to higher differences between the elastic and the viscoelastic models.

Figure 1.2 – Results from elastic and viscoelastic analyses: (a) deflections and (b) strains (Mejlun et al., 2017)

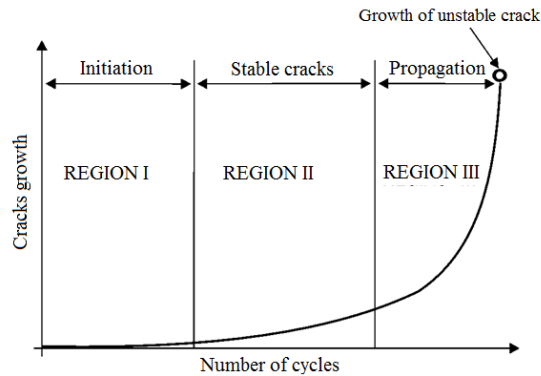


1.2.2 Fatigue cracking

Timoshenko (1953) provided a discussion on concepts related to the fatigue of metals, which can be applied to other engineering materials. This author stated that under repeated loading and unloading or reversed stresses, failure can occur due to stresses that are smaller than the ultimate strength of the material. The endurance limit concept was proposed as being the stress level below which the material tested would not fatigue under reversed loading.

The fatigue cracking phenomenon has been described as a process of permanent structural deterioration in any kind of material. Cracking initiates and progresses as the material is submitted to load applications, with repeated stresses and strains causing cracks or total rupture of the material (Pinto and Preussler, 2002). This distress is related to the decrease of resistance caused by the process of progressing micro-cracking, which corresponds to the modification of the internal structure of a pavement when the stress levels are lower than the material strength (Balbo, 2007). The fatigue cracking process has three defined stages: (i) occurrence of the first micro structural changes and beginning of the irreversible damage zones, (ii) occurrence of macro-cracks after the coalescence of the micro-cracks, and (iii) growth of macro-cracks, leading to a rapid rupture of the material (Figure 1.3).

Figure 1.3 – Fatigue cracking stages (Bernucci et al., 2007)



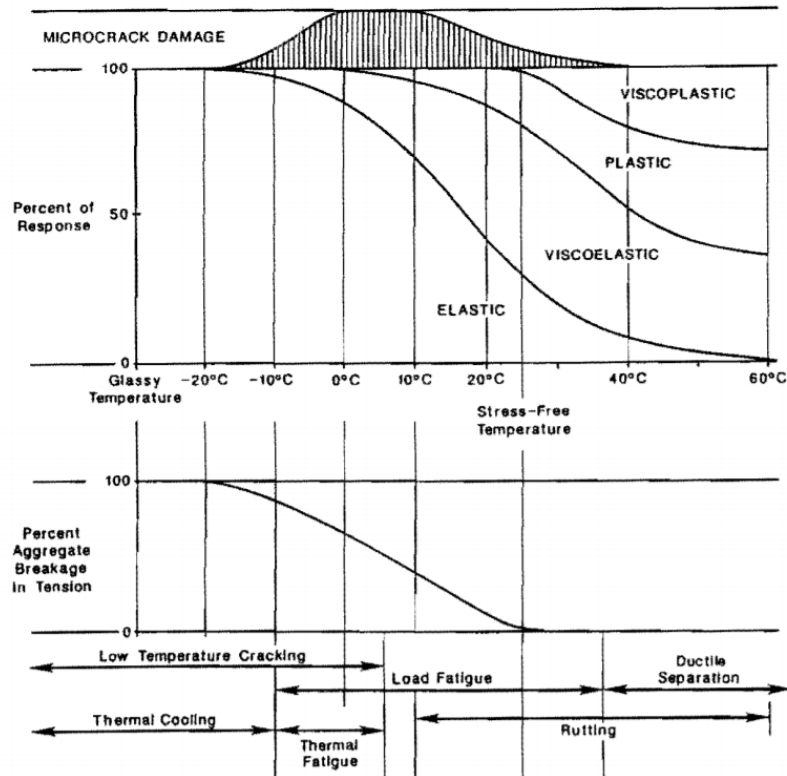
According to Ceratti (1991), fatigue damage is the result of two isolated processes: (i) crack initiation, and (ii) cracks growth. Both processes lead to pavement failure. The crack propagation might occur slowly, but weaken the structural components of an asphalt pavement, leading to total failure when damage reaches a critical level. Balbo (2007) states that crack propagation can be visually observed on the surface of asphalt layers, affecting other layers on the pavement structure.

Epps and Monismith (1973) state that fatigue cracking resistance of an asphalt mixture is normally defined in the laboratory by fracture life (N_f) or service life (N_s). The first is related to the number of load applications need to result in fatigue failure, while the latter corresponds to the total number of load applications need to reduce the performance of specimen. Other authors also define fatigue cracking resistance as the total number of repetitions that is need to lead to the total rupture of the specimen (Loureiro, 2003).

1.2.3 Variables influencing the fatigue cracking of asphalt pavements

There are many factors that influence the fatigue cracking performance of asphalt pavements. Most of these variables are normally considered in the different test methods used to characterize asphalt mixes in laboratory. It has been widely accepted that fatigue cracking occurs in intermediate temperatures, but there is no worldwide consensus on which temperature range should be considered for the characterization of asphalt materials. Little, Crockford and Gaddam (1992) illustrated the influence of temperature/frequency on the responses and failure mechanisms of asphalt mixes (Figure 1.4).

Figure 1.4 – Components of asphalt concrete material response as a function of temperature/frequency (Little, Crockford and Gaddam, 1992)



According to Ongel and Harvey (2004), thick asphalt concrete layers (thicker than 100mm) tend to crack due to fatigue damage at intermediate to high temperatures (15 to 40°C); for asphalt concrete layers thinner than 100mm, fatigue normally occurs at lower temperatures. On the other hand, the Superpave methodology (Cominsky et al., 1994) provided an equation (Equation 1.9) to obtain the effective test temperature to be used for fatigue testing based on the estimated mean annual pavement temperature (MAPT). The MAPT should be an average annual value obtained at one-third of the depth of the asphalt layer.

$$T_{\text{eff}} = (0.8 \times \text{MAPT}) - 2.7 \quad (1.9)$$

Where: T_{eff} is the effective temperature for fatigue cracking testing (°C);
 MAPT is the mean annual asphalt layer temperature.

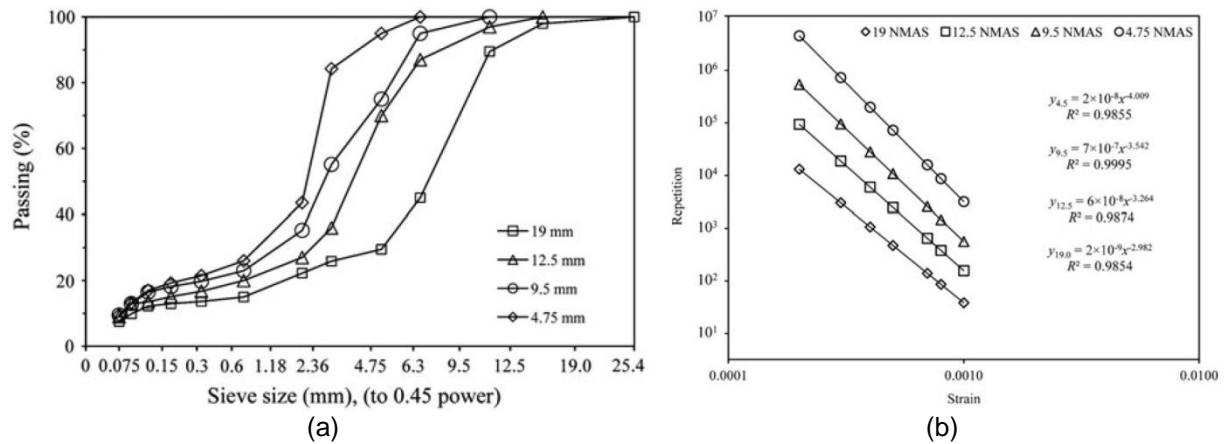
Regarding the temperature used in the different fatigue testing methods, Pramesti et al. (2013) performed the four-point bending beam test (4PBTT) at 5, 20, and 30°C, and concluded that higher testing temperatures lead to better fatigue resistance and

lower strain susceptibility. Inverted results were found by Kim et al. (1991), as fatigue cracking resistance at 0°C was higher than at 20°C, considering the recoverable horizontal strain. According to these authors, this could be explained by the fact that the elastic portion of the deformation found in the 20°C-specimens was very small in comparison to what was found in the 0°C-specimens.

The properties of aggregate particles constituting an asphalt mixture, e.g., their gradation size, shape characteristics (form, surface texture and angularity), and mineralogical compositions have a major influence on distresses related to rutting, but these should also be considered to predict the fatigue cracking behavior.

Sousa et al. (1998) concluded that finer gradations tend to have higher binder contents, which leads to better fatigue resistance. Hafeez, Kamal and Mirza (2015) found similar results after characterizing the fatigue performance of an asphalt mixture by means of the strain-controlled 4PBBT. Four different aggregate size gradations (Figure 1.5a) were used in this study, by varying the nominal maximum aggregate size (NMAS). The asphalt content for a 4.0% void content ranged from 6.2 to 6.9%. The results (Figure 1.5b) indicated that the coarser the asphalt mixture, the less resistant to fatigue cracking it was. In terms of aggregate type, Kim et al. (1992) performed the ITT in two asphalt mixes with the same gradation but constituted by two aggregates with different surface texture and mineralogical characteristics. The rough aggregate type provided better fatigue resistance in comparison to the polished aggregate. These authors also observed that the fatigue cracking occurred through the interface bonding between the aggregate particles and the asphalt binder if polished particles were used; on the other hand, for rough surface materials, fracture appeared on the internal structure of the aggregate particles, which required a higher number of cycles to occur.

Figure 1.5 – Fatigue performance for different gradations: (a) aggregate size distributions and (b) fatigue life (Hafeez, Kamal and Mirza, 2015)

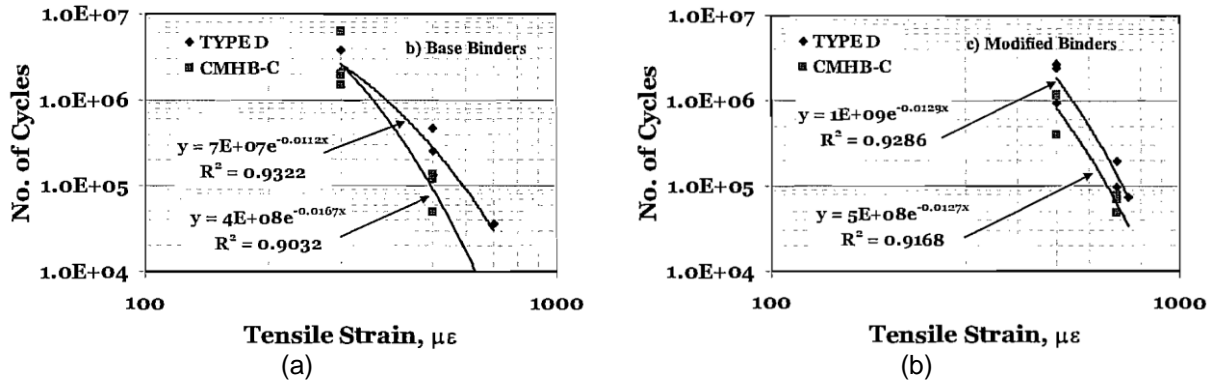


In order to enhance the performance of asphalt mixes and to meet the criteria proposed by Superpave methodology, e.g., values of dynamic shear modulus times the sine of the phase angle ($|G^*| \times \sin \delta$) less than 5,000kPa (Cominsky et al., 1994), the modification of asphalt binders have become a common practice for use in asphalt pavement structures. Each type of modifier (polymers, rubber, lime and anti-stripping agents) has its own function when they are incorporated into asphalt mixes, but they are generally used to prevent the asphalt layer from early distresses. In general, thermoplastic elastomers and crumb rubber are good for improvement of the rutting, fatigue cracking and thermal cracking resistances. Thermoplastic polymers enhance the performance related to rutting; and lime and hydrated lime are good for moisture damage resistance and to minimize the oxidation processes (Hunter, Self and Read, 2015).

In relation to fatigue cracking, many studies have proposed the use of asphalt binder modifiers, especially polymers, to increase the fatigue life of asphalt mixes. This has been observed by both asphalt binder tests and asphalt mixes tests, as well as by field studies. Sugandh et al. (2007) compared two asphalt mixes in two conditions: with neat binder and with modified binder. The modification resulted in better fatigue resistance, as the number of cycles to failure was higher for both asphalt mixes evaluated, but the increase in fatigue life was more pronounced in the finer asphalt mix (also, with more asphalt binder content), as seen in Figure 1.6. The differences between Type D and CMHB-C mixes are related to their aggregate gradation, as the

first was a dense mix and the latter a gap graded type of mix. The asphalt binder content was very similar (4.5 and 4.9%).

Figure 1.6 – Fatigue performance for different types of asphalt binder: (a) neat binders and (b) modified binders (Sugandh et al., 2007)



Fakhri, Hassani and Ghanizadeh (2013) performed the 4PBBT in a conventional asphalt mix and in a SBS-modified asphalt mix. Different methods of analysis and different failure criteria were considered. In general, the polymer-modified mixes had fatigue lives that lasted three times longer than the conventional ones. Also, the increase in loading frequencies did not necessarily affect the fatigue life of the SBS-modified mix in comparison to the conventional mix, so this means that the modified material has less sensibility to different traffic speeds. Other researchers have found the same tendency. Khattak and Baladi (1998) studied asphalt mixes with neat binder and SBS- and SEBS-modified binders in different contents. The fatigue life of the polymer-modified mixes was considerably higher, with the best resistance occurring for the 5% of polymer-modified mixes, even though 7% of polymer was also tested. The authors considered that this increase in fatigue life with the addition of polymer was due to in the tensile strength and enhancement in the plastic properties of the asphalt mixes evaluated. Awanti (2013) compared stone matrix asphalt (SMA) mixes with neat and SBS-modified binders by means of stress-controlled ITT fatigue testing and concluded that the polymer-modified material had 36% higher fatigue life.

The rheological properties of asphalt binders containing polymers have also been evaluated, especially to be compared to neat binders. Mazumder, Kim and Lee (2016) compared an SBS-modified asphalt binder with a neat binder, also combined with two types of wax additives: leadcap (L) and sasobit (S). Fatigue cracking

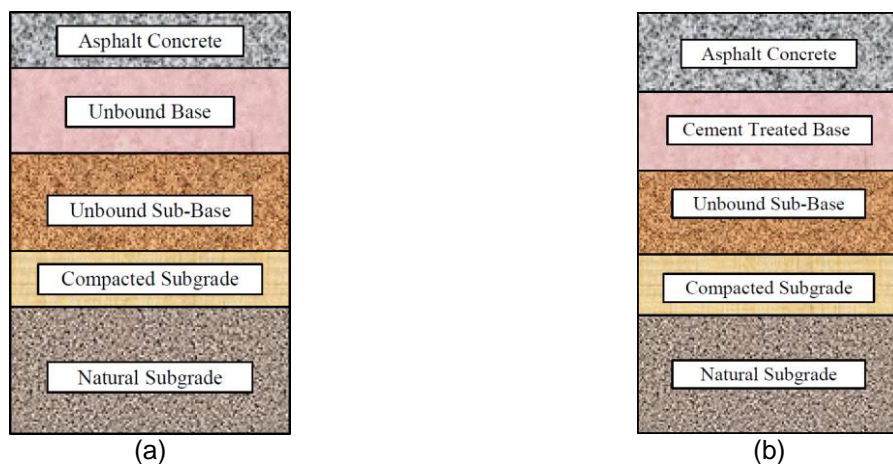
resistance was obtained in terms of the Superpave fatigue parameter ($|G^*| \times \sin \delta$). The results indicated that the modified binder would lead to a lower fatigue life, especially with the addition of sasobit wax. In respect to the limits considered by the Superpave methodology, all the asphalt binders tested had $|G^*| \times \sin \delta$ values lower than 5,000kPa. The initial motivation of using these additives was related to the increase on rutting resistance.

1.2.4 Fatigue cracking in flexible and semi rigid asphalt pavements

This section provides the main differences between these two types of structures, the stress and strain characteristics found in two types of pavement structures: flexible and semi rigid asphalt pavements, and the general fatigue cracking performance that normally occurs on each type of structure.

According to Balbo (2007), the concept of flexible and semi rigid asphalt pavements can vary in the existing literature. In general, the main difference between them is the base course layer. A flexible asphalt pavement is constituted by an asphalt surface layer and an unbound course base layer, whereas a semi rigid asphalt pavement also has an asphalt layer but the base layer is constituted by a material stabilized with any kind of hydraulic binder (most commonly, the Portland cement), as presented in Figure 1.7.

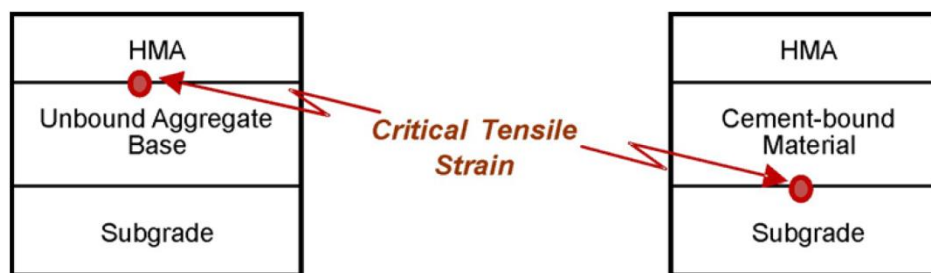
Figure 1.7 – Types of asphalt pavements: (a) flexible and (b) semi rigid (Christopher, Schwartz and Boudreau, 2006)



These structures perform differently on the field, since the semi rigid asphalt pavement provides better performance in terms of structural and functional

conditions in comparison to flexible asphalt pavements, and can still be an economically viable alternative. The cement-treated base also provides a strong support to the asphalt layer and can be well preserved by the surface layer throughout the time (Flintsch, Diefenderfer and Nunez, 2008). Figure 1.8 shows the different location of the critical tensile strain in each type of asphalt pavement mentioned, with hot mix asphalt (HMA) as wearing course. The hypothesis of bonded layers is considered.

Figure 1.8 – Location of critical tensile strain: (a) flexible and (b) semi rigid asphalt pavement (Flintsch, Diefenderfer and Nunez, 2008)



Flintsch et al. (2008) used the Asphalt Institute (AI) model to predict the fatigue failure of one HMA layer constructed over two types of base course: unbound material and cement-treated material. The number of equivalent single axle loads (ESALs) need to reach failure of the HMA layer was found to be infinite for the semi rigid pavement structure, and the tensile strain at the bottom of the HMA layer for the semi rigid solution was 60 times lower. In this case, the fatigue life to be considered was referred to the cement-treated base layer.

1.3 INPUT OF FATIGUE CRACKING IN ASPHALT PAVEMENT DESIGN

The design of asphalt pavement structures is under constant improvement worldwide, but the empirical method used in Brazilian standard regulations still considers the California bearing ratio (CBR) parameter. This is the official method currently used in most highway projects in Brazil. Only a few climate adaptations are often provided for each scenario (Fritzen, 2015).

Many researchers have been trying to enhance the performance of Brazilian asphalt pavements by providing contributions and more realistic concepts to the current design methods. Rodrigues (1987) introduced the mechanistic approach for the

rehabilitation of airport asphalt pavement structures by using the software Tecnapav, which considered data related to the stiffness of each layer, traffic and costs data. Motta (1991) proposed a design method that included the calculation of stress and strain levels found in flexible pavement structures and estimated the fatigue life of the referred project by means of number of ESALs. Traffic, climate factors, materials and constructive techniques were also considered. In the past decades, other researchers developed and calibrated models to use as input in analyses software for mechanistic-empirical asphalt pavement design projects (e.g., Franco, 2007).

The São Paulo municipality (Brazil) proposed a design method for public highway constructions that included a few modifications to the CBR method. It included the possibility of using asphalt mixes with polymer modification and base layers constituted by recycled aggregates, with crushed stone or with cement. It also included a mechanistic analysis regarding the fatigue resistance of the asphalt structures proposed by the method (PMSP IP-08, 2004). The fatigue verification is done by means of the elastic layered system theory, and stress/strain levels are obtained by computational software. For HMA mixtures, the fatigue life model proposed by this method is described by Equation 1.10.

$$N_f = 6.64 \times 10^{-7} \left(\frac{1}{\varepsilon} \right)^{2.93} \quad (1.10)$$

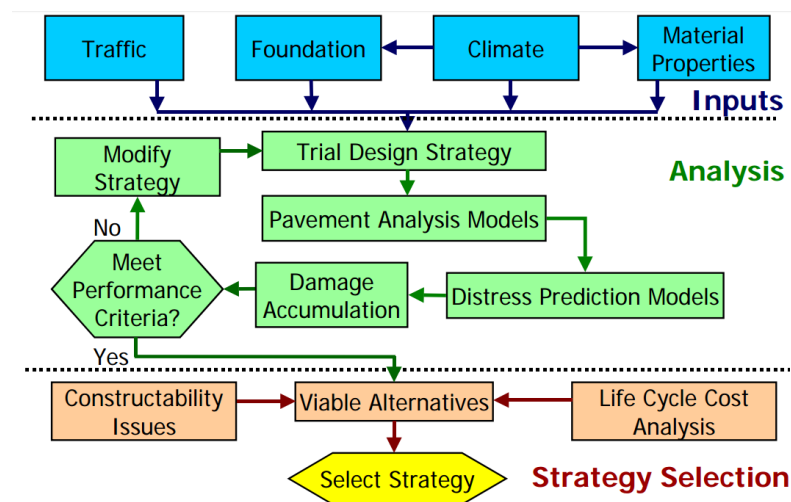
Where: N_f is the number of cycles to failure;
 ε is the strain level at the bottom of the surface layer.

During the 1950s, AASHTO performed an extensive analysis of results from an experimental test site monitored during two years, in the state of Illinois (US). After several updates and addition of new concepts, the 2002 AASHTO Design Guide was released and provided a mechanistic-empirical method to design asphalt pavements.

The procedure included in the 2002 AASHTO Design Guide follows the steps on Figure 1.9. First, a trial design should be assembled, including the subgrade support, the asphalt concrete's and the other layers' properties, the traffic configuration, the climate conditions, the pavement type and the construction techniques. Criteria

related to pavement performance should be established for the performances related to: fatigue cracking, rutting, thermal cracking, and roughness. After that, the structural responses, i.e., stresses and strains, are obtained by means of computational processes, for each damage-calculation increment, throughout the entire pavement life. The accumulated damage and distresses are calculated for each analysis period, including the period at the end of the pavement life. The main distresses are predicted by means of the calibrated mechanistic-empirical performance models.

Figure 1.9 – 2002 AASHTO design guide overall procedure (NCHRP, 2004)



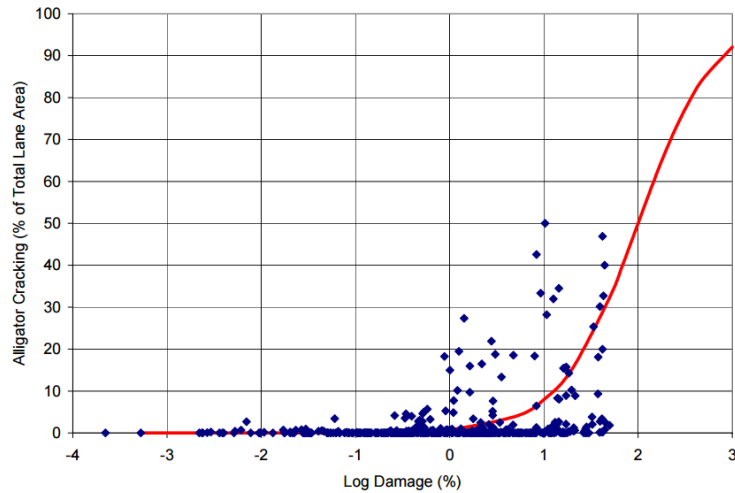
For the prediction of fatigue cracking performance, the critical response variable is the tensile horizontal strain at the bottom of the HMA layer. The damage prediction is based on a transfer function that correlates damage to cracked area (CA), presented in Equation 1.11. Figure 1.10 shows the relationship between the measured and the predicted cracking, in terms of fatigue damage of the asphalt layer.

$$CA = \left(\frac{6,000}{1 + e^{(C_1 \times C'_1 + C_2 \times C'_2 \log_{10}(D \times 100))}} \right) \times \left(\frac{1}{60} \right) \quad (1.11)$$

Where:

- CA is cracked area (%);
- D is the accumulated damage;
- C_1 is equal to: 1.0;
- C'_1 is equal to: $-2 \times C'_2$;
- C_2 is equal to: 1.0;
- C'_2 is equal to $-2.40874 - 39.748 \times (1 + h_{ac})^{-2.856}$.

Figure 1.10 – Predicted damage versus percentage of cracked area (NCHRP, 2004)



1.4 FATIGUE CRACKING PREDICTION

The developed and calibrated methods of fatigue cracking prediction to be used into the design methods for asphalt pavements can be generally divided into two groups: empirical and mechanistic-empirical methods. Originally, both take into consideration the horizontal strain at the bottom of the asphalt layer to predict the damage caused by fatigue cracking, and the vertical strain at the top of the subgrade to control rutting. The mechanistic-empirical approach is limited in the sense that the models are normally developed from experiences performed with specific materials and climatic conditions, and mostly considers the theory of elasticity for the materials behavior and sometimes might include concepts from the theory of viscoelasticity.

The pavement design standard of the Department of Transportation of the state of São Paulo, Brazil, (PMSP IP-DE-P00-001, 2006) requires the elastic parameters of the asphalt pavement layers in order to perform a mechanistic verification of the asphalt pavement structures. Different experimental fatigue cracking models can be used to predict the fatigue cracking of the surface asphalt layer. Earlier, the traditional models normally took into consideration only strain values (Equation 1.12), as presented by Verstraeten, Veverka and Francken (1982), Powell et al. (1984) and Thompson (1987). Table 1.1 presents the fitting coefficients for the aforementioned models.

$$N = k_1 \times \left(\frac{1}{\varepsilon_t}\right)^{k_2} \quad (1.12)$$

Where: N is the number of accumulated ESALs to fatigue failure;
 ε_t is horizontal tensile strain at the bottom of the asphalt layer;
 K and n are fitting coefficients.

Table 1.1 – Fitting coefficients of early fatigue prediction models

| Reference | k_1 | k_2 |
|--|------------------------|-------|
| Verstraeten, Veverka and Francken (1982) | 4.92×10^{-14} | 4.76 |
| Powell et al. (1984) | 1.66×10^{-10} | 4.32 |
| Thompson (1987) | 5.00×10^{-6} | 3.00 |

More recent methods, such as the one provided by the mechanistic-empirical pavement design guide (MEPDG), have provided new performance models that use some of the materials' properties, including the materials stiffness. Equation 1.13 shows the fatigue cracking performance prediction general model by the MEPDG. A set of different fitting coefficients can be used in this equation, and the two most commonly used are those developed by Shell Oil and the AI. The general form of these prediction models is the same, as shown below. The differences between them rely on the fitting coefficients (Table 1.2), normally obtained by means of laboratory tests, and on the laboratory-to-field adjustment factors, which can be based on the materials volumetric and properties.

$$N = Ck_1 \times \left(\frac{1}{\varepsilon_t}\right)^{k_2} \times \left(\frac{1}{E}\right)^{k_3} \quad (1.13)$$

Where: N is the number of accumulated ESALs to fatigue failure;
 ε_t is horizontal tensile strain at the bottom of the asphalt layer;
 E is the stiffness modulus of the asphalt mixture at the intermediate temperature (psi);
 k_1 , k_2 and k_3 are fitting coefficients;
 C is a correction factor.

Table 1.2 – Fitting coefficients of AI and Shell Oil fatigue prediction models

| Reference | k_1 | k_2 | k_3 |
|------------------------|-----------------------|-------|-------|
| Asphalt Institute (AI) | 7.96×10^{-2} | 3.291 | 0.854 |
| Shell Oil | 1.0 | 5.000 | 1.400 |

For the AI model, the correction factor C is calculated by Equation 1.14, and for the Shell Oil model, this coefficient is calculated by Equation 1.15 (for pavement sections with asphalt surface layers between 2 and 8 inches). The final prediction (N_f) is based on 20% of cracked area in the entire pavement surface.

$$C = 10^{4.84 \left(\frac{V_b}{V_a + V_b} - 0.69 \right)} \quad (1.14)$$

Where: C is the correction factor;
 V_b is the percentage of effective binder content, in volume;
 V_a is the percentage of air voids.

$$C = \left(1 + \frac{13909E^{-0.4} - 1}{1 + \exp(1.354h_{ac} - 5.408)} \right) (0.0252PI - 0.00126PI(V_b) + 0.00673V_b - 0.0167)^5 \quad (1.15)$$

Where: C is the correction factor;
 V_b is the percentage of effective binder content, in volume;
E is the stiffness modulus of the asphalt mixture at the intermediate temperature (psi);
 h_{ac} is the asphalt layer thickness;
PI is the penetration index of the asphalt binder.

From the general equation, different modifications have been introduced by several researchers throughout the years. The so-called calibrated models, also known as transfer functions, use different values for their coefficients. Among these calibrated models, the AI and the Shell equations have been widely used (Rajbongshi, 2009). Table 1.3 shows the coefficients used in both models.

Table 1.3 – Modified fitting coefficients of AI and Shell models (Rajbongshi, 2009)

| Reference | k_1 | k_2 | k_3 |
|------------------------|------------------------|-------|-------|
| Asphalt Institute (AI) | 1.133×10^{-3} | 3.291 | 0.854 |
| Shell | 5.350×10^{-7} | 5.671 | 2.363 |

Rajbongshi (2009) calculated the fatigue life of an asphalt mix using the AI and Shell models and found major differences among the results. For very low strain levels, the AI number of ESALs to failure was 10 times higher than the Shell model. For higher strain levels, the ratio was 2.5. Stubbs, Saleh and Jeffery-Wright (2010) presented another transfer function proposed by Shell that considers the stiffness modulus of the asphalt mixtures and the asphalt binder content (Equation 1.16).

$$N = \left[\frac{6918 \times (0.856V_B + 1.08)}{S_{mix}\epsilon} \right]^5 \quad (1.16)$$

Where: N is the number of accumulated ESALs to fatigue failure;
 ϵ is horizontal tensile strain at the bottom of the asphalt layer ($\mu\epsilon$);
 V_B is the asphalt binder content (%);
 S_{mix} is the stiffness modulus of the asphalt mixture (psi).

The referred authors used two typical asphalt pavement structures from New Zealand to calibrate and to validate the proposed model. After the 4PBBT was performed, at the temperature of 20°C and loading frequency of 10Hz, the results indicated that the Shell transfer function tends to generally underestimate the fatigue life of the asphalt mixture in more than five times. Saleh (2012) used two asphalt mixtures with asphalt cement (AC) 60/70 and two different aggregate maximum nominal sizes: 10 and 14mm. The 4PBBT was used to characterize the asphalt mixtures and to develop a calibrated version of the Shell model. According to this study, a shift factor of 4.8 should be multiplied to the original equation.

Adhikari and You (2010) performed the 4PBBT with varying frequency and temperature and compared their results with fatigue cracking prediction models by AI and Shell. An asphalt concrete with 4.0% of voids content, commonly used in the

state of Michigan, with a PG 64-28 asphalt cement, binder content of 5.5%, and NMAS of 9.5mm. The results indicated that the AI model overestimates the fatigue life and that the Shell model underestimates it. Denneman et al. (2011) tested five typical South African asphalt mixtures and an extra high modulus asphalt concrete in order to calibrate the parameters used in the MEPDG fatigue cracking prediction model. The results showed that the coefficients k_1 , k_2 and k_3 varied in 10^7 , 2 and 10 times, respectively, which indicates that they are highly dependent on the type of asphalt mix and asphalt binder evaluated.

1.4.1 Proposed methods for Brazilian asphalt pavement structures

Nascimento (2015) defined a transfer function to correlate the averaged damage (N/N_f) to cracked area of real pavement sections. In this research, damage simulations were done in the layered viscoelastic pavement analysis for critical distresses (LVECD) program, and part of the input data were the asphalt mixture properties obtained by means of the compression-tension test along with the simplified viscoelastic continuum damage (S-VECD) protocol provided by the author. Other parameters such as number of ESALs and climate conditions were also considered in the program. In this research, 27 pavement sections from the Fundão project, subjected to real traffic loading, were selected.

First, the data from the pavement monitoring (evolution of cracked area) and from damage simulations were recorded for each period of time. Then, the averaged damage was calculated by simply obtaining the mean damage value (for 10% of cracked area) of the entire set of pavement sections that were part of the project (the averaged damage was found to be 0.5). The shift function used to transform averaged damage into *averaged reduced damaged* considered these indices: the period, in months, to reach damage value of 0.35 ($T_{0.35}$) and the secant rate between twelve months and one month (R_{12-1}).

Equation 1.17 and Equation 1.18 present the two shift factor functions from the study by Nascimento (2015). This study used the 2004 MEPDG transfer function as the first candidate, but the author decided not to choose it, because a sigmoidal shape was not observed for the 'damage versus cracked area' curves in his research. Finally, a power function was selected for the reduced damage-to-cracked area transfer

function, as presented in Equation 1.19. It should be noticed that predicted cracked area values higher than 100% should be considered as 100%. The fitting coefficients for the equations provided are shown in Table 1.4.

$$S_{T_{0.35}} = A \times T_{0.35} + B \quad (1.17)$$

$$S_{R_{12-1}} = \beta_1 \times (R_{12-1})^2 + \beta_2 \times (R_{12-1}) + \beta_3 \quad (1.18)$$

Where: $S_{T_{0.35}}$ is the shift factor based on $T_{0.35}$;
 $S_{R_{12-1}}$ is the shift factor based on R_{12-1} ;
 A and B are fitting coefficients;
 β_1 , β_2 and β_3 are fitting coefficients.

$$CA = C_1 \times \left(\frac{N}{N_f} \text{red} \right)^{C_2} \quad (1.19)$$

Where: CA is predicted fatigue cracked area (%);
 $\frac{N}{N_f} \text{red}$ is the averaged reduced damage (damage multiplied by the shift factor, S);
 C_1 and C_2 are fitting coefficients.

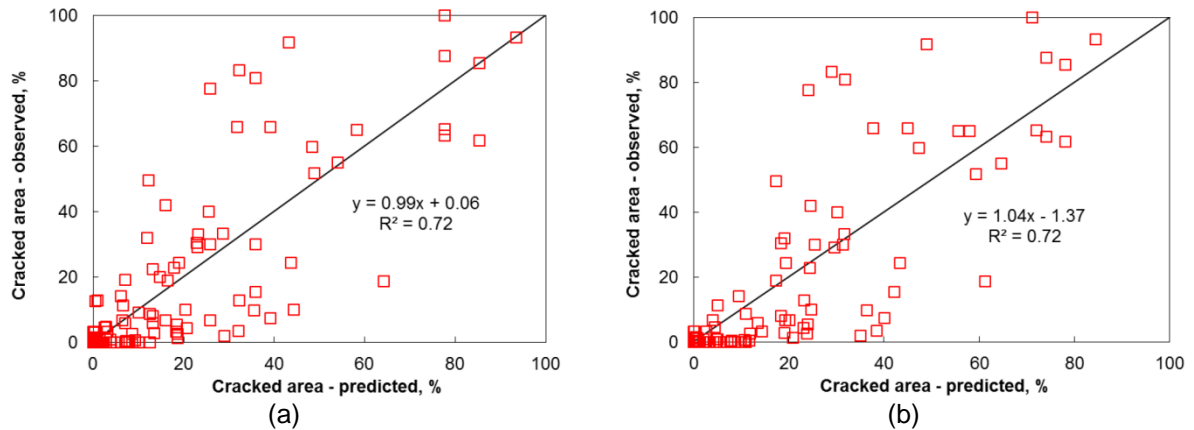
Table 1.4 – Fitting coefficients from Nascimento (2015)

| Coefficient | | Value | |
|-------------------|-------------------------|-----------|----------|
| Shift function | Based on $T_{0.35}$ | A | 0.008274 |
| | | B | 0.635237 |
| | Based on $R_{R_{12-1}}$ | β_1 | 836.913 |
| β_2 | | -50.496 | |
| β_3 | | 1.399 | |
| Transfer function | Based on $T_{0.35}$ | C_1 | 7272.68 |
| | | C_2 | 8.6629 |
| | Based on $R_{R_{12-1}}$ | C_1 | 3700.98 |
| | | C_2 | 7.4006 |

The author compared the observed and predicted values of cracked area for all the 27 pavement sections monitored during the research, for the different periods of

traffic accumulation. Figure 1.11 shows the correlation obtained, with a R^2 value of 0.72 for both damage criteria considered.

Figure 1.11 – Comparison between observed and predicted cracked area: (a) based on $T_{0.35}$ and (b) based on R_{12-1} (Nascimento, 2015)

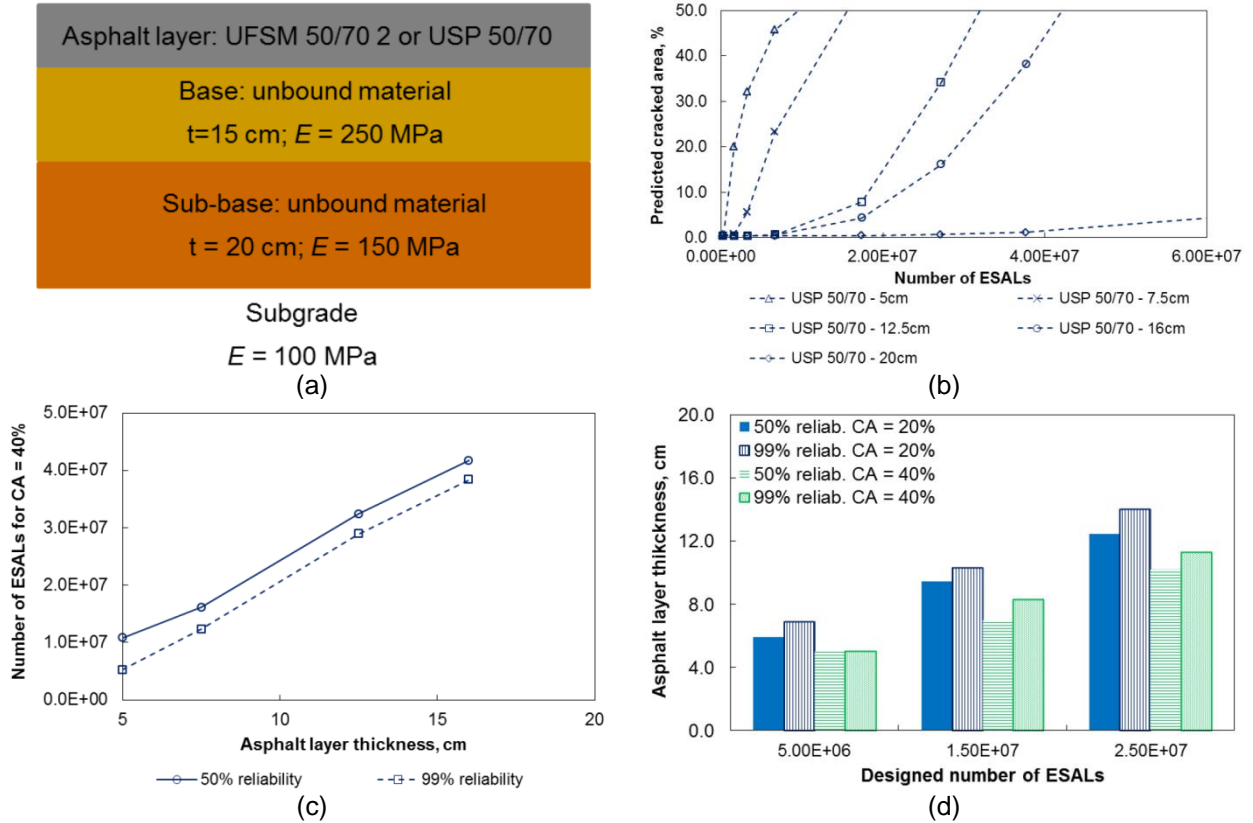


Nascimento (2015) proposed a protocol for asphalt pavement design in Brazil based on their findings and the averaged reduced damage-to-cracked area transfer function developed by his study. A typical pavement structure was chosen (Figure 1.12a) and some assumptions were made: yearly traffic growth rate of 3% and three different traffic levels, based on these number of ESALs, calculated by the United States Army Corps of Engineers' (USACE) method: 5.0×10^6 , 1.5×10^7 and 2.5×10^7 . The main objective of the pavement design is to determine the asphalt layer thickness, and Nascimento (2015) considered two reliability levels (50 and 99%) and two failure criteria (20 and 40% of cracked area). The proposed design methodology is summarized next.

First, the LVECD program performs simulations using different thicknesses for the asphalt layers. Then, the transfer function (based on $T_{0.35}$) is applied to obtain the predicted cracked area (Figure 1.12b). Curves of cracked area versus cumulative traffic for each thickness proposed are plotted (Figure 1.12c), and the number of ESALs for each failure criterion is determined. The last step of the methodology is the definition of the asphalt layer thicknesses that should be considered for each traffic level and condition (Figure 1.12d). This definition is based on the traffic levels assumed in the beginning of the protocol. Figure 1.12 shows an example of the proposed design for a typical asphalt pavement structure that was used in the

calibration of the transfer function. In this example, the level of reliability is 99% and the failure criterion is 40% of cracked area.

Figure 1.12 – Asphalt pavement design protocol: (a) typical pavement structure used in Brazil, (b) predicted cracked area versus traffic, (c) traffic accumulation versus layer thickness, and (d) designed asphalt layer (Nascimento, 2015)



Following the concepts provided by Nascimento (2015), Fritzen (2016) developed and calibrated a transfer function for Brazilian materials and pavement conditions, by considering a classical mechanical characterization testing, with the use of the resilient modulus test and the ITT. Forty-five segments from different experimental test sites were constructed and monitored for eight or more years, with a total of six types of asphalt mixtures analyzed. The objective was to predict the damage related to fatigue cracking by means of an experimental procedure and computer calculations.

In order to obtain the accumulated damage, Fritzen (2016) used an elastic analysis software for multiple layers developed by Franco (2007). The averaged damage for a total of 110 points in the surface asphalt layer was calculated for each accumulated traffic considered in the analysis. The main objective of Fritzen (2016) was to find a

correlation between simulated damage and cracked area of the several pavement sections studied, by developing a transfer function that could properly fit different types of asphalt mixtures. The author used a damage shift approach based on the initial simulated damage growth rate. This would ensure that there was a unique relationship between the shifted damage and the cracked area of the real pavement. The averaged reduced damage was determined at 10% of cracked area.

The protocol used to develop the transfer function was similar to what can be found in Nascimento (2015), with different assumptions. In this case, damage values were still considered at 10% of cracked area, but the averaged damage value was 0.8. The period in months in which the damage of 10% of cracked area occurred was found through regression, for each pavement analyzed.

With all the necessary parameters determined (damage values and period in months at 10% of cracked area; number of ESALs and period in months at the averaged damage), the shift factor was calculated (Equation 1.20) so that the accumulated damage was converted into a parameter called *averaged reduced damage*. The *damage-to-fatigue cracked area* transfer function was found to be a power law equation (Equation 1.21), with its coefficients obtained after the use of the solver function in the Excel software, in which the minimum mean square error should be considered between the predicted and the observed cracked areas. The fitting coefficients are provided in Table 1.5.

$$S = A \times (T_{0.8})^B \quad (1.20)$$

Where: S is the shift factor;
 $T_{0.8}$ is the period of time in months at 0.8 of damage;
 A and B are fitting coefficients.

$$CA = C_1 \times (D_{red})^{C_2} \quad (1.21)$$

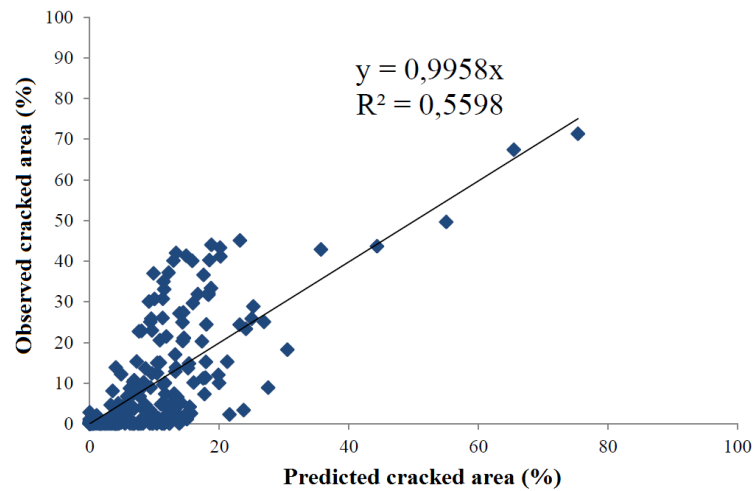
Where: CA is predicted fatigue cracked area (%);
 D_{red} is the averaged reduced damage (damage multiplied by the shift factor, S);
 C_1 and C_2 are fitting coefficients.

Table 1.5 – Fitting coefficients from Fritzen (2016)

| Coefficient | | Value |
|-----------------------|-------|--------------------|
| Shift factor function | A | 0.8756 |
| | B | 0.0307 |
| Transfer function | C_1 | 1.50×10^5 |
| | C_2 | 40.61338 |

To validate the transfer function that was developed and calibrated, Fritzen (2016) compared the observed cracked area with the predicted cracked area for all pavement sections monitored in their research. Figure 1.13 shows the correlation between both parameters, with a R^2 of 0.56, which was considered to be very good in comparison to the 2004 MEPDG transfer function. Plots related to each pavement section were done to compare the predicted cracked area to the observed cracked area, and most of the results provided a good correlation, so the transfer function was finally validated. In general, the observed cracked area values were higher than the predicted values, which can be explained by issues that the prediction model is not capable of capturing after a certain level of cracked area, such as water infiltration.

Figure 1.13 – Comparison between observed and predicted cracked area (Adapted from Fritzen, 2016)



The methodology used by Fritzen (2016) to develop and calibrate the transfer function proposed required simpler inputs regarding asphalt mixtures characterization and computer simulations. Those inputs can be obtained by means of classical fatigue tests normally performed in Brazilian research centers and design project companies.

1.4.2 Traffic input in fatigue cracking models

Traditionally, performance prediction models for asphalt pavements consider the traffic by simply transforming the different types and loads in loading axles of 80kN, based on the empirical tests done in AASHTO test roads. The use of the entire real load spectrum is important to understand the fatigue cracking of asphalt pavements better, therefore, the weigh-in-motion (WIM) technique is a strong tool capable of collecting the real data that come from loading configuration. These data can be used in mechanistic-empirical methods for pavement design (Berthelot, Loewen and Taylor, 2000).

Regarding the study of asphalt pavements performance using field data, Otto, Momm and Valente (2013) monitored an instrumented experimental test site and collected information of traffic, strain and stress levels in each layer, as well as information on the moisture content of the granular layers and temperature of the asphalt layer. The fatigue cracking performance of this asphalt pavement was studied, and the main conclusions were that the deterioration of an asphalt pavement is influenced by the

axle configuration, types and speed of vehicles passing, which are factors that are normally not considered in the usual models.

Priest (2005) developed a fatigue cracking performance model by calibrating the MEPDG equations for a pavement structure designed by a mechanic-empirical method. Experimental test sites instrumented with temperature and moisture measurement sensors, load cells and strain gauges were studied. A total of eight test sections with varying layers composition and thicknesses were evaluated. After a few years of field data collection, two fatigue cracking prediction models were developed, one for HMA thinner layers (127mm) and the other for thicker HMA asphalt layers (approximately 180 to 230mm). Equation 1.22 and Equation 1.23 show these models, respectively.

$$N = 0.4801 \times \left(\frac{1}{\varepsilon_t}\right)^{3.143} \times \left(\frac{1}{E}\right)^{0.4834} \quad (1.22)$$

$$N = 0.4875 \times \left(\frac{1}{\varepsilon_t}\right)^{3.0312} \times \left(\frac{1}{E}\right)^{0.6529} \quad (1.23)$$

Where: N is the number of accumulated ESALs to fatigue failure;
 ε_t is horizontal tensile strain at the bottom of the asphalt layer;
 E is the stiffness modulus of the asphalt mixture (MPa).

Hafeez et al. (2013) evaluated twelve field asphalt mixtures with different properties: two asphalt binders (AC 60/70, and AC 80/100), three types of filler (sand, stone dust, and sand), and two gradation sizes (fine, and coarse). These asphalt mixtures were compacted in the field, but the samples were extracted before any traffic passed on. 4PBBT was performed at different temperatures (5, 15, and 25°C). In terms of fitting coefficients to be considered in fatigue life curves, the results varied a lot for each condition and type of mixture tested. The parameter k varied from 0.00009 to 0.76, and the parameter n varied from 2.03 to 4.25. The authors concluded that there was a correlation between these coefficients (Equation 1.24).

$$k_2 = 2.044 - 0.275 \log(k_1) \quad (1.24)$$

Where: k_1 and k_2 are fitting coefficients.

Wen and Li (2013) evaluated asphalt mixtures with different types of asphalt binder (modified or not) by means of fatigue cracking prediction models found in the literature. Tensile strength and dynamic modulus tests were performed in the laboratory, and field analysis was done by means of an instrumented experimental test site. The comparison between the predicted and the observed data using models from the literature was not satisfying, so the authors decided to develop and to propose a new fatigue cracking prediction model, which took the dissipated energy during the tensile strength test in consideration along with the dynamic modulus of the asphalt mixture. This model provided good correlations with field data (R^2 equal to 0.99). Equation 1.25 presents the proposed model.

$$N_f = 5.43 \times 10^{13} \times \left(\frac{1}{\varepsilon_t}\right)^{3.963} \times \left(\frac{1}{E}\right)^{2.149} \times (\text{CSED})^{1.705} \times h^{0.30} \quad (1.25)$$

Where: N_f is the number of accumulated ESALs to fatigue failure;
 ε_t is horizontal tensile strain at the bottom of the asphalt layer;
 E is the stiffness modulus of the asphalt mixture (MPa);
 CSED is the critical strain-energy density during the ITT;
 h is the asphalt layer thickness (mm).

Park, Buch and Suh (2001) developed a fatigue cracking prediction model by using a non-linear regression technique that combined factors related to traffic loading with field variables, such as environmental aspects and materials properties. To complete this research, 39 asphalt pavements sections from an experimental test site in the state of Michigan were gathered to provide the data used to develop and to calibrate the model (Equation 1.26), which results in a R^2 value of 0.99.

$$\begin{aligned} \ln(N) = & -3.454 \ln(SD) + 0.018CA - 0.223 \ln(\varepsilon_t) \\ & + 3.477 \ln(H_{AC}) - 3.52 \ln(KV) + 0.053 \ln(E_{AC}) - 1.027 \ln(E_{BS}) \\ & - 1.515 \ln(E_{SG}) + 32.156 \end{aligned} \quad (1.26)$$

Where: N is the number of accumulated ESALs to fatigue failure;
SD is the asphalt pavement surface deflection;
CA is the cracked area;
 ε_t is horizontal tensile strain at the bottom of the asphalt layer.
 H_{AC} is the asphalt layer thickness (in);
 E_{AC} is the resilient modulus of the asphalt concrete (psi)
KV is the kinematic viscosity (centistokes);
 E_{BS} is the base layer modulus (psi);
 E_{SG} is the resilient modulus of the subgrade (psi).

1.5 ACCELERATED TESTING FOR FATIGUE CRACKING PREDICTION

Tests performed in full-scale pavement sections, also known as accelerated pavement testing (APT), Yeo, Suh and Mun (2008) used a real-scale asphalt pavement structure and induced the infiltration of water to subgrade soil during the construction and loading applications on the surface layer. The falling weight deflectometer (FWD) equipment was used to measure the deflections and using a backcalculation process the stiffness values were obtained. Instrumentation was done in the pavement structure in order to provide strain values. These authors developed a fatigue model (Equation 1.27) based on the cumulative damage and correlated it with results obtained in the APT and in the laboratory tests. The failure criterion for the asphalt pavement sections was the crack initiation. Later, the same authors compared the fatigue life using the proposed model to other fatigue models found on the literature. In general, field models led to similar results in comparison to lab models, which all underestimated the fatigue life of the asphalt pavement studied.

$$N_f = 1.29 \times 10^{-6} \left(\frac{1}{\varepsilon_t} \right)^{3.02} \quad (1.27)$$

Where: N_f is the number of ESALs to fatigue failure;
 ε_t is the tensile strain at the bottom of the asphalt layer.

The use of traffic simulators in APT sections has been an alternative procedure to obtain more precise and more realistic performance-related data, in short periods of time. Metcalf (1996) states that accelerated testing in full-scale consists in the application of controlled wheel loading at the highway weight limit or higher to a pavement structure in order to determine the response in terms of displacements, stresses and strains, and to obtain the performance of this structure under a controlled, accelerated, accumulation of damage in a shorter amount of time.

APT using traffic simulators has helped on the development and calibration of performance models related to the main distresses that occur in asphalt pavements, including fatigue cracking. This procedure has different objectives, including: to evaluate the existing asphalt pavements for heavier traffic, to allow the use of new materials and new structures, to evaluate the possible use of geosynthetics, to evaluate the effects of new combinations of axles loads and tire configurations, among others.

According to Metcalf (1996), there are basically three types of real-scale traffic simulators: (i) test roads, which provide good evidence of the pavement performance but poor environmental control; (ii) circular tracks, which have the advantages of operating at high speed and are capable of testing several pavement sections at the same time, but they can offer some difficulty during the construction of the circular pavement with the conventional equipment and techniques; (iii) linear tracks, which normally use a two-way loading that can affect pavement performance. Several countries have performed different trials throughout the past decades: Australia, Canada, China, France, Germany, Italy, Japan, South Africa, Switzerland, the USA, among others.

In Brazil, the Instituto de Pesquisas Rodoviárias (IPR) circular track has been used since the 1980s to study different types of wearing courses, including asphalt concrete and cement concrete, and also recycled materials as base layer. The Universidade Federal of Rio Grande do Sul (UFRGS) has a linear track that has provided different studies, such as the use of geotextiles, rubber-modified asphalt binders and the implementation of new techniques for monitoring purposes, including instrumentation and temperature measurements (Negrão, 2012).

2 CHARACTERIZATION OF FATIGUE CRACKING RESISTANCE OF ASPHALT BINDERS USING DIFFERENT METHODS

2.1 INTRODUCTION

Several researchers have created and developed different test methods with the objective of predicting the fatigue cracking resistance of asphalt mixes by means of asphalt binder characterization. Fatigue cracking is a distress that is highly dependent on the type and quality of the asphalt binder used in a HMA. The stiffness and damage characteristics of asphalt binders normally provide a good indication of the fatigue resistance of asphalt mixes constituted by them (SHRP-A-404, 1994).

In 1987, the Strategic Highway Research Program (SHRP) project entitled 'Binder Characterization and Evaluation' was created to provide a better understanding of asphalt binders chemical and physical properties and how those properties affect the performance of asphalt pavement structures. Before SHRP was conceived, the existing empirical specification tests used for asphalt binder characterization could not properly address performance-related properties of these materials and could not describe or predict in-field performance of asphalt pavements (Petersen et al., 1994). Also, the empirical characterization did not truly differentiate the behavior of modified asphalt binders from neat binders (Gershkoff, Carswell and Nicholls, 1997). Thus, rheological tests were implemented by SHRP and a new classification based on their performance grade (PG) was developed.

The traditional Superpave parameter $|G^*| \times \sin \delta$ is used to characterize the fatigue resistance of asphalt binders when the Performance Grade (PG) specification is considered. Despite that, several researches have unsuccessfully tried to correlate this parameter to the fatigue resistance of asphalt mixtures containing modified binders, especially considering that this parameter is obtained in the linear viscoelastic (LVE) region of the asphalt binders. Therefore, other test methods and new parameters have been developed (Bahia et al., 2001), such as the use of damage-induced tests, by means of load repetitions. The PG specification currently limits the value of $|G^*| \times \sin \delta$ to 5,000kPa and 6,000kPa for standard (L) and heavy/very heavy traffics (H/V), respectively, at the testing frequency of 10rad/s (AASHTO M 320, 2009).

Among the main existing laboratory tests that provide the fatigue life of asphalt binders, the time sweep test (TST) and the linear amplitude sweep (LAS) test have been widely used in the past years (Tabatabaee and Tabatabaee, 2010; Perez-Jiménez, Botella and Miró, 2012; Willis et al., 2012; Bahia et al., 2013; Pamplona, 2013; Martins, 2014; Nuñez et al, 2014; Ameri, Jelodar and Moniri, 2015; Safaei and Castorena, 2015; Camargo, 2016; Wang et al., 2016; Nunes, 2017). Both tests are performed in the dynamic shear rheometer (DSR).

The TST can be a stress- or a strain-controlled test and consists in the application of cyclic loading at a constant frequency. For the strain-controlled mode, which will be used further in this dissertation, there are no standard values for frequency and strain amplitude. Some authors indicate the use of 10rad/s and 10% of strain to accelerate the test, in order to avoid time-consuming tests in other conditions. It is important to ensure that the test is performed at strain levels that are outside the LVE region, since asphalt pavements have a non-linear damage behavior (Clyne and Marasteanu, 2004).

The LAS test (AASHTO TP 101, 2014) consists in applying a cyclic loading divided into two steps. The first step corresponds to a frequency sweep from 0.2 to 30Hz at 0.1% of strain amplitude; the second step is an amplitude sweep from 0 to 30% with linear increment on the strain value, during 300 seconds and at a constant frequency of 10Hz. The first part of the test (frequency sweep at low strain amplitude) is performed in order to obtain the LVE properties of the specimen, including the stiffness modulus, which is later used in the calculation of the accumulated damage.

This section of the present dissertation has the main objective of comparing results from different fatigue cracking resistance tests performed in asphalt binders. Three materials are studied: one neat asphalt binder used as part of the asphalt wearing course of an experimental test site that will be presented later on this dissertation, and two modified binders (SBS-modified and one highly modified binder, HiMA).

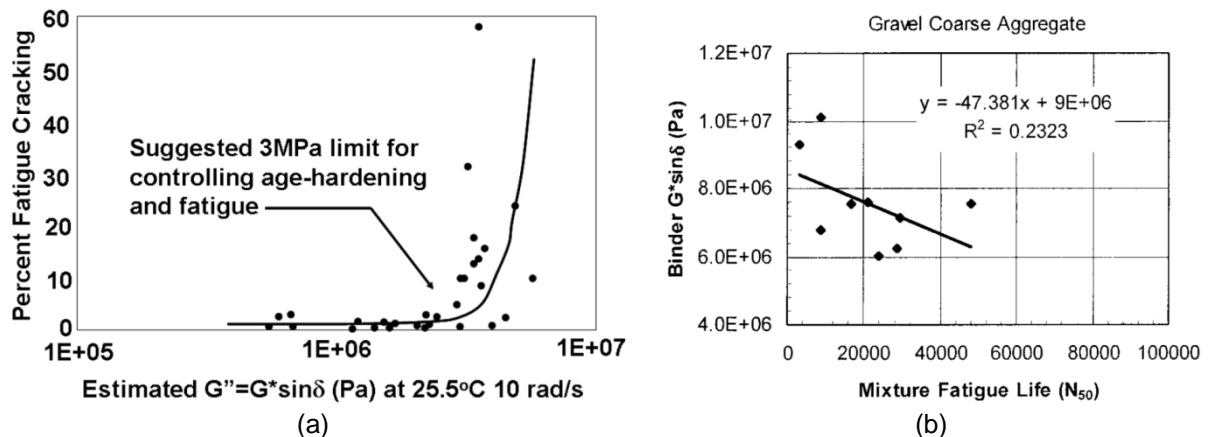
2.2 REVIEW OF LITERATURE

The Superpave specification's first attempt to address fatigue cracking of asphalt binders was based on an experimental test site built in the 1950s in the state of

California (USA). The Zaca-Wigmore road test assisted the development of asphalt binder parameters to be considered in highway design projects and the durability of this type of material. The parameter $|G^*| \times \sin \delta$ of different asphalt binders from the constructed sections was compared to the percentage of fatigue cracking, and it was decided to limit the value of $|G^*| \times \sin \delta$ to 3,000kPa at the predicted annual average pavement temperature in the region of interest, at the frequency of 10rad/s (Petersen et al., 1994). Figure 2.1a presents the correlation data used for specification purposes. The failure criterion considered to limit the maximum value of $|G^*| \times \sin \delta$ was 10% of fatigue cracking after approximately 9 to 10 years of pavement evaluation based on crack surveys (Finn e al., 1990). Later, the Federal Highway Administration (FHWA) suggested increasing the limit to 5,000kPa, which was included into the AASHTO's specification for design purposes (Gibson et al., 2012).

After a few years, another study (Bahia et al., 2001) concluded that the Superpave parameter did not address the modified binders' characteristics correctly, therefore asphalt mixes were tested by means of four point beam bending tests, and a poor correlation was found between these results and the values of $|G^*| \times \sin \delta$ (Figure 2.1b). The failure criterion for the asphalt mixes was based on the 50% reduction of initial stiffness. It is important to notice that all values of $|G^*| \times \sin \delta$ found on the binder tests were higher than any Superpave specification (i.e., higher than 6,000kPa), because these tests were performed at the frequency of 10Hz and at short-term aged materials, in order to meet the same test conditions established by the four point bending beam test.

Figure 2.1 – Comparisons between fatigue cracking and Superpave parameter: (a) Petersen et al., 1994 and (b) Bahia et al., 2001

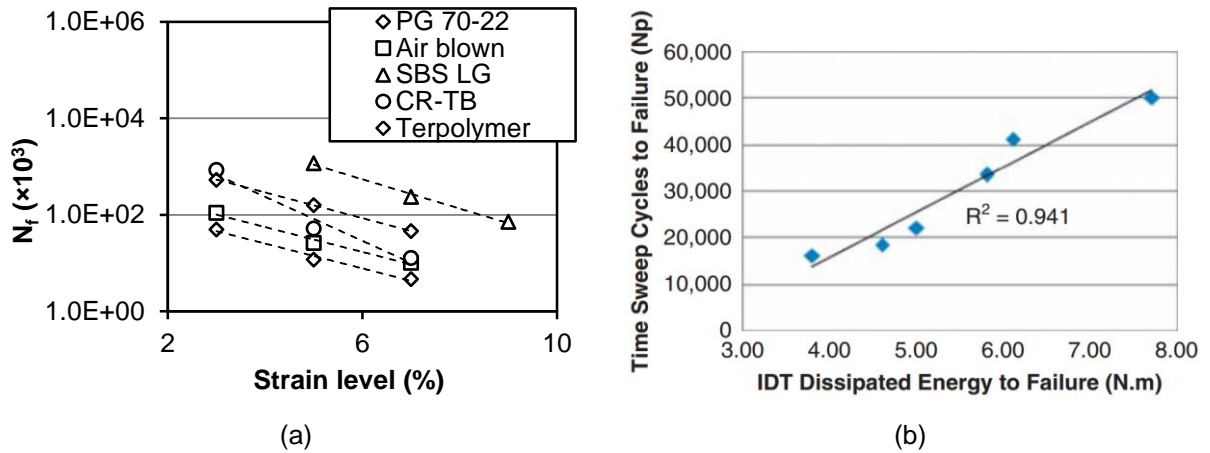


Martono and Bahia (2008) conducted the TST at three strain levels at 19°C and 10Hz. They considered the point of failure as the point where the $|G^*|$ value reached 50% of its initial value. Modified binders had a better resistance to fatigue cracking if compared to the neat PG 70-22 binder studied, with the SBS-modified binder having the best fatigue resistance in comparison to the other materials. Figure 2.2a presents the fatigue lives of each binder tested, where N_f is the number of cycles to failure.

Johnson (2010) performed TSTs in four different asphalt binders (neat binder, SBS-modified binder, and two Elvaloy-modified binders – one with PG 64-34 and the other with PG 58-34), with strain variation from 5 to 7%. The results indicated that at 5% strain, the SBS-modified asphalt binder had a better fatigue resistance if compared to other binders. At 7% of strain amplitude, the three modified binders had similar results among them and also better resistance in comparison to the neat binder. The selection of the strain level used in the TST is normally arbitrary, and in the referred research, the strain levels were chosen according to good correlations found with results from experimental test sites. Although it might not seem a simple task, it is important to simulate a wide range of strain levels through laboratory testing for a better understanding of the materials behavior and for understanding their performance in field under different loading and structural conditions.

Tabatabaee and Tabatabaee (2010) performed the TST using strain level of 10% and loading frequencies of 15Hz and 1.59Hz (10rad/s), but discarded the 1.59Hz-tests because most binders did not fail in a reasonable amount of time. Testing temperatures were initially 5 and 30°C, but the first was discarded due to high stiffness of the asphalt binders, which prevented the equipment to reach the target strain during the test. They compared the results from TST at 10% controlled-strain (using 50% of $|G^*|$ reduction as failure criterion) performed in asphalt binders to results of dissipated energy taken from ITT performed in asphalt mixes. The correlation was found to be better than the correlation between the Superpave parameter $|G^*| \times \sin \delta$ to the results obtained for the asphalt mixes (Figure 2.2b).

Figure 2.2 – Time sweep tests results: (a) Martono and Bahia (2008), and Tabatabaee and Tabatabaee (2010)



Previous studies have considered the strain distribution in asphalt mixes to select the strain levels to be applied during the TST. For example, Mannan, Islam and Tarefder (2015) compared the results from the 4PBTT performed in asphalt mixes to the results from TST performed on binders. For the binder characterization, they used strain levels that were 100 times higher than the ones used for the asphalt mixes characterization, based on the modeling of strain distribution by Masad et al. (2001). Masad et al. (2001) estimated that the maximum binder strain is about 90-100 times that of the mix, so 4% would represent $400\mu\epsilon$ in the asphalt mix, which tends to be very high in the field.

Planche et al. (2004) studied the influence of several parameters that are not normally considered in asphalt binder fatigue resistance tests, especially in time sweep tests, which might demand a great amount of time to be finished. These authors concluded that any of these parameters might interfere with the fatigue response of asphalt binders: the initial value of $|G^*|$; the increase in $|G^*|$ value in the beginning of the test, which might be caused by self-heating of the material; steric hardening occurring with time, which might cause an increase of $|G^*|$ values during a portion of the test; and the influence of rest periods, which might cause healing effects to the binders.

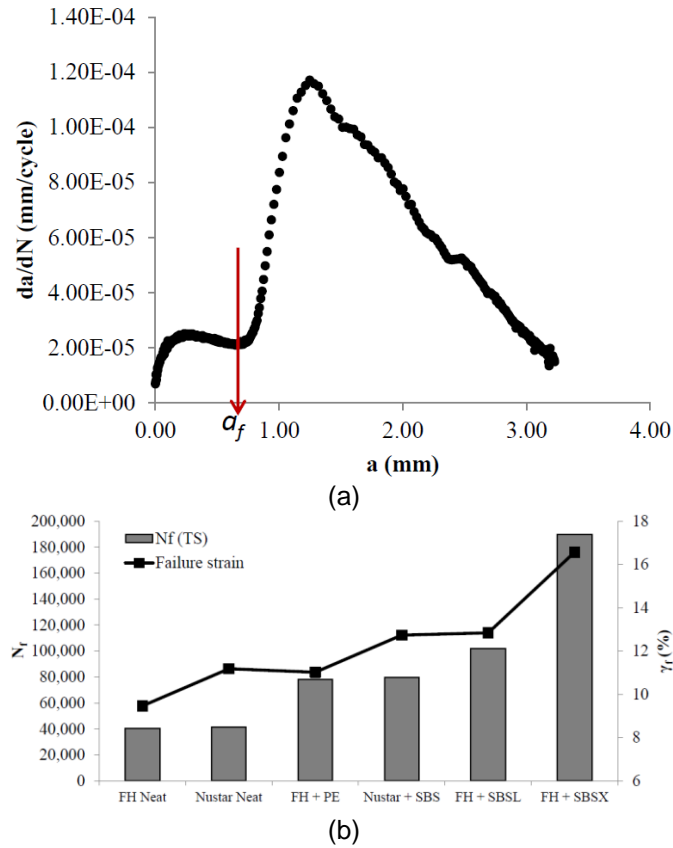
Wang et al. (2016) compared different analysis approaches to define fatigue failure during time sweep tests. They concluded that the dissipated energy based method is

better than the traditional failure definition based on 50% reduction in the initial value of $|G^*|$. Al-Haddad (2015) found similar results.

Despite correlating well with asphalt mixes results, the TST might not be suitable for design purposes due its time-consuming characteristic. Therefore, accelerated fatigue tests have been proposed. The LAS test was developed by Johnson (2010) and has been the focus of several studies in the past years. The analysis of the results obtained in this test was proposed based on viscoelastic continuum damage (VECD) mechanics by means of damage accumulation rate. This author correlated and validated the results to asphalt mixes behavior in laboratory and field performance.

Since its development, other approaches have been considered to obtain the fatigue resistance of asphalt binders by means of the LAS test. Hintz (2012) studied the fracture mechanics applied to asphalt, as she considered this to be one of the multiple phenomena that contribute to changes in its properties during fatigue testing. Edge fracture was considered to initiate at the periphery of the binder specimen and to propagate into the inner part of the sample. In this method, the failure criterion proposed was the local minimum crack growth rate before the rapid increase in the crack growth rate (Figure 2.3a). This author obtained a good comparison ranking between the numbers of cycles to failure (from the TST) to the crack length at failure (from the LAS test), as shown in Figure 2.3b.

Figure 2.3 – LAS test: (a) crack growth rate approach and (b) comparison between LAS test and TST (Hintz, 2012)



The fracture mechanics approach requires the calculation of the crack size at each cycle during the test, as the following (Martins, 2014):

- First the torsional stiffness is calculated at each data point (Equation 2.1). Then, the effective radius at each data point (r_N) is obtained by Equation 2.2.

$$k = \frac{T}{\varphi} \quad (2.1)$$

Where: k is the torsional stiffness;
 T is the torque;
 φ is the deflection angle amplitude.

$$r_N^4 = r_i^4 \frac{k_N}{k_i} \quad (2.2)$$

Where: r_N is the radius at cycle N;
 r_i is the initial radius;
 k_N is the torsional stiffness at cycle N;
 k_i is the initial torsional stiffness.

- The effective crack length (a) is calculated by Equation 2.3.

$$a = r_i - r_N \quad (2.3)$$

Where: a is the crack length (mm);
 r_N is the sample radius at cycle N;
 r_i is the initial sample radius.

- Finally, the crack growth rate is calculated (da/dN), as a function of a (Equation 2.4).

$$\frac{da}{dN} = \frac{\Delta a}{\Delta N} \quad (2.4)$$

Where: Δa is the change in crack length;
 ΔN is the change in number of loading cycles.

The current analysis method used for analyzing LAS test results is based on the VECD theory. The calculation steps based on AASHTO TP 101 (2014) are presented next.

- First the damage accumulation $D(t)$ for the specimen is calculated using Equation 2.5.

$$D(t) \cong \sum_{i=1}^N [\pi y_0^2 (C_{i-1} - C_i)]^{\frac{\alpha}{1+\alpha}} (t_i - t_{i-1})^{\frac{1}{1+\alpha}} \quad (2.5)$$

Where: $D(t)$ is the accumulated damage at the time 't';
 C_i is the specimen's integrity at the time 't', which is equal to $|G^*|$ at the time 't' divided by the initial value of $|G^*|$;
 $|G^*|$ is the value of dynamic shear modulus (MPa);

y_0 is the applied strain for a given data point (%);
 α is the inverse value of m , which is slope of the log-log $|G'|$ versus frequency (from the frequency sweep step of the LAS test), where $|G'|$ is the storage modulus;
 t is the testing time (s).

- Then, the C_1 and C_2 parameters are calculated by fitting Equation 2.6 to the integrity versus damage ($C \times D$) curve:

$$C = C_0 - C_1(D)^{C_2} \quad (2.6)$$

Where: C is the material's integrity at the time 't';
 C_0 is the initial value of integrity, which can be considered as 1.0;
 C_1 and C_2 are fitting coefficients.

- The failure damage level is defined by Equation 2.7. D_f is the value of $D(t)$ which corresponds to the reduction in initial value of $|G^*|$ at the peak shear stress. Then, Equation 2.8 and Equation 2.9 calculate the parameters A and B for the fatigue law equation.

$$D_f = \left(\frac{C_1 - C_{\text{at peak stress}}}{C_1} \right)^{\frac{1}{C_2}} \quad (2.7)$$

$$A = \frac{f(D_f)^k}{k(\pi C_1 C_2)^\alpha} \quad (2.8)$$

$$B = 2\alpha \quad (2.9)$$

Where: f is the loading frequency (Hz);
 k is equal to $1 + (1 - C_2)\alpha$.

- Finally, the number of cycles to failure (N_f) can be calculated according to Equation 2.10.

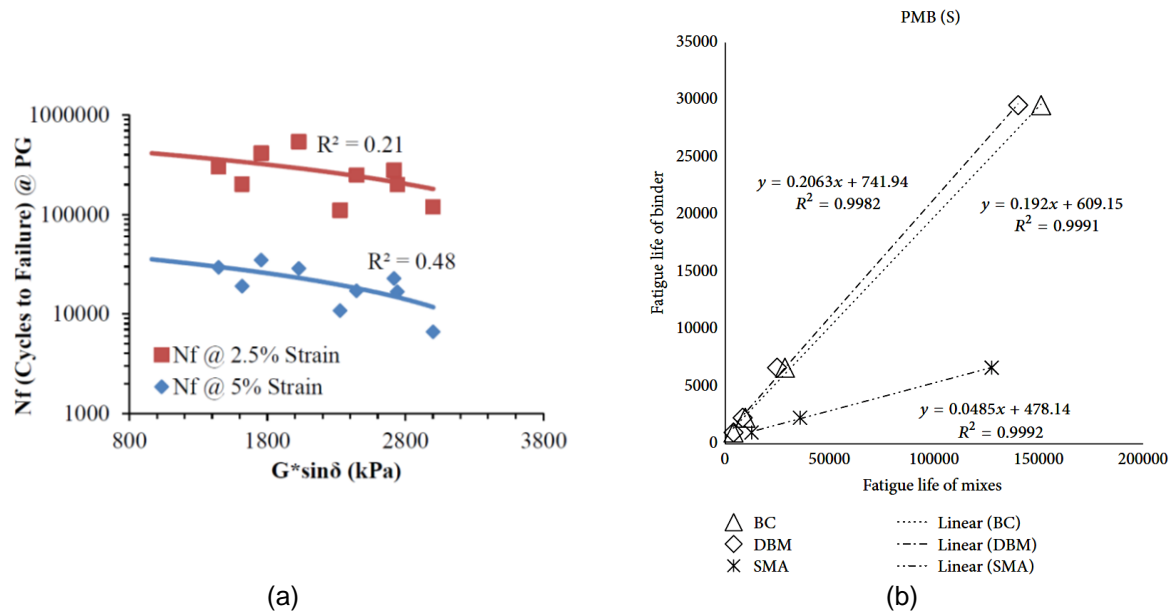
$$N_f = A(\gamma)^{-B} \quad (2.10)$$

Where: N_f is the number of cycles to failure;
 γ is the strain level considered;
 A and B are the coefficients previously calculated.

Hintz et al. (2011) compared results from 15 samples of asphalt binders to the performance of actual asphalt pavements structures constituted by the same materials. For the asphalt binders, the failure criterion was the number of cycles at failure using the LAS test calculation at 4% of strain amplitude. For the field mixtures, the failure criterion used was cracked area. The correlation between the results was considered to be good among most of the asphalt binders tested, except for a PG 64-28 binder ($R^2 = 0.64$). One should notice that 4% could be too high for the strain levels found in the binder. Other strain amplitudes could be simulated and compared to field cracking in order to validate the LAS test with better results.

Lyngdal (2015) tried to correlate the number of cycles to failure taken from the LAS test at two strain levels (2.5 and 5.0%) with values of $|G^*| \times \sin \delta$. The correlation was found to be very poor (Figure 2.4a). Other researchers have also tried to correlate the results from LAS test asphalt characterization to asphalt mixes tests results. Saboo and Kumar (2016) performed the 4PBBT in asphalt mixes using four different strain levels (400; 600; 800 and 1,000 $\mu\epsilon$), and LAS test using the strain levels of 2, 3, 4 and 5%, assuming that the strain in asphalt mixes are 50 times lower than the strain in asphalt binders. There were neat and modified binders and mixes among the materials tested, and the mixes had different gradations: asphalt concrete (BC), dense bituminous macadam (DBM) and SMA. The main conclusion was that the fatigue life (number of cycles to failure) can be linearly correlated between both scales. Figure 2.4b shows the results for the SBS polymer modified materials, named as PMB (S).

Figure 2.4 – Comparison between: (a) traditional Superpave parameter and LAS test results (Lyndgal, 2005) and (b) fatigue life of binder and fatigue life of mixes (Saboo and Kumar, 2016)



Many Brazilian researchers have been using the LAS test to evaluate different types of asphalt binders and to correlate the results to the fatigue cracking resistance of asphalt mixtures. Nuñez (2013) and Pamplona (2013) evaluated the fatigue resistance of modified binders using the crack growth rate concept from the LAS test, and concluded that the binder modification enhances the behavior of the materials studied. Camargo (2016) studied a field-blended rubber asphalt and compared the results obtained from the VECD model proposed after the LAS test to a neat and to a SBS-modified binder, and concluded that rubber asphalt had a better resistance to fatigue than the other ones evaluated. The LAS has been used for other asphalt materials. Coutinho (2012) tested FAM type of asphalt mixes in relation to fatigue characterization by means of the TST and the LAS test and found similar results in terms of fatigue lives for both types of tests.

Nuñez (2013) evaluated several types of asphalt binders (one neat binder and twelve modified binders) by means of LAS tests. The asphalt binders were submitted to short-term and long-term aging processes by the use of rolling thin film oven test (RTFOT) and pressure aging vessel (PAV), respectively. Using the VECD theory, the neat asphalt binder had the worst fatigue resistance behavior, while the EVA-modified asphalt binder had the best behavior. Another methodology to analyze the results obtained by the LAS test is to consider the resistance to fatigue cracking in

terms of fracture mechanics, by means of crack growth rate during the test (Nuñez, 2013). Normally a modified binder will also have better resistance considering this method.

2.3 MATERIALS AND METHODS

Three types of asphalt binders were tested in this section, by means of three different methodologies: Superpave traditional parameter, time sweep test (TST), and linear amplitude sweep (LAS) test. One neat 30/45 penetration grade binder was used for binder characterization and for other studies done in this dissertation, such as asphalt mixtures characterization and for the construction and monitoring of an experimental test site. Two modified binders were only tested in this section: one SBS-modified asphalt binder and one HiMA, with 2.5 and 7.0% of polymer, respectively. Table 2.1 presents the empirical properties of the three materials. It is important to state that the SBS-modified binder was originally classified as E 60/85 (elastomeric binder classified by the rate minimum softening point/minimum elastic recovery).

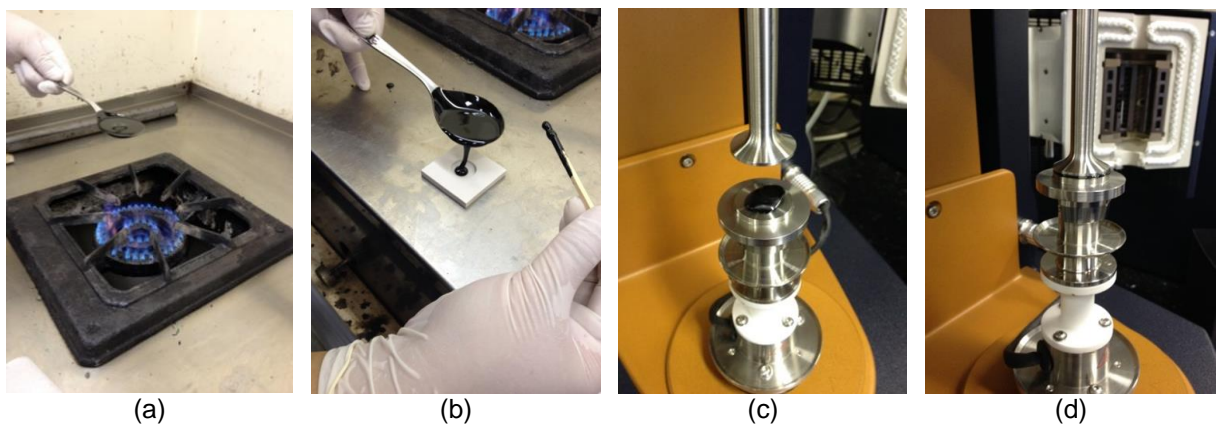
Table 2.1 – Empirical characterization of the asphalt binders

| Property | 30/45 | SBS | HiMA |
|-----------------------------|--------------|------------|-------------|
| Penetration (10^{-1} mm) | 31 | 54 | 45 |
| Softening point (°C) | 53.2 | 66.0 | 84.0 |
| Elastic recovery (%) | – | 87.5 | 96.0 |
| Flash point (°C) | 352 | > 235 | 308 |
| Specific gravity | 1.007 | 1.008 | 1.003 |
| Brookfield viscosity (cP): | | | |
| at 135°C | 468 | 1,989 | 2,170 |
| at 150°C | 226 | 805 | 997 |
| at 177°C | 78 | 227 | 309 |

The characteristics presented above meet with the required criteria provided by Brazilian standards for asphalt binders. As expected, the viscosity of the modified binders is higher than the viscosity of the neat binder. Comparing both modified materials, they have similar values of viscosity and elastic recovery, but the results of both parameters are approximately 10% higher for the HiMA in comparison with the SBS-modified binder.

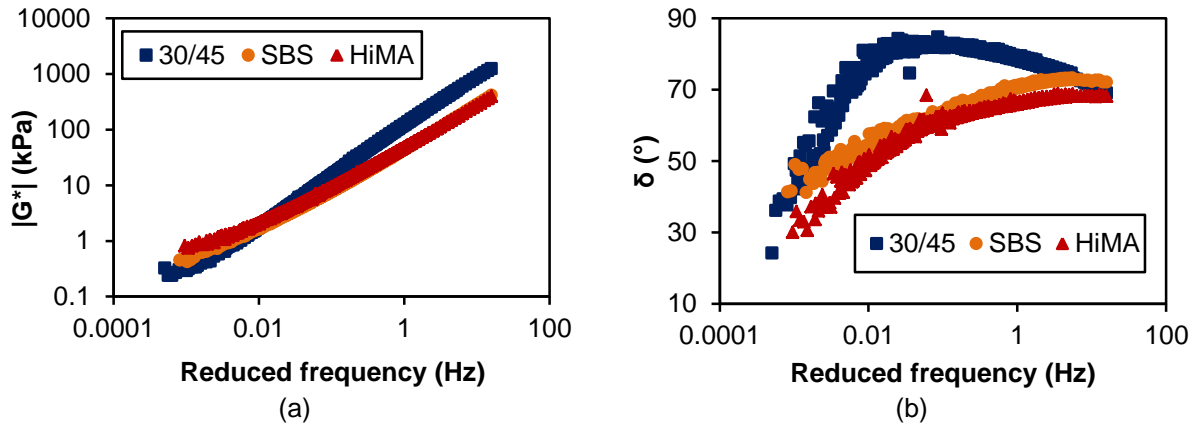
All the tests performed in the DSR followed the same sample preparation: first, the binder is heated until a minimum handling temperature (Figure 2.5a), then the fluid material is molded according to the specimen size required by each test (Figure 2.5b). The specimen is properly placed between the parallel plates (Figure 2.5c) and the final adjustments, such as gap corrections and trimming, are done (Figure 2.5d). The rheometer chamber is closed and the testing parameters are selected in order to begin the test.

Figure 2.5 – Asphalt binder sample preparation: (a) heating, (b) molding, (c) placing in the DSR, and (d) final adjustments



Before the characterization of the asphalt binders in relation to their fatigue cracking resistance performance, master curves for dynamic shear modulus ($|G^*|$) and phase angle (δ) were plotted, and are shown in Figure 2.6. The master curves were obtained after a frequency sweep (0.1 to 100rad/s) and a temperature sweep (10 to 76°C, with intervals of 6°C) at a small constant strain amplitude of 0.01% (to guarantee that the materials were tested on their LVE region). The 8mm- parallel plate geometry with a 2mm- gap testing was used for lower temperatures (from 10 to 40°C) and 25mm- parallel plate geometry with a 1mm- gap was used for higher temperatures (from 40 to 76°C). The master curves were all plotted for a reference temperature of 40°C.

Figure 2.6 – Master curves at 40°C for unaged binders: (a) dynamic shear modulus $|G^*|$ and (b) phase angle δ

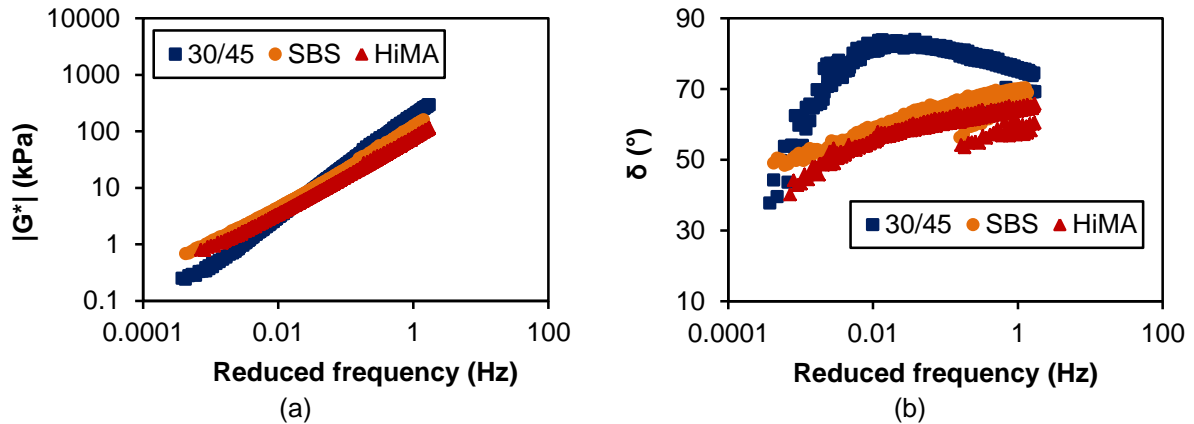


The master curves indicate that there are differences between the neat and the modified binders. At high frequencies (which is related to low temperatures), the neat binder has higher values of $|G^*|$, while at low frequencies (or high temperatures), $|G^*|$ values are lower for this binder type. The comparison between the modified binders is not conclusive, with both materials having similar behavior regarding their linear viscoelastic.

Regarding the elastic properties of the materials studied, the neat binder has higher values of phase angle at most of the temperatures analyzed, and the HiMA has the lowest values for this parameter. This indicates that the modified binders are more elastic than the neat binder, which is expected, since the polymers added to the binders tend to make them more flexible. The comparison between the SBS-modified binder and the HiMA indicates that the latter is more elastic (lower phase angle values) in the entire temperature/frequency spectrum, especially for the highest and the lowest temperatures.

After the characterization of their rheological properties, the three asphalt binders were submitted to a short-term aging process with the use of the RTFOT equipment, according to ASTM D 2872 (2012). The reference temperature for master curves purpose was also 40°C. Figure 2.7 presents the master curves for the short-term aged samples.

Figure 2.7 – Master curves at 40°C for aged binders: (a) dynamic shear modulus $|G^*|$ and (b) phase angle



The master curves for the aged materials present similar tendencies in comparison to the curves for the unaged binders, but the SBS-modified binder has higher values of $|G^*|$ if compared to the HiMA at high and low frequencies, which was not a clear tendency found for the unaged samples. The comparison between the aged and unaged master curves indicated that the SBS-modified binder was more affected by the aging processes than the other binders. The curve slopes were very similar for both unaged and aged materials, so $|G^*|$ values at 10rad/s were compared (Table 2.2).

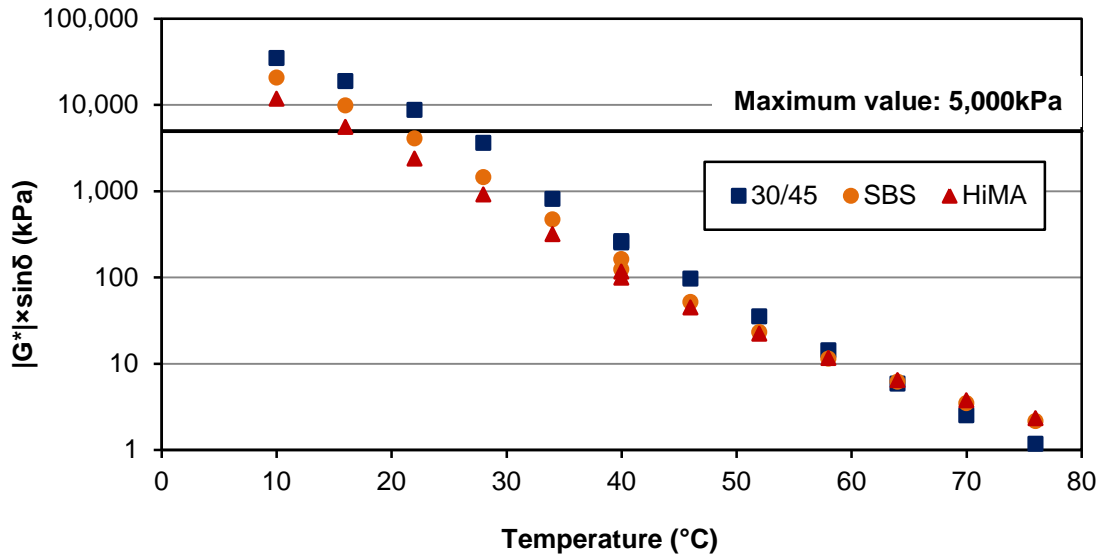
Table 2.2 – $|G^*|$ values of unaged and aged binders at the reference temperature

| Binder | $ G^* $ (kPa) | | Percent of increase |
|---------------------|---------------|-------|---------------------|
| | Unaged | Aged | |
| 30/45 neat binder | 186.5 | 274.8 | 47.3 |
| SBS-modified binder | 62.5 | 172.3 | 175.7 |
| HiMA | 68.2 | 106.4 | 56.0 |

2.4 RESULTS AND DISCUSSIONS

2.4.1 Superpave fatigue parameter

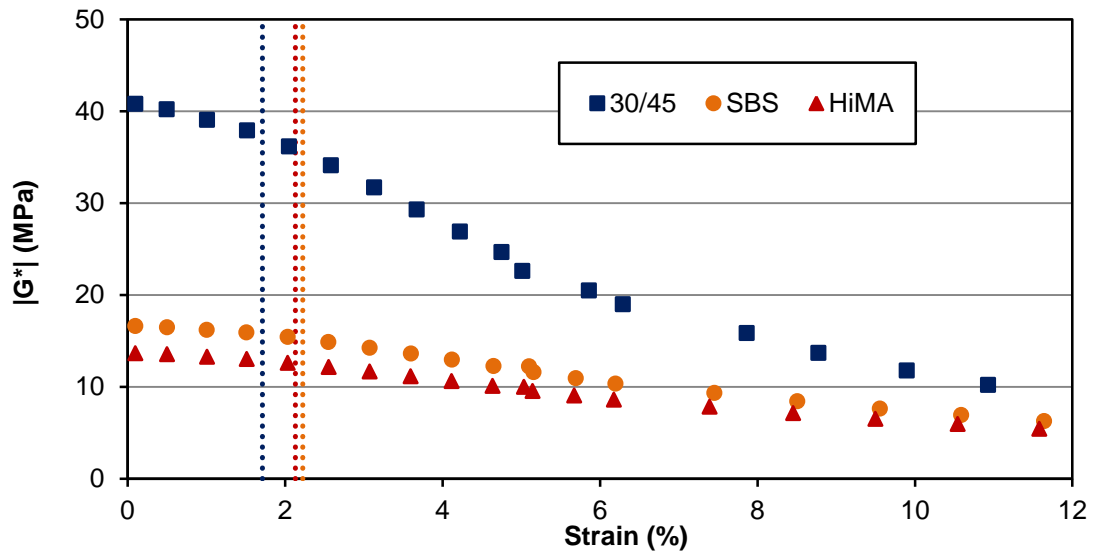
Different approaches and analyses were performed in order to characterize the fatigue life of the asphalt binders studied in this section of the dissertation. First, the Superpave parameter $|G^*| \times \sin \delta$ was obtained at the frequency of 10rad/s for RTFOT-aged specimens. Figure 2.8 presents the values of $|G^*| \times \sin \delta$ at the several testing temperatures; the limit value of 5,000kPa (for low traffic levels) was also plotted.

Figure 2.8 – Parameter $|G^*| \times \sin \delta$ at different temperatures

The results indicate that the three binders studied have similar behavior regarding the Superpave parameter for fatigue cracking characterization. According to the results, the modified binders would likely have a good resistance to this type of distress for 20°C or higher temperature levels, but the neat binder would only meet the Superpave criterion for temperatures higher than 25°C, which is still satisfying, considering that the fatigue cracking occurs at intermediate temperatures. According to the slopes for each curve, if the entire temperature range is considered, the neat binder is more susceptible to temperature changes and the HiMA has the least temperature susceptibility.

2.4.2 Time sweep test (TST)

Since many researchers started to conclude that the Superpave parameter was probably not able of capturing differences among neat and modified binders, other fatigue testing methods were performed in this study. First, strain sweep tests were performed (ASTM D 7175, 2008) in order to obtain the strain percentage in which each binder would go from the linear viscoelastic region to the non-linear/damage region. The test was conducted in RTFOT-aged specimens at 10Hz and the strain sweep was done from 0.1 to approximately 12%. The results are presented on Figure 2.9.

Figure 2.9 – $|G^*|$ values from strain sweep test

There are different methodologies to identify the LVE region of asphalt materials (Airey and Rahimzadeh, 2004). The present dissertation uses the American Society for Testing and Materials (ASTM) standard method, which considers 90% of the initial value of $|G^*|$ as the limit for the LVE region. Therefore, the values obtained for the neat binder, the SBS-modified binder, and for the HiMA were respectively: 1.7, 2.2, and 2.1%. In order to avoid any issues related to testing variability, these values were rounded up to 2.0, 2.5, and 2.5%, respectively.

The TST was performed at 10Hz at different strain levels for RTFOT-aged materials, which were chosen (2, 4 and 6% for the neat binder; and 6, 8 and 10% for the modified binders) based on the LVE region of each material, in order to guarantee damage-induced tests. The strain level of 6% was used for the three binders. Bahia et al. (2001) consider the frequency of 10Hz to be very high, but this value was selected in order to reduce the testing time and to correlate to results from the 4PBBT performed in asphalt mixes, which uses the same frequency level. Strain levels outside the linear viscoelastic zone were used to account for the damage behavior of the materials. Figure 2.10 shows the curves obtained. Table 2.3 presents the parameters for the fatigue law curves (Equation 2.10) for each material tested.

There is a lack of consensus about some parameters considered during the time sweep test. The initial value of $|G^*|$ is normally considered as the value obtained in

the first cycle of the test, but in every test performed in the present research, the value of $|G^*|$ required a few number of cycles to be stabilized before it would actually start decreasing. Therefore, in order to maintain a standard method for every sample tested, it was decided to consider the fifth cycle as the initial value of $|G^*|$. This choice was made based on the visual analysis of the evolution of $|G^*|$. At this specific cycle, most of the tests had already stabilized the values of $|G^*|$. Another issue that has not been well addressed in the literature is whether the initial value of $|G^*|$ should be considered from the first cycles of the TST test or from the LVE characterization.

Figure 2.10 – Fatigue behavior of the asphalt binders at time sweep test

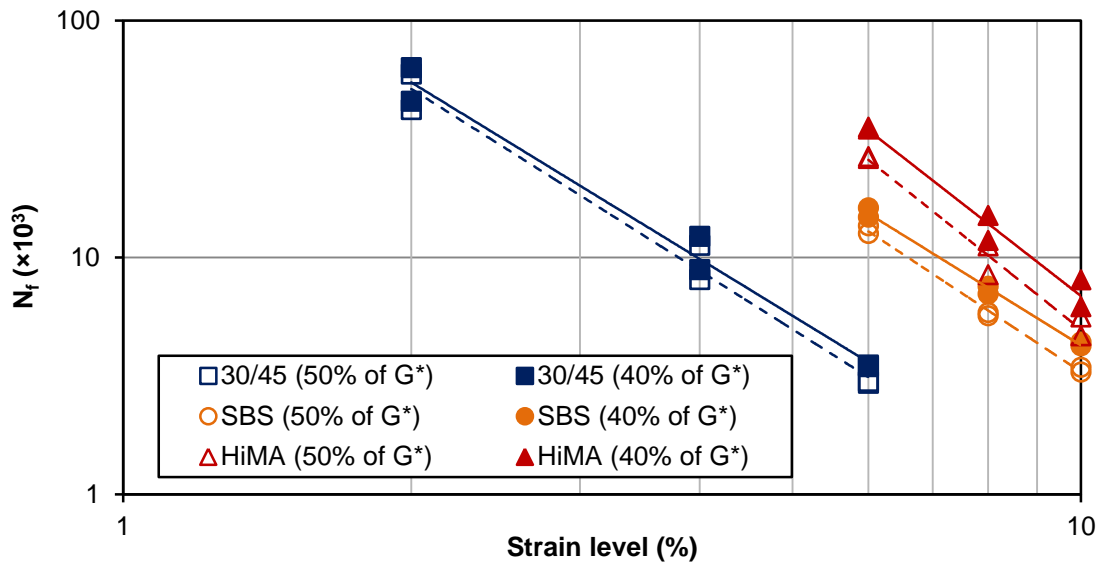


Table 2.3 – Parameters of the fatigue curves for the time sweep test

| Binder | 40% of $ G^* $ | | 50% of $ G^* $ | |
|---------------------|-------------------|------|-------------------|------|
| | A | B | A | B |
| 30/45 neat binder | 0.3×10^6 | 2.47 | 0.3×10^6 | 2.55 |
| SBS-modified binder | 1.4×10^6 | 2.51 | 1.5×10^6 | 2.67 |
| HiMA | 9.8×10^6 | 3.15 | 8.4×10^6 | 3.23 |

The parameters A and B provide tendencies on the fatigue cracking of asphalt binders, as higher values of A provide higher fatigue resistance. Regarding the values of B, the higher they are, the more susceptible to changes on strain levels, the materials are. This means that, for both criteria, the HiMA has the better fatigue cracking resistance (high values of A) and is the most susceptible to changes on

strain values. At low strain levels, this binder would provide a much higher resistance in comparison to the neat binder. Normally, binders with higher elasticity tend to have better fatigue resistance in strain-controlled tests. One thing that can be noticed by analyzing the results is that the number of cycles to failure does not change much when using any of the failure criteria proposed (40 or 50% of initial $|G^*|$ value). The HiMA seems to be more influenced by these different criteria in comparison to the other materials.

Also regarding the TST, some authors (Rowe and Bouldin, 2000; Safaei et al., 2014; Wang et al., 2015) state that the peak value of normalized $|G^*|$ (Equation 2.11) is a good representative of the failure point of an asphaltic material. According to Wang et al. (2016), this phenomenological failure parameter correlates well with cracking propagation initiation when considered in asphalt mixes characterization and has also been very promising for asphalt binders fatigue life. Figure 2.11a presents the evolution of values of normalized $|G^*|$ with the increasing number of cycles (for 6% of strain level), and Figure 2.11b provides a correlation between the number of cycles to failure considered in this approach and the number of cycles to failure obtained for the analysis that considers the reduction to 50% of $|G^*|$. The comparison between the two failure criteria indicates that they both provide similar number of cycles, since the results are very close to the equality line. It is important to state that the HiMA did not reach the peak value of normalized $|G^*|$, which clearly shows that the fatigue life of this material would be higher if this criterion was considered. This shows that the test should be carefully evaluated and finished after the peak of $|G^*|_{\text{norm}}$ is finally reached.

$$|G^*|_{\text{norm}} = N_i \times \frac{|G_i^*|}{|G_0^*|} \quad (2.11)$$

Where: $|G^*|_{\text{norm}}$ is the normalized shear stiffness;
 N is the number of cycles at cycle i ;
 $|G_i^*|$ is the value of $|G^*|$ at cycle i ;
 $|G_0^*|$ is the initial value of $|G^*|$.

Figure 2.11 – TST test results: (a) evolution of normalized $|G^*|$ and (b) comparison between $|G^*|_{\text{norm}}$ and 50% reduction

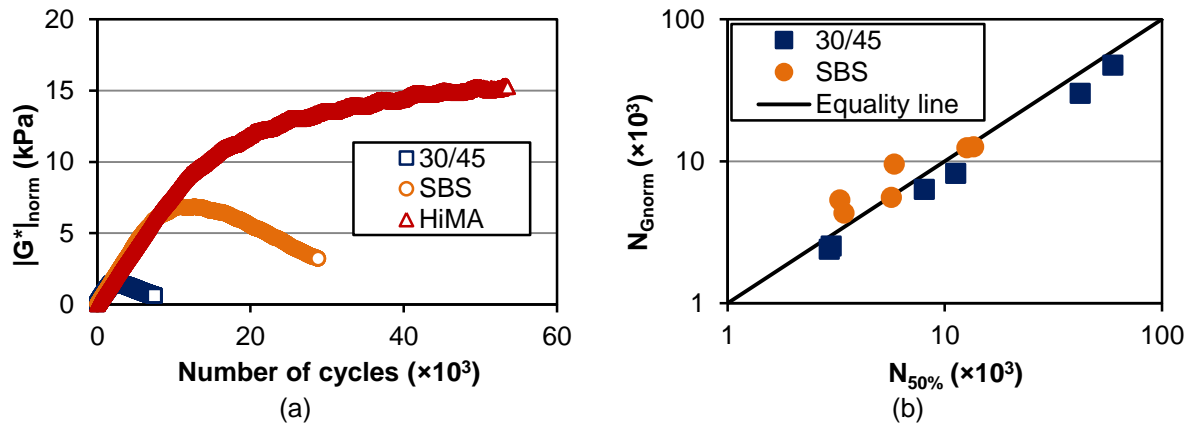
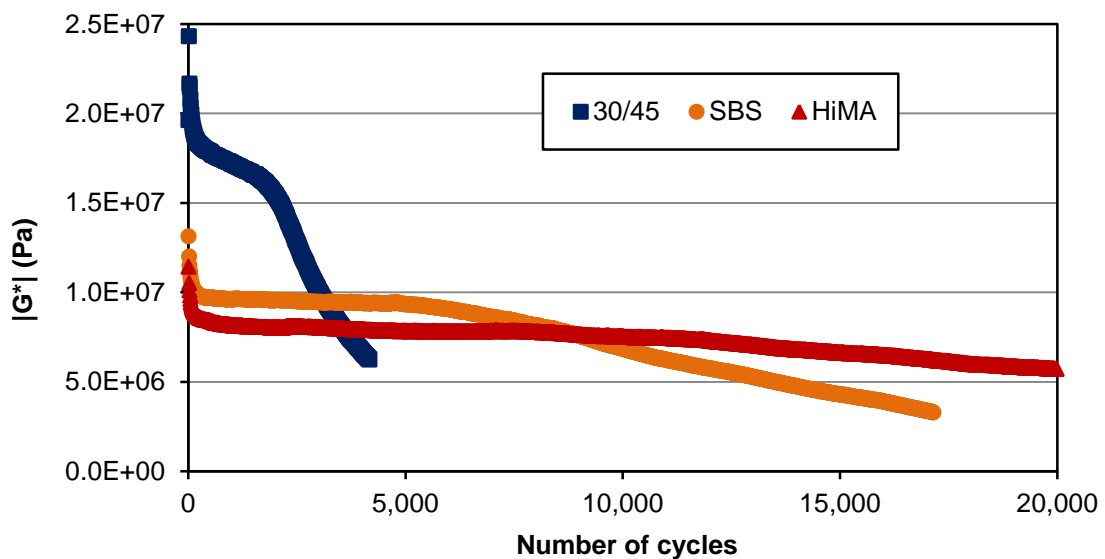


Figure 2.12 presents the evolution of $|G^*|$ during the TST. The strain level of 6% was chosen to represent the behavior of the three binders tested at the same conditions. The neat binder has the highest value of $|G^*|$ at the beginning of the test, but it decreases much faster than the values of $|G^*|$ for the modified binders, which is expected. The modified binders have similar $|G^*|$ values, and both decrease during the first cycles. Then, there is a plateau value of $|G^*|$ until it starts decreasing once again, around 6,000 cycles and 12,000 cycles, for the SBS-modified binder and the HiMA, respectively. This indicates that the HiMA has a better fatigue life in comparison to the other binders tested, by reaching the last portion of the fatigue behavior much after the other binders.

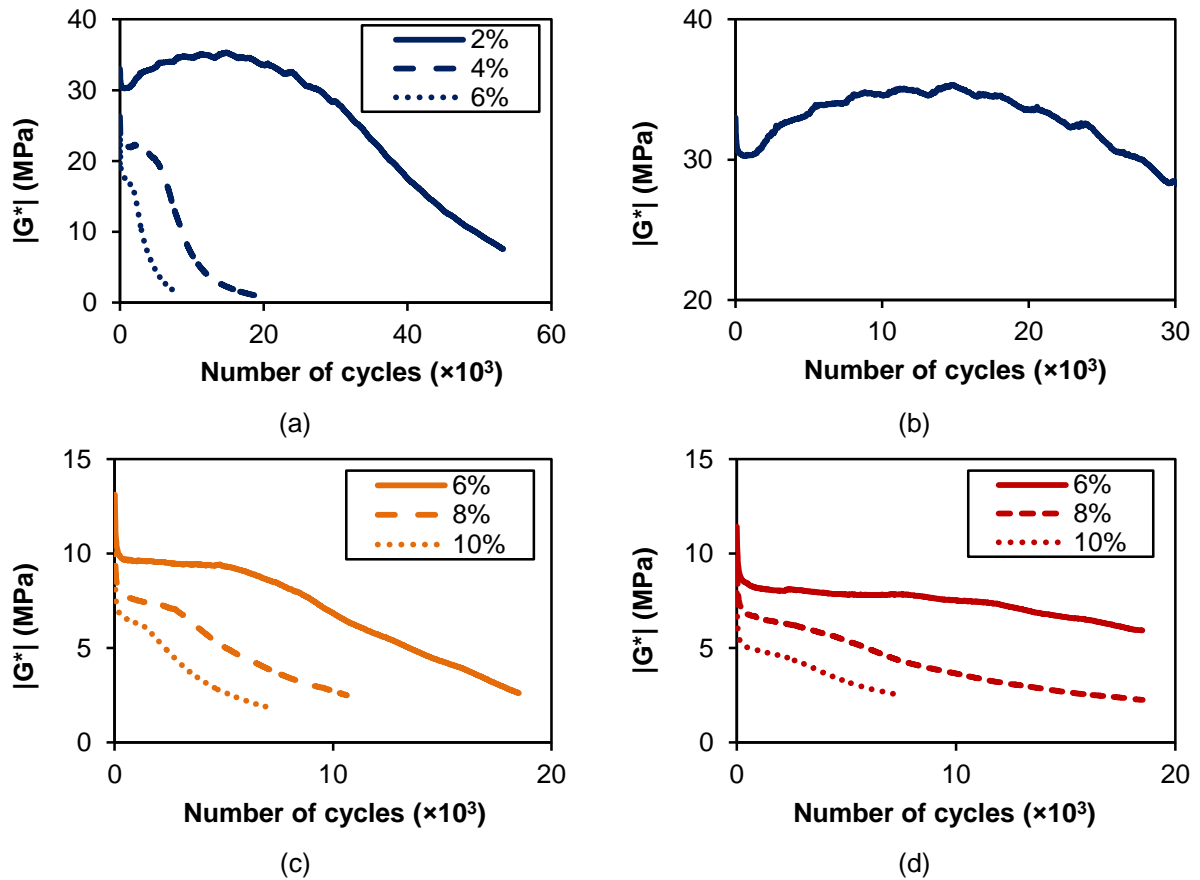
Figure 2.12 – Evolution of $|G^*|$ during the time sweep test (6% strain)



The comparison among the three binders showed that there is a tendency of the neat binder to have its $|G^*|$ value dropping more rapidly than the $|G^*|$ values of the modified binders, with the HiMA having the slowest drop among all. Gauthier, Le Hir and Plance (2004) consider that this approach might not represent the fatigue cracking of an asphalt binder well, because it indicates that the material fails during phase II of the fatigue cracking process, which is incorrect, since the failure point should be in the transition from phase II to phase III. Figure 2.13 shows the comparison among the three strain levels tested for each binder.

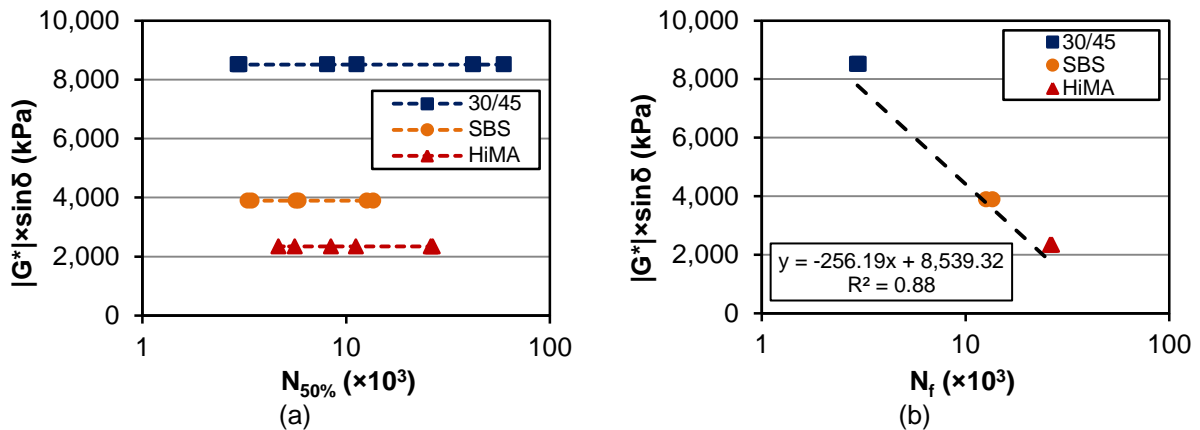
The neat binder had a different behavior in the evolution of its $|G^*|$ value during the time sweep test for 2% of strain (Figure 2.13a). In the first cycles, the value of $|G^*|$ tends to decrease but then starts to increase before dropping once again. This increasing phase corresponds to a phenomenon known as steric hardening, and is normally hard to be determined in higher strain levels (Gauthier, Le Hir and Plance, 2004). The steric hardening is an isothermal increase in binder's stiffness due to molecular rearrangements occurring during the test performed in more than one specimen (Figure 2.13b).

Figure 2.13 – Evolution of $|G^*|$ during TST: (a) neat binder, (b) steric hardening on neat binder (2%), (c) SBS and (d) HiMA



The comparison between the number of cycles to failure by means of the time sweep test and the parameter $|G^*| \times \sin \delta$ is presented on Figure 2.14a. It is clear that the fatigue life of the asphalt binders is dependent on the strain amplitude to which the materials are subjected. Figure 2.14b presents the correlation considering the same strain level (6%). The lower the fatigue life, the higher is the value of $|G^*| \times \sin \delta$, which is expected, since the Superpave specification limits a maximum value for the parameter. The neat binder should not be used in an asphalt pavement if the average temperature is 20°C, considering that the value of $|G^*| \times \sin \delta$ is higher than 5,000kPa.

Figure 2.14 – Superpave parameter versus TST results: (a) all the strain levels tested and (b) 6% strain



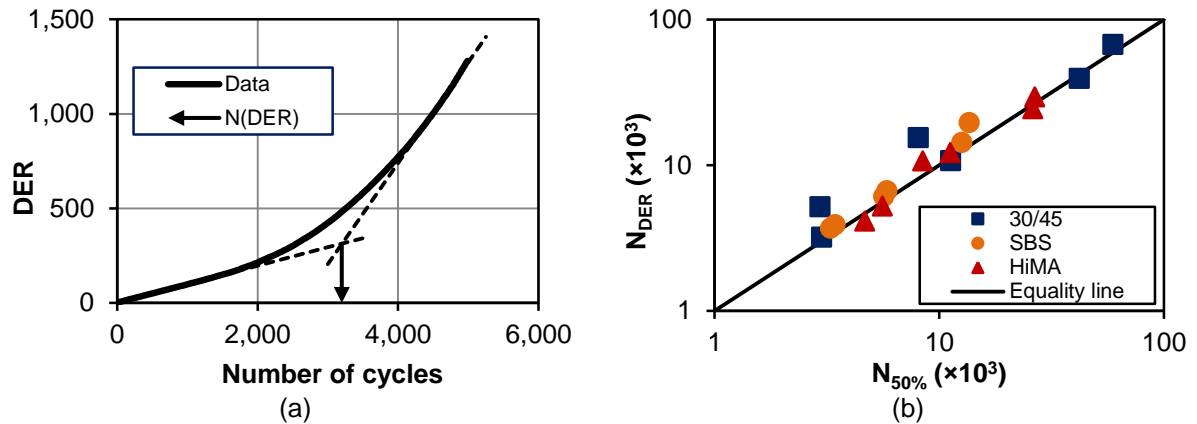
Some researchers have used the dissipated energy approach to characterize asphalt binders in relation to fatigue cracking. The concept of dissipated energy ratio (DER) was proposed by Ghuzlan and Carpenter (2000). This parameter is calculated through Equation 2.12. A typical plot of DER values versus number of cycles during the time sweep test is presented in Figure 2.15a. The initial part of the curve represents a linear increase on DER values and the second part is a transition to the second linear increase of DER. The intersection point between the two linear parts of the curve is considered to be the failure point of the sample (N_f). In the present research, the first linear part of the curve was set until 1,000 cycles, while the last linear portion of the curve was in the last 1,000 cycles of the test. Figure 2.15b presents the comparison between N_f values from two different approaches: considering 50% of decrease in $|G^*|$ values and the point where the DER evolution becomes nonlinear. It is possible to see that the values are close to the equality line, which means that both criteria might indicate similar fatigue resistance to the asphalt binders.

$$W_i = \pi \sigma_i \varepsilon_i \sin \varphi_i \quad (2.12)$$

Where:

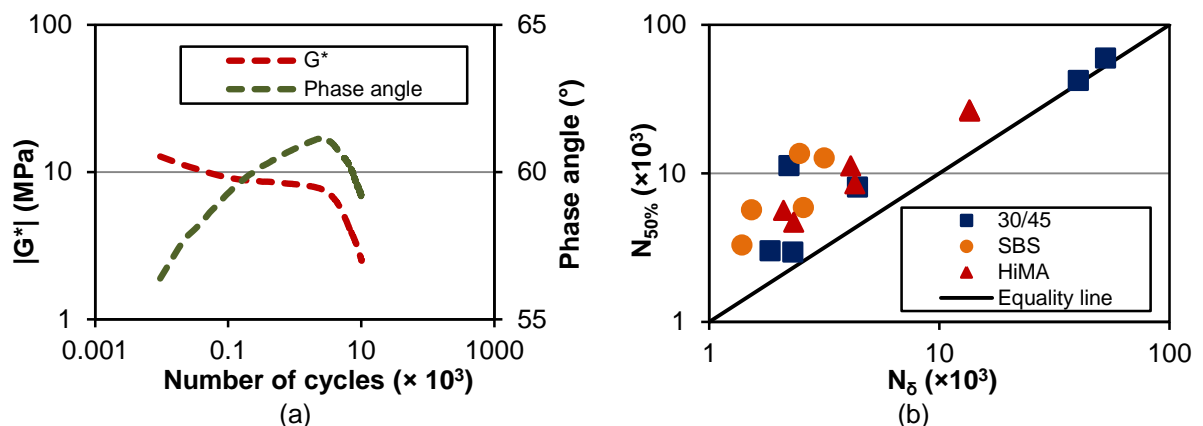
- W_i is the dissipated energy at load cycle i ;
- σ_i is the stress amplitude at load i ;
- ε_i is the strain amplitude i ;
- φ_i is the phase angle.

Figure 2.15 – DER values: (a) evolution during the time sweep test and (b) comparison with traditional fatigue life criterion



Another failure criterion proposed in the literature has been used especially for asphalt mixes: the peak of phase angle during the test. The main explanation for that is that the rapid decrease in the phase angle means that the material is not capable of resisting any additional loading. The peak phase angle point tends to coincide with the rapid decrease in the material's stiffness. Other researchers have used this same parameter for asphalt binder characterization. Figure 2.16a presents an example of phase angle evolution for the three binders tested, at 6% strain. Figure 2.16b presents a comparison between the fatigue obtained by means of the peak phase angle value and by means of stiffness reduction (50%).

Figure 2.16 – Peak phase angle results: (a) evolution of phase angle during the test and (b) comparison with traditional fatigue life criterion (50% stiffness reduction)



The results obtained from peak phase angle do not meet with the 50% decrease in initial stiffness, but in general meet with the rapid decrease on $|G^*|$ value, which means that 50% of the initial $|G^*|$ value is probably not the point where the sample

rapidly loses its strength. The fatigue life considering the 50% criterion was generally higher than the fatigue life that considers the peak phase angle, which means that this percentage of stiffness reduction might be too high for fatigue damage. Table 2.4 presents the percentage of $|G^*|$ that corresponds to the peak in phase angle value, for each binder and condition tested.

Table 2.4 – Percentage of $|G^*|$ at peak phase angle value

| Binder | % strain | Percentage of initial $ G^* $ |
|---------------------|----------|-------------------------------|
| 30/45 neat binder | 2 | 60% |
| | 4 | 90% |
| | 6 | 70% |
| SBS-modified binder | 6 | 85% |
| | 8 | 78% |
| | 10 | 77% |
| HiMA | 6 | 72% |
| | 8 | 73% |
| | 10 | 72% |

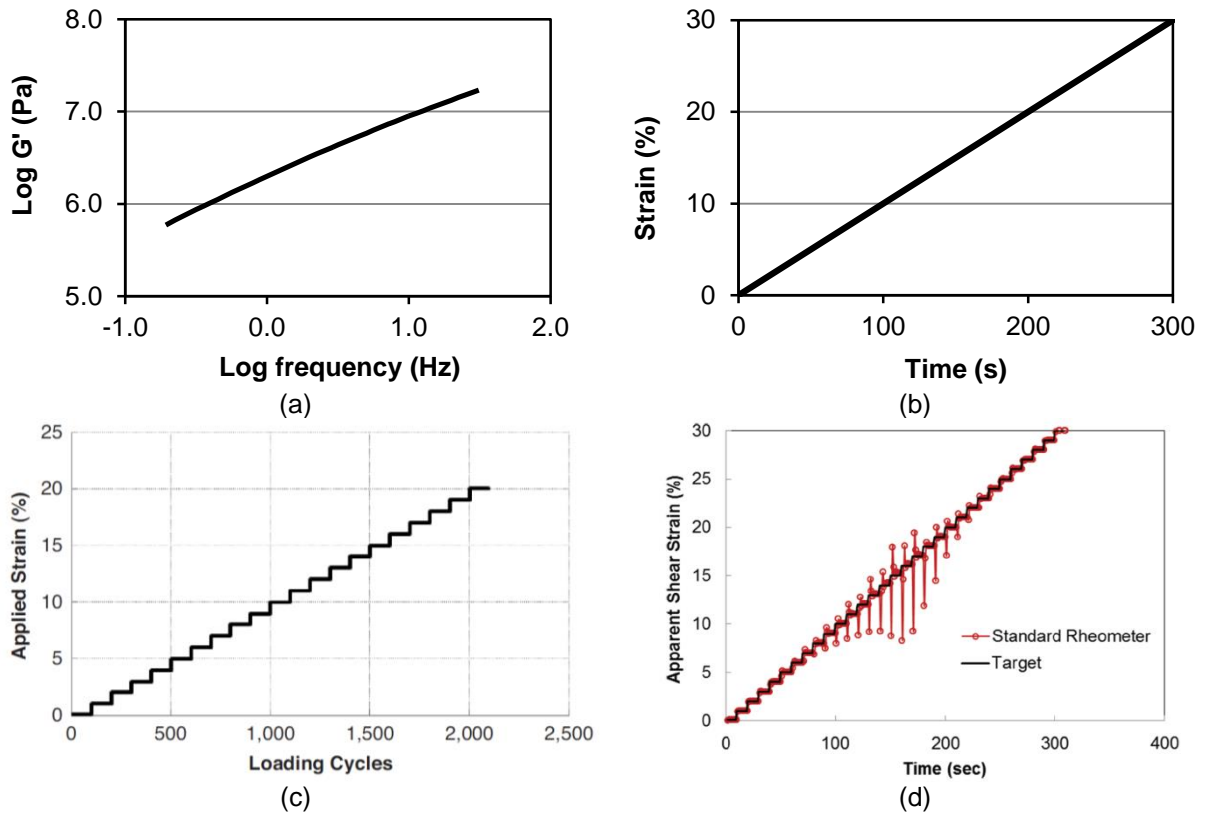
2.4.3 Linear amplitude sweep (LAS) test

The LAS test consists in two parts. The first part is a frequency sweep from 0.2 to 30Hz at strain amplitude of 0.1%. This procedure is done in order to obtain the LVE properties of the asphalt binder at its initial condition, without any damage. The parameter alpha (α), which is later used for amplitude sweep data analysis, is calculated as the reciprocal value of the straight line slope (m) of the log storage modulus (G') versus log frequency curve (Figure 2.17a). The second part of the test is the amplitude sweep, conducted at a frequency of 10Hz, with linear increments of strain amplitude from 0 to 30% (Figure 2.17b).

When the LAS test method was first introduced, the strain amplitude range went from 0 to 20%, but Hintz et al. (2011) concluded that some asphalt binders exhibit small damage levels under this condition, so they decided to extend the strain amplitudes up to 30%. Other modification was recommended by Hintz and Bahia (2013): instead of the original stepwise amplitude sweep (Figure 2.17c), these authors indicated that continuous amplitude sweep, using small increments in loading amplitude at every cycle, should be used. This would resolve issues on the use of some rheometers that

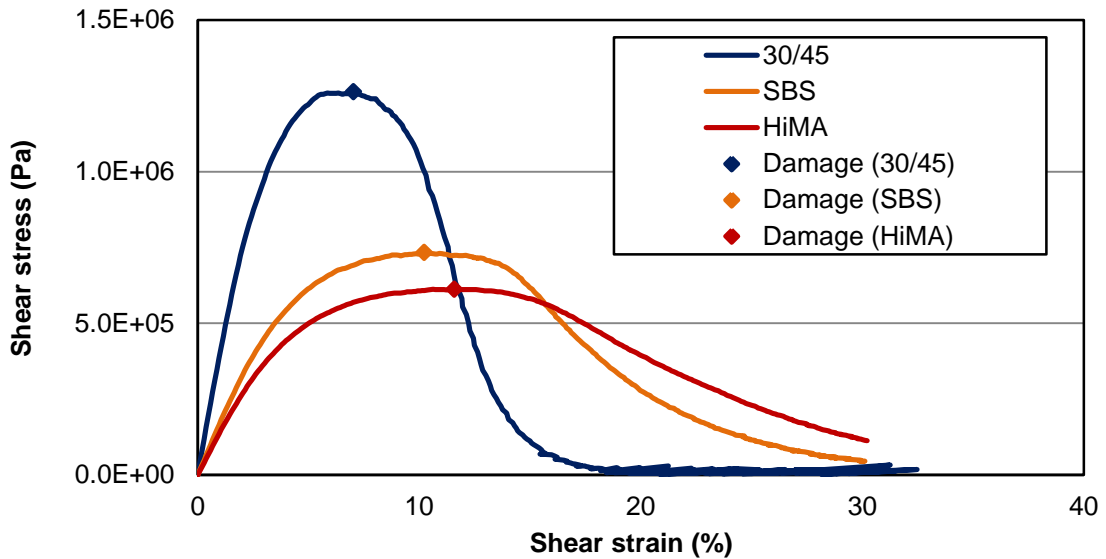
are not capable of increasing the strain amplitudes in abrupt steps (Figure 2.17d). Also, this new procedure eliminates crack tip formation on the specimens.

Figure 2.17 – LAS test procedure: (a) frequency sweep and (b) current ramp amplitude sweep; (c) old stepwise amplitude sweep (Hintz et al., 2011) and (d) output data found using the old procedure (Hintz and Bahia, 2013)



The LAS tests were performed in the present research at the temperature of 20°C. The analyses of the results were firstly based on the VECD method, considering the peak stress value is the failure criterion. Figure 2.18 presents the change in shear stress with amplitude sweep. The peak value is considered is the point in which the asphalt binder is more likely to fail.

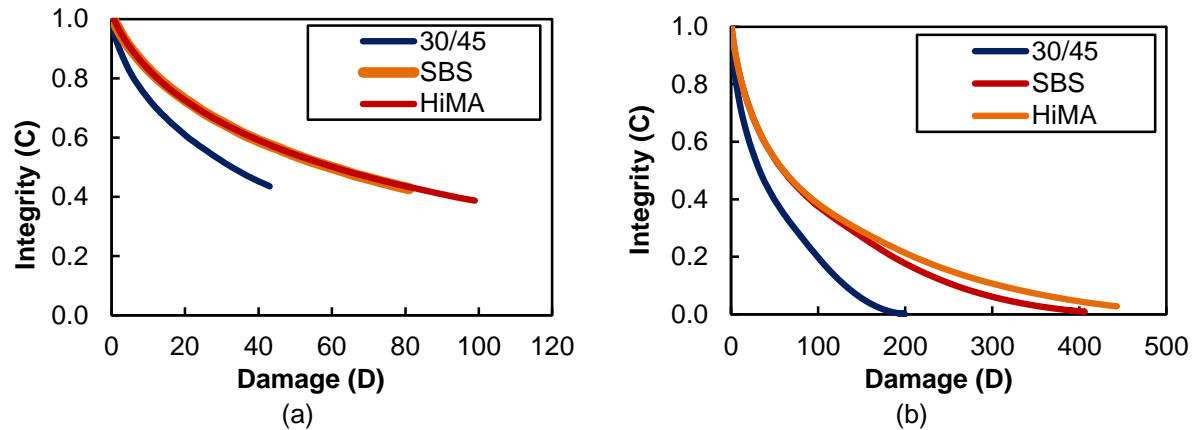
Figure 2.18 – Stress-strain curves after LAS test



The neat 30/45 penetration grade binder has a rapid increase in its shear stress in comparison to the modified binders, with a peak value of 1.26MPa at the strain of 7.0%. The modified binders have a slower increase of their shear stress value, with their peak occurring in a value that is around 50% less than the value obtained for the neat binder. The SBS-modified binder has a shear stress peak value of 0.73MPa at 10.2% of strain and the HiMA has a peak value of 0.61MPa at 11.6% of strain.

The LAS test provides the information needed to plot the damage characteristic curve: integrity (C) versus damage (D). These curves represent the decrease on the initial integrity of the materials as the damage increases. Figure 2.19a presents the curves for the three binders studied, until fatigue failure (peak shear stress). Note that the curves from the SBS-modified and the HiMA materials collapse, showing that they have similar behavior regarding damage evolution until the failure point. Figure 2.19b shows the entire C x S curves, which corresponds to the whole test from 0 to 30% strain amplitude. From these curves, it is possible to conclude that the HiMA has a better damage tolerance than the SBS-modified binder at the last portion of the test. The initial integrity considered here is the value of dynamic shear modulus ($|G^*|$).

Figure 2.19 – Damage characteristic curves the three binders tested: (a) until failure and (b) entire curves



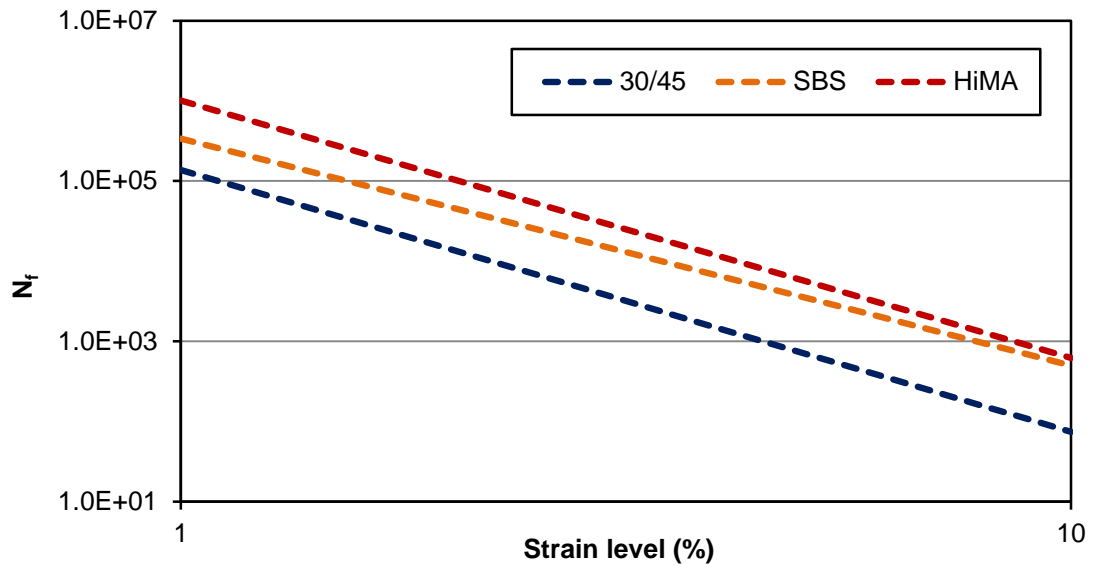
The integrity of the neat binder decreases faster than the integrity of the modified binders, which is expected. The modified binders have similar behavior, but when the integrity of both modified binders reach the value 0.4, the HiMA integrity starts decreasing in a lower rate if compared to the SBS-modified binder. Also, the HiMA does not seem to reach zero integrity at the end of the test (strain amplitude of 30%), while both neat and SBS-modified binder do, with the neat binder having zero integrity at the damage intensity of approximately 200, two times lower than the SBS-modified binder.

Table 2.5 presents the inputs for modeling the fatigue law for the three binders analyzed. The parameters presented here correspond to the strain levels in which each binder was tested at the time sweep tests. It is important to state that the higher the parameter A is, the better fatigue resistance the material will have. Figure 2.20 illustrates the fatigue curves.

Table 2.5 – Parameters of fatigue curves for LAS test

| Binder | A | B |
|---------------------|---------------------|-------|
| 30/45 neat binder | 1.366×10^5 | 3.264 |
| SBS-modified binder | 3.382×10^5 | 2.830 |
| HiMA | 1.007×10^6 | 3.210 |

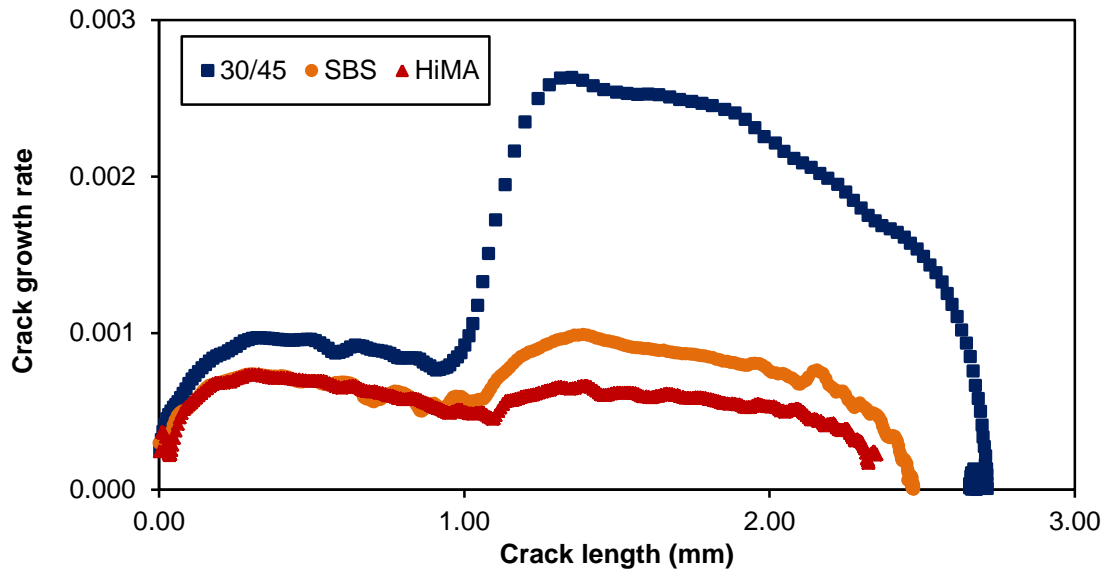
Figure 2.20 – Fatigue life curves obtained from LAS test



The fatigue curves presented indicate that the neat binder has a lower fatigue resistance if compared to the modified binders. The slopes are very similar for the neat binder and the HiMA, but the SBS-modified binder has a less pronounced slope, which indicates that the fatigue resistance of this material is more affected by the strain levels it would be subjected to. The HiMA is the most resistant among the three binders analyzed, providing twice the number of cycles to failure if compared to the SBS-modified binder.

The other method used to characterize the fatigue resistance of asphalt binders by means of LAS tests is the crack growth during the test. Figure 2.21 plots crack length versus crack length grow rate. Normally, the failure crack length (a_f) is considered at the minimum value of crack growth rate, in which the micro-cracks coalesce. This occurs right before the fatigue resistance starts to rapidly decrease, i.e., when the materials starts to fail. This means that the higher the value of a_f , the more resistance to fatigue cracking the asphalt binder will be.

Figure 2.21 – Crack growth rate evolution from LAS test

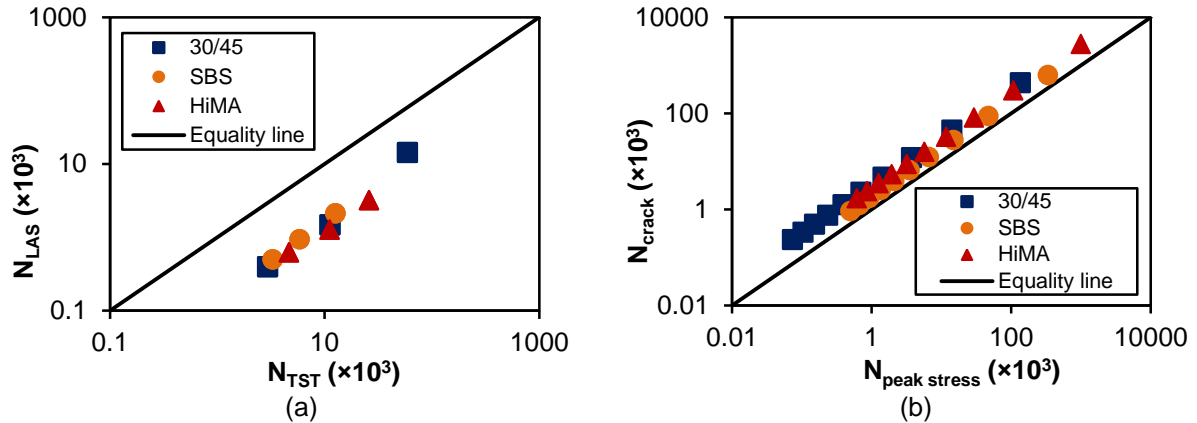


Due to scale issues, it is not very clear seeing through the graphs, where the a_f point is, for each of the binders tested. Observing the values of crack length and crack growth rate, the lowest point between the two peaks of crack growth rate corresponds to: 0.91mm, 0.93mm, and 1.09mm, for the neat binder, the SBS-modified binder, and the HiMA, respectively. Martins (2014) found similar results for the neat binder, but higher crack length values for the HiMA. These values indicate that the HiMA has the best fatigue resistance among the binders tested, while the neat binder has the lowest resistance. One can observe that there is a lot of noise in the data presented for crack length growth. This noise made it difficult to obtain the exact value of a_f , so it is possible to conclude that this criterion might not be suitable for the materials evaluated in this dissertation. Other researchers have also found difficulties on finding the minimum value of crack growth rate, especially for modified binders (Nuñez, 2013). Further investigation on this parameter needs to be done.

Figure 2.22a presents the comparison between the fatigue life from the VECD analysis (LAS test) and the fatigue life from the TST (50% reduction on the $|G^*|$ value). Figure 2.22b shows the correlation between the two models provided by the LAS test: one obtained from the peak stress analysis and the other one obtained from the fracture mechanics analysis. Ten strain levels were considered for both models (from 1 to 10%, with 1% increment). It is possible to conclude that the crack growth model is not capable of providing clear differences between the asphalt

binders studied, and that it overestimates the fatigue resistance of the materials in comparison to the peak stress analysis.

Figure 2.22 – Comparison between LAS test approaches: (a) crack growth rate and (b) peak stress



2.5 SUMMARY AND FINDINGS

The present chapter of this dissertation evaluated three different asphalt binders (a neat 30/45 penetration grade binder, a SBS-modified binder, and a highly modified binder – also known as HiMA) in relation to their fatigue resistance by means of different methods and approaches. The original Superpave parameter $|G^*| \times \sin \delta$ was firstly introduced, and then time sweep and LAS tests were performed. Strain levels of 2, 4, and 6% were selected for the neat binder, while strain levels of 6, 8 and 10% were used for the modified binders. The different approaches considered in this research were the conventional fatigue criteria (40 and 50% of reduction on the initial value of $|G^*|$), the dissipated energy concept approach, fracture mechanics concepts and the VECD methodology. The main findings in this chapter are:

- The modified asphalt binders resulted in higher fatigue lives in comparison to the neat material, and the HiMA provided the best resistance;
- The parameter $|G^*| \times \sin \delta$ has a good correlation with TST results;
- The two approaches used to analyze the TST data (dissipated energy and 50% reduction in the initial value of stiffness) resulted in similar values of fatigue life (N_f);
- The results from the VECD analysis performed for the LAS test were, in general, five times lower than the traditional method of the TST.

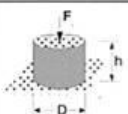
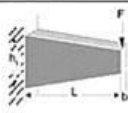
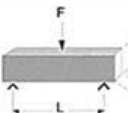
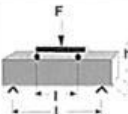
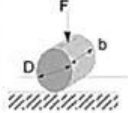
3 DIFFERENT PROCEDURES TO EVALUATE FATIGUE CRACKING RESISTANCE OF ASPHALT MIXES

3.1 INTRODUCTION AND BACKGROUND

Laboratory tests used to characterize fatigue resistance of asphalt mixes can be divided into different methods, depending on the loading characteristics, the failure criteria, and the specimen geometry. Nuñez (2013) listed some of these tests currently in use worldwide: simple flexure, supported flexure, direct axial, diametral (also known as ITT), triaxial, and also wheel-track testing.

Di Benedetto et al. (2004) organized an interlaboratorial study that included several European countries with the main objective of analyzing the fatigue resistance characteristics of asphalt mixes using eleven different test methods. A total of 150 laboratory tests were performed, which included stress- and strain-controlled methods, with different characteristics of the loading application and specimens' geometry (Figure 3.1). The tests results based on the classic approach of fatigue cracking evaluation (number of cycles until 50% of stiffness is reached, for example) were much influenced by the loading mode. The ones based on the continuum damage theory were capable of isolating the intrinsic characteristics of fatigue cracking resistance from the influence of the test methods. In terms of asphalt mixes, the literature review presented in this dissertation focuses on laboratory tests related to ITT, flexure bending (4PBBT) and tension-compression, because these are the test methods to be used throughout the research.

Figure 3.1 – Characteristics of the laboratory tests studied by Di Benedetto et al. (2004)

| Type | Test Geometry | Type of loading/ Country of the team | Amplitude (10^{-6} m/m or MPa) |
|------|--|--|---|
| T/C |  | Tension- Compression "Homogeneous" F_1, S_1 | Strain: (80), 100,140, 180 Stress: 0.9 |
| 2PB |  | Two-Point Bending "Non Homogeneous" F_2, B_1, B_2 | Displacement; max strain: 140, 180, 220 Load; max stress: 1.4 |
| 3PB |  | Three-Point Bending "Non Homogeneous" N_1 | Displacement; max strain: 140, 180, 220 Load; max stress: 1.4 |
| 4PB |  | Four-Point Bending "Non Homogeneous" N_2, P, PL, UK | Displacement; max strain: 140, 180, 220 Load; max stress: 1.4 |
| ITT |  | Indirect Tensile Test "Non Homogeneous" S_2 | Load; max strain: at first cycle: ~25, ~40, ~65 |

Among the several factors that influence the fatigue life characterization of asphalt mixes, temperature and loading frequency are two very important variables to be considered. Most researchers indicate that fatigue tests should be performed at 20°C and 10Hz, but several studies have suggested other conditions. In terms of testing frequency, there have been only a few authors that tried to correlate the vehicles speed to stress/strain loading time, which consequently relates to the frequency of passing vehicles on the pavement structure. Al-Qadi, Xie and Elseifi (2008) commented on earlier attempts to address the stress pulses in asphalt pavements: Barksdale (1971) and Brown (1973). Barksdale (1971) used fine element modeling and the elastic theory to calculate stress pulse widths as a function of vehicles speed and pavement depth. Due to viscous effects and inertia forces observed in the AASHTO road test, this author reported that the loading times were not inversely proportional to the vehicle speed. This author developed a chart that correlated depth, speed and loading time. Later, Brown (1974) developed an equation that relates the loading time to vehicle speed and pavement depth (Equation 3.1).

$$\log(t) = 0.5d + 0.2 - 0.94 \log(V) \quad (3.1)$$

Where: t is the loading time;
 d is the depth (m);
 V is the vehicle speed (km/h).

In Brazil, Medina and Motta (1995) also correlated vehicles speed and depth to loading times. Their investigation resulted in slightly higher values of times and the same tendency observed by Barksdale (1971), since the increasing speed led to lower time values and the increasing depth led to higher values.

In terms of temperature, the USA FHWA has implemented the direct tension test for fatigue characterization at such temperature that it is not too hot for the binder to exhibit viscous and plastic effects (FHWA, 2016). Equation 3.2 is considered to obtain the testing temperature, and the maximum value should be higher than 21°C. In France, fatigue cracking resistance is normally characterized at 10°C, and the results are corrected to 15°C for pavement designs in metropolitan areas (Corté and Goux, 1996).

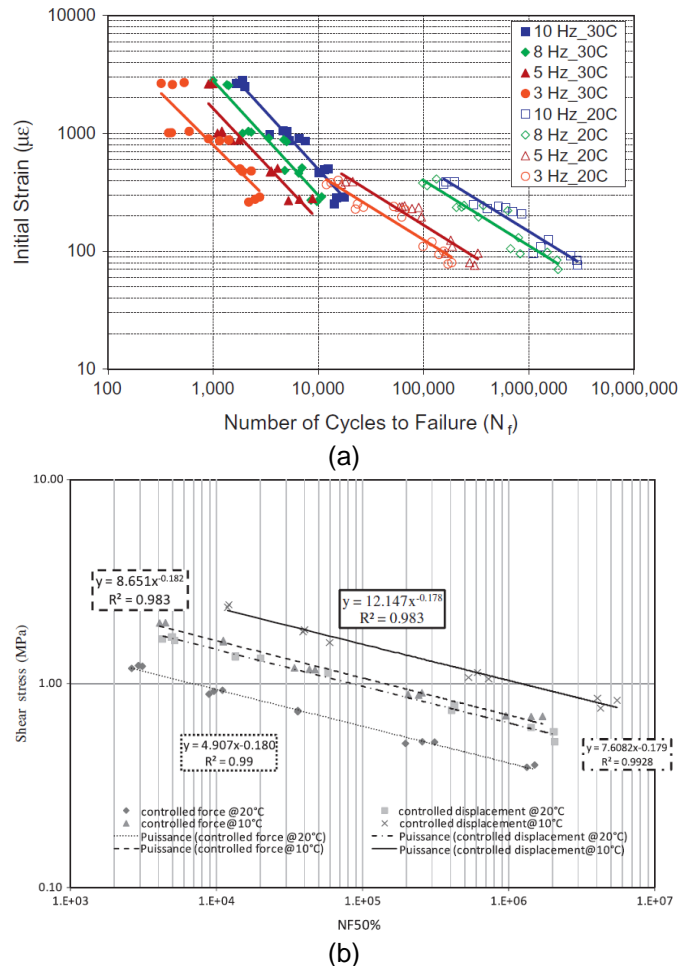
$$T = \frac{(HTPG + LTPG)}{2} - 3 \quad (3.2)$$

Where: T is the testing temperature (°C);
 HTPG is the high temperature performance grade;
 LTPG is low temperature performance grade.

Al Khateeb and Ghuzlan (2014) studied the influence of different values of loading frequency (3, 5, 8 and 10Hz) and temperature (20 and 30°C) on the fatigue life of asphalt mixes. The stress-controlled mode ITT was performed, and some of the results included: the fatigue life decreased in more than 90% when the temperature increased from 20 to 30°C, and the fatigue lives were higher for high loading frequencies (Figure 3.2a). Boudabbous et al. (2013) compared two modes of load for fatigue characterization (stress- and strain-controlled tests) using 50% decrease in E* value as the failure criterion and concluded that there are major differences on the

fatigue lives, although the fatigue curves slopes are similar for both modes (Figure 3.2b).

Figure 3.2 – Testing conditions influencing fatigue life: (a) different frequencies and temperatures (Al-Khateeb and Ghuzlan, 2014) and (b) stress- or strain-controlled modes (Boudabbous et al., 2013)



Other studies have compared the fatigue life of asphalt mixes in different temperatures. Bodin et al. (2010) characterized the fatigue resistance of different materials by means of strain-controlled trapezoidal beam tests in the range of 0 to 30°C and concluded that there is not a linear correlation between fatigue life and temperature, as lower and higher temperatures provided better fatigue resistance and medium temperatures provided low resistance. Bhattacharjee and Malick (2012) instrumented asphalt mixes slabs and submitted them to a wheel load simulator under controlled temperature. During the tests, they measured the transverse and longitudinal strains and used them in a fatigue cracking model. The results indicated that lower temperatures provide better resistance, especially at higher strain levels. Asadi, Leek and Nikraz (2013) performed the four point beam bending test and

concluded that higher temperatures lead to better fatigue resistance. Also, these authors indicated that both Shell and Asphalt Institute models are more compatible to the results obtained for the specimens tested at 40°C.

Nejad, Aflaki and Mohammadi (2010) tested SMA and HMA samples, analyzed the results by means of the traditional approach (number of cycles to complete failure) and concluded that the HMA provides higher resistance to fatigue cracking, which is explained by the dense gradation and lower air voids content. Other findings by those authors include: the decrease of the stiffness modulus with increasing temperature; and better resistance to fatigue cracking with finer aggregate gradation, even with similar asphalt binder content.

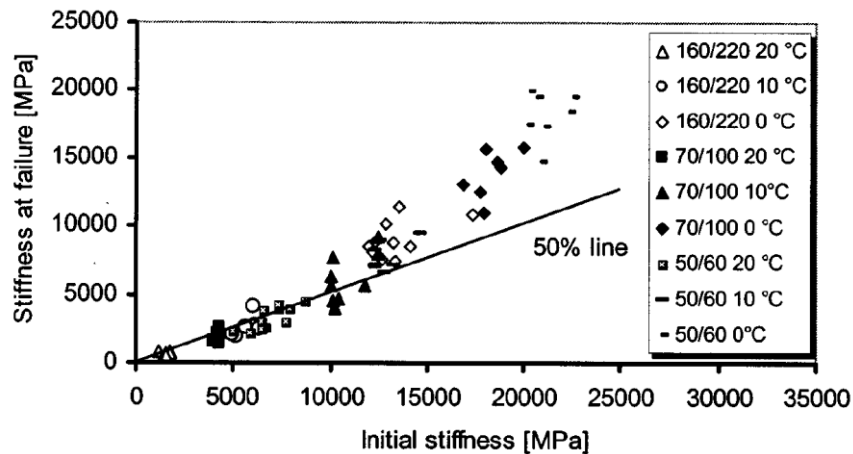
3.2 FATIGUE CHARACTERIZATION OF ASPHALT MIXES

In general, laboratory tests are done according to either one of these two types of loading application: stress-controlled and strain-controlled (Porter and Kennedy, 1975). The stress-controlled test consists on applying a vertical controlled stress, which subjects the specimens to increasing deformation (Preussler, 1983). The stress-controlled type of tests used to be recommended for thick asphalt pavements, in which the asphalt surface layer provides higher bearing capacity (Huang, 2003). The strain-controlled test consists in applying cyclic loading at a constant strain level, which decreases the stress level. The specimen's stiffness decreases throughout the test, until it reaches a pre-established value (Pinto, 1991. Medina and Motta, 2015). Some authors considered that the strain-controlled should be performed for thin thick asphalt layers (less than 50mm), due to the support provided by the inferior layers, which is supposedly not affected by the surface layer stiffness (Huang, 1993; Medina and Motta, 2015).

Lately, changes in the structural design of asphalt pavement structures and complex traffic loading distribution has made it more difficult to identify the fatigue damage mechanisms occurring the asphalt surface layers under both modes (Shan et al., 2016). Many researchers have tried to unify the results from both stress-controlled and strain-controlled tests, and energy concepts approaches have been mainly considered.

The initial stiffness values have also been considered as a major effect on the fatigue characterization of asphalt mixes in laboratory. Lundstrom et al. (2004) compared the initial stiffness asphalt mixes constituted by different binders classified as penetration grade (AC 50/60, AC 70/100, and AC 160/220) to the stiffness observed at the failure point, by means of the tension-compression test. Failure was considered to occur at the point of rapid decrease in the stiffness value. Figure 3.3 presents the results found for three temperatures (0, 10, and 20°C). The conclusion was that the classical fatigue failure criterion (50% reduction on the initial value of E^*) did not correspond to the actual failure for high initial stiffness (low temperature or high binder consistency).

Figure 3.3 – Stiffness at failure versus initial stiffness in controlled-strain tests (Lundstrom et al., 2004)



On the other hand, Harvey and Tsai (1996) made some remarks regarding the influence of stiffness on the fatigue life of asphalt mixes, as their results indicated that higher initial stiffness and higher fatigue life occurred when the voids content was low. This relationship is the opposite of what is normally expected, since stiffer materials tend to have lower fatigue life in strain-controlled testing. These authors suggested that the stiffness value of the asphalt mixes should not be considered in fatigue cracking models; instead, the mix variables should be included.

In terms of stress-controlled tests, Mashaan et al. (2014) performed ITT tests in SMA mixes with different contents of crumb rubber (from 0 to 12%). The increasing content increased the material's stiffness and led to higher fatigue lives at different stress amplitudes (200, 300, and 400kPa).

3.2.1 Indirect tensile test

In Brazil, the most common fatigue test used to characterize asphalt mixes is performed by means of diametral compression, which is known as the ITT. The test provides indirect tensile loading applications to the specimen (Figure 3.4) at a stress level of 10 to 50% of the material's indirect tensile strength (ITS) value and it is performed at a frequency of 1Hz with 0.1s of sinusoidal load application and 0.9s of rest period before the next loading application. The test finishes when the specimen reaches complete failure (total rupture of the specimen) due to an increase on the strain level (for stress-controlled test), or when the specimen's stiffness decreases to a pre-established percentage of its initial stiffness (for strain-controlled test). Equations 3.3, 3.4 and 3.5 present the fatigue laws that can be obtained at the end of the test.

$$N_f = k_1 \left(\frac{1}{\sigma_t} \right)^{n_1} \quad (3.3)$$

$$N_f = k_2 \left(\frac{1}{\Delta\sigma} \right)^{n_2} \quad (3.4)$$

$$N_f = k_3 \left(\frac{1}{\varepsilon_t} \right)^{n_3} \quad (3.5)$$

Where: N_f is the number of load cycles until total rupture of the specimen;
 σ_t is the tensile stress applied to the specimen;
 $\Delta\sigma$ is the difference between the horizontal and the vertical stresses at the middle of the specimen;
 ε_t is the tensile strain measured at the middle of the specimen;
 k_i and n_i are the coefficients obtained for the linear regression taken from the N versus σ_t or N versus $\Delta\sigma$ or N versus ε_t curves, in logarithmic scales.

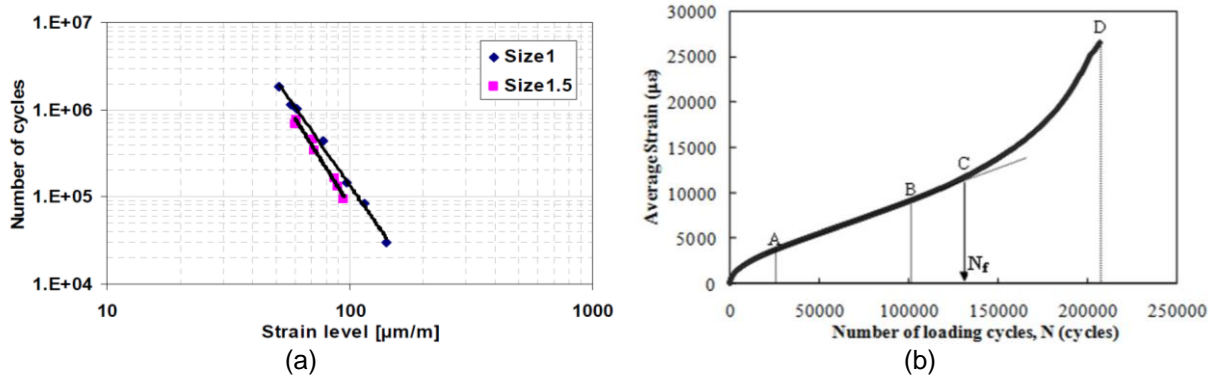
Figure 3.4 – Indirect tensile test: (a) stresses during the test and (b) equipment commonly used



The ITT has the advantage of being very simple and easy to be performed, in terms of testing execution as well as in terms of laboratory sample production. Besides that, field cylindrical samples can also be tested. The main disadvantages of this test are, among others: the possibility of having cumulative permanent deformation during the test, depending on the testing temperature and the stress state. This might underestimate the fatigue life of the material tested (Colpo, 2014).

Despite the well-known issues and concerns related to the use of the ITT, this test method is still performed in many agencies and research laboratories, especially in Brazil. Some of the variables related to this test are the mode of loading and the specimen size. Li (2013) performed the ITT in specimens with standard diameter size (100mm) and in specimens with 150mm-diameter size (Figure 3.5a). The major objective was to compare different specimen sizes and to obtain the relationship between the results obtained from each size. The results were similar for both sizes in terms of fatigue curve slopes and number of cycles to failure. Nguyen et al. (2013) used two different failure criteria to characterize four types of asphalt mixes in relation to ITT: (i) vertical deformation of 9.0mm, and (ii) average strain, or the value in which the strain during the test increases rapidly and becomes nonlinear (point C in Figure 3.5b). They concluded that the average strain criterion presented a better correlation between stress amplitude and fatigue life than the 9.0mm vertical deformation at 20°C.

Figure 3.5 – Indirect tensile test: (a) influence of specimen size (Li, 2013) and failure criterion by Nguyen et al. (2013)

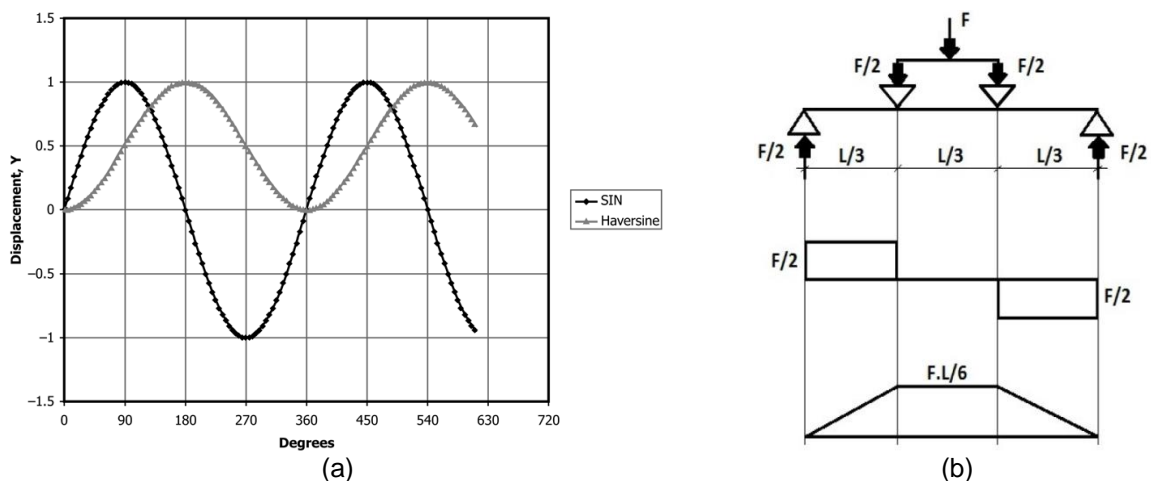


In the past few years, several researchers have developed and improved tests for fatigue life characterization. Different specimen configurations (geometry sizes and formats), forms of load application, and analysis methods, have been tested with the main objective of improving the acquisition of the fundamental material properties of the asphalt mixes tested. Some of these tests are presented next.

3.2.2 Four point beam bending test

The four point beam bending test (4PBBT) uses a two-point supported specimen with the loading application points and consists in applying a cyclic haversine displacement (Figure 3.6a) in the central area of asphalt mixes compacted beams (Figure 3.6b). This configuration provides maximum constant bending moment and zero shear in the center third of the specimen. This ensures the appearance of cracks under a pure flexural state during the test.

Figure 3.6 – Four point beam bending test: (a) loading pulse (ASTM D 7460, 2010) and (b) shear force and bending moment diagrams during the test



Fontes (2009) listed the main advantages of performing flexural tests: normally, these tests are easy to be analyzed; the results can be directly used in asphalt pavements designs by considering an appropriate field/laboratory transfer function, which might decrease the variability among results from different specimens. Despite some criticism related to its uniaxial stress state, the good representation of field loading conditions provided by the 4PBBT is very relevant (Ceratti, 1991).

The strain-controlled four point beam bending test is described by AASHTO T 321 (2007) and ASTM D 7460 (2010) and it is normally performed at the frequency of 5.0 or 10.0Hz at the temperature of 20°C. The initial strain is selected by the operator and might depend on field strains and on the specimen's stiffness. The failure point, or number of cycles to failure, is not a consensus among the several researchers that have been studying fatigue characterization of asphalt materials. The AASHTO standard considers failure when the specimen's stiffness decreases in 50%, and the ASTM standard considers that failure occurs at the maximum (peak value) of the plot between normalized modulus and number of cycles (E^*_{NORM}). The initial stiffness of the specimen is considered at the 50th cycle.

Arao (2014) performed the 4PBBT to evaluate the behavior of different types of asphalt mixes (dense and gap graded mixes), constituted by two different aggregates and four different asphalt binders (AC 30/45 neat binder, rubber binder, AC 60/85 neat binder and SBS-modified binder). The results indicated that asphalt mixes with rubber binder presented better fatigue resistance if compared to the other mixes. This might be explained by the stiffness values of this particular mix, which was the lowest among the materials tested. This tendency is normally observed for strain-controlled tests.

3.2.3 Tension-compression test

The tension-compression test was firstly developed based on the fact that real asphalt pavements are subjected to three continuous alternating load pulses, produced by the vehicles, which is different to most of laboratory tests try to represent. The bottom of the surface layer is primarily under pressure when the vehicle wheel is close to a given point of the pavement; the bottom of the layer is under tension when vehicle crosses the given point; and then, it is under pressure

once again when the vehicle leaves. By the end, the pavement structure is under tensile and compressive stresses (Qian et al., 2013). The test consists in applying a tension-compression sinusoidal loading in a cylindrical asphalt mix sample at 10Hz of frequency at different temperatures. The tension-compression cycle creates a homogeneous stress-strain state in the center of the specimen, where the axial strain is measured (Nguyen, Di Benedetto and Sauzéat, 2012).

In a study conducted by Nascimento et al. (2014), the tension-compression test was performed along with calculation of the VECD model to evaluate the fatigue resistance of asphalt mixes. According to these authors, there were still some experimental and analyses factors to be improved to make this method of analysis more practical and more precise. This test is considered as a homogeneous test, once it guarantees that the entire specimen is subjected to the same stress-strain state. In case of cylindrical specimens, 100mm × 130mm samples are used (Figure 3.7). The axial strain is measured by three extensometers and are located in the middle section of the specimen, which avoids border effects.

Figure 3.7 – Specimen prepared for tension-compression test (Nascimento et al., 2014)



Fatigue tests are normally performed at a previously selected intermediate temperature (chosen from 10 to 30°C, for example), as the strain-controlled specimens are subjected to a cyclic sinusoidal loading at the frequency of 10Hz. The loading application is repeated until the specimen fails. Previous researches have considered different failure criteria for this type of test. Mangiafico (2014) considered the fatigue life until the stress amplitude was equal to 10% of its initial value, i.e., until

the complex modulus value decreased in 90%. Nascimento et al. (2014) used the initial drop on the phase angle as the failure criterion.

Nascimento (2015) proposed the use of the viscoelastic continuum damage (VECD) for characterizing Brazilian asphalt mixes in terms of fatigue cracking. This model is based on three main concepts: (i) Schapery's work potential theory, (ii) the elastic-viscoelastic correspondence principle based on pseudo strain, and (iii) the time-temperature superposition (TTS) principle. Two parameters are calculated using the VECD model: the pseudo stiffness, also known as the material's integrity (C) and the damage (S). Equation 3.6 and Equation 3.7 provide the calculation of these parameters, and the plot $C \times S$ (damage characteristic curve) is always the same, independent of the type of loading (stress- or strain-controlled), frequency, strain or stress amplitude and the temperature used in the test. This is the reason why the damage characteristic curve is considered to be a fundamental property of the material tested. The pseudo strain (ϵ^R) can be calculated by Equation 3.8. In the present research, controlled-on-specimen (COS) uniaxial fatigue testing was performed.

$$C = \frac{\sigma}{\epsilon^R} \quad (3.6)$$

$$dS_i = \left(-\frac{1}{2} (\epsilon^R)_i^2 \Delta C_i \right)^{\frac{\alpha}{1+\alpha}} (\Delta \xi)_i^{\frac{1}{1+\alpha}} \quad (3.7)$$

Where:

- C is the material's integrity;
- σ is the stress level;
- S_i is the material's damage;
- ϵ^R is the pseudo strain;
- ξ is the reduced time;
- α is the damage evolution rate, $1 + 1/m$, in which m is the relaxation modulus log-log slope.

$$\varepsilon^R = \frac{1}{E_R} \int_0^{\xi} E(\xi - \tau) \frac{d\varepsilon}{d\tau} d\tau \quad (3.8)$$

Where: ε^R is the pseudo strain;
 E_R is the LVE relaxation modulus;
 ε is the strain;
 ξ is the reduced time;
 α is the damage evolution rate, $1 + 1/m$, in which m is the relaxation modulus log-log slope;
 τ is an integration term.

The simplified VECD (S-VECD) was proposed by Underwood et al. (2009) in order to make the VECD model calculation for cyclic tests characterization easier but still very accurate. The present research follows the method presented by Nascimento (2015), which provides more details on the S-VECD. The damage characteristics curve ($C \times S$) can be represented by an exponential function (Equation 3.9) or a power function (Equation 3.10). The damage is calculated by Equation 3.11.

$$C(S) = e^{aS^b} \quad (3.9)$$

$$C(S) = 1 - C_{11}S^{C_{12}} \quad (3.10)$$

$$S_{i+1} = S_i + \left(\frac{1}{2} (\varepsilon_{0,ta}^R)^2 C_{11} C_{12} S^{C_{12}-1} \right)^\alpha K_1(d\xi) \quad (3.11)$$

Where: C is the material's integrity;
 S is the material's damage;
 a , b , C_{11} , C_{12} and K_1 are coefficients;
 $\varepsilon_{0,ta}^R$ is the pseudo strain tensile amplitude;
 ξ is the reduced time.

3.2.4 Other fatigue tests

The French trapezoidal-shaped fatigue test is also used to evaluate the fatigue cracking resistance of asphalt mixes. The test consists in applying alternate loads in two points of the specimen, with failure occurring at the middle third section of the specimen, where the bending moment is at its highest (Barra, 2009). Fatigue life corresponds to the number of load repetition so that the initial strength is reduced to

50% (Loureiro, 2003; Barra, 2009). The trapezoidal test presents some difficulties to be done as the specimens are hard to be produced in the laboratory due to their geometry. Also shear forces might appear along with the flexural moments, which is undesired for the analysis of results (RDT-CONCEPA/ANTT, 2014). Figure 3.8 shows the specimens used in this type of test as well as the equipment used to perform it.

Figure 3.8 – Trapezoidal fatigue test: (a) specimens used in the test (Barra, 2009) and (b) LCPC equipment (RDT-CONCEPA/ANTT, 2014)



(a)



(b)

With the main objective of simulating the load effects provided by the vehicles' tire on an asphalt pavement, the wheel tracking test (WTT) was developed to evaluate the fatigue life parameters. With two cameras used to detect and correlate the cracking initiation as the tires pass by the specimen, the WTT aims to define a model that is capable of simulating the beginning and the propagation of field cracking in a more realistic manner (Loureiro, 2003).

Despite being most commonly used to evaluate rutting of asphalt mixes, the asphalt pavement analyzer (APA) is also capable of testing fatigue cracking resistance. It can simulate the real field conditions in prismatic specimens for that purpose. (Figure 3.9). The test utilizes a steel tire passing on a rubber pressurized hose capable of simulating the pressure provided by the tires (Skok, Johnson and Turk, 2002).

Figure 3.9 – APA equipment (Loureiro, 2003)



3.3 ASPHALT MIXES DESIGN

The experimental study involving the asphalt mix characterization was performed in terms of three different fatigue cracking resistance tests: the stress-controlled ITT, the 4PBBT and the axial tension-compression test. In this part of the study, only one type of mix was studied, which is the same mix used in the experimental test site.

The 12.5mm dense HMA was constituted by granite aggregate, obtained on quarry DS2-SP, located in the city of Bragança Paulista, in São Paulo state (Brazil). The aggregates were collected from the quarry during the week of the experimental test site construction in order to guarantee that the materials had the same characteristics, i.e., shape, specific gravity and mineralogical composition properties, as the ones used in the field pavement structure – to be further presented and discussed on this dissertation. The aggregates collected were taken to laboratory and then they were homogenized, divided, sieved and stored according to their sizes. Hydrated lime was also used in the asphalt mix composition. Table 3.1 presents the aggregates characterization.

Table 3.1 – Aggregates characterization

| Aggregate | Parameter | | |
|----------------|---------------------------|------------------|----------------|
| | Apparent specific gravity | Specific gravity | Absorption (%) |
| 19.0mm granite | 2.776 | 2.746 | 0.40 |
| 9.5mm granite | 2.781 | 2.739 | 0.60 |
| 4.75mm granite | 2.762 | 2.748 | 0.20 |
| Hydrated lime | 2.344 | – | – |

Regarding the HMA design, the asphalt binder used in its composition was the AC 30/45 penetration characterized in Chapter 2 (specific gravity of 1.007). The proportion of aggregates was 40% of the 19mm; 45% of the 9.5mm; 13.5% of the 4.75mm; and 1.5% of hydrated lime. The aggregate size distributions and the mix gradation (Superpave 19mm) are presented in Figure 3.10. The mix design was done by means of the Marshall methodology, with 75 blows per face of each specimen at the mixing temperature of 150°C. Short-term conditioning process was also performed for a period of 2 hours. Design parameters are presented in Table 3.2.

Figure 3.10 – Size distributions: (a) aggregates and (b) asphalt mix composition

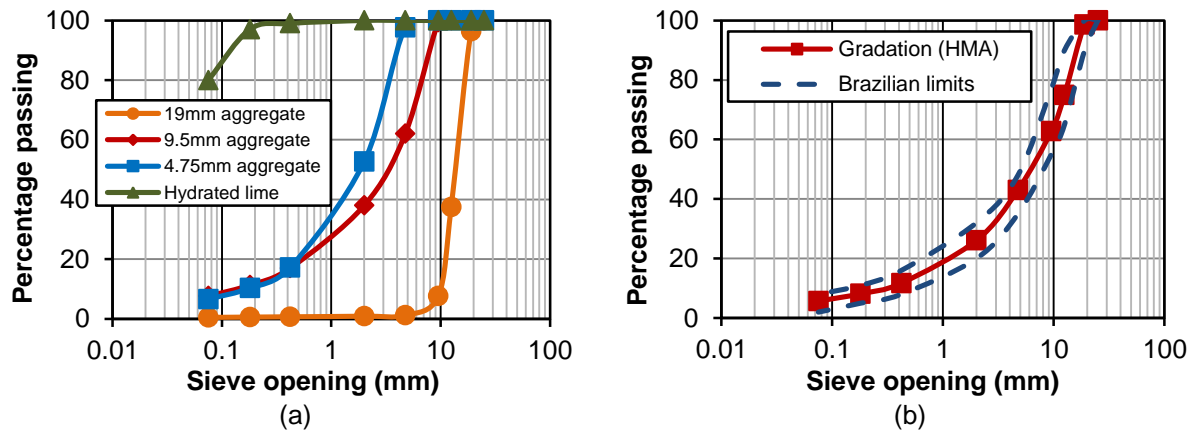


Table 3.2 – HMA design parameters

| Parameter | Value |
|---|-------|
| Asphalt binder content (%) | 4.4 |
| Maximum specific gravity, G_{mm} | 2.533 |
| Bulk specific gravity, G_{mb} | 2.451 |
| Voids content, V_v (%) | 4.0 |
| Voids in mineral aggregate, VMA (%) | 14.4 |
| Voids filled with bitumen, VFB (%) | 72.2 |
| Filler / asphalt ratio | 1.1 |
| Indirect tensile strength at 25°C, ITS (MPa) | 2.4 |
| Percentage of flat/elongated particles (%) ¹ | 18.0 |

¹Percentage of aggregate particles with ratio between their thickness (shortest dimension) and length (longest dimension) higher than 1:3.

The HMA was used as the asphalt surface layer in the experimental test site. The main difference among the two sections constructed and used in the study was related to the materials constituting their base layers. Different types of base layer were used: crushed stone and crushed stone with cement. The aggregates used in the base layer mixes were the same as the ones used in the asphalt layer, with the addition of cement for the latter.

3.4 RESULTS AND DISCUSSIONS

Different test methods and analyses were performed for characterizing the HMA specimens produced in the laboratory and samples collected in the field. Indirect tensile and four point bending tests were performed in laboratory and field specimens, while tension-compression tests were done only in laboratory specimens. The main objective of this section was to find correlations between different test methods usually done for fatigue cracking resistance characterization, trying to find the most representative test and analysis method. Also, comparisons between the behavior of lab-produced specimens and real field samples are carried out.

The ITT is the most traditional procedure used in Brazil to determine the fatigue resistance of asphalt mixes. In the present research, the stress-controlled test is performed and consists in submitting the specimen to repeated diametral loading in form of controlled compression stress. The loading – which is a percentage of the ITS value of the referred asphalt mix – was applied in a frequency of 1Hz (0.1s of loading and 0.9s of unloading) with the use of a materials testing system (MTS) hydraulic equipment at 20°C. During the test, tensile strain increases until the complete failure of the specimen, and this represents the fatigue life of the sample, in terms of number of cycles to failure (N_f). The ITT can also be performed as a strain-controlled test, but this method is not much common in Brazil and requires other accessories to be performed.

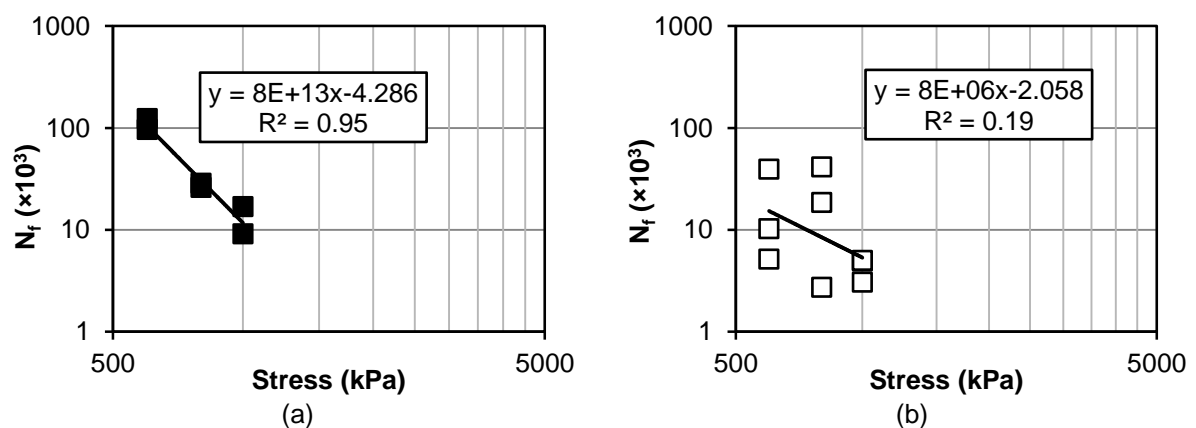
In the present research, the ITT was performed at 20°C, a typical intermediate temperature used in fatigue testing. Laboratory and field specimens were tested at three different stresses values: 30, 40, and 50% of the ITS value of the asphalt mix studied. Due to extensive time needed to perform the tests in 10, 20%, or other stress levels, they were not considered in this dissertation. Lower stress values are

normally suggested, because using high stress levels might induce other variables not related to fatigue cracking responses, and the fatigue curve slopes tend to fit better with a wider range of stress levels.

For the ITT, the classical fatigue analysis has been widely used in order to predict the fatigue life of asphalt mixes. This analysis normally defines the failure point of a specimen as the number of cycles in which the asphalt mix reaches complete failure (for stress-controlled tests) or its stiffness reduces to 40 or 50% of its initial value (for strain-controlled mode tests). If the strain amplitude is very low, some asphalt mixes might reach an endurance limit, which is the point in which the specimen can be submitted to loading cycles and never reaches the failure criteria proposed.

In the present research, the ITT was performed in terms of stress-controlled mode of loading. The failure criterion was the point where the strain growth rate of the specimen was no longer linear, as previously explained in this dissertation. Figure 3.11 presents the results in terms of fatigue laws for both laboratory and field samples. At least two specimens for each stress condition were tested, and due to the inherent variability normally obtained for fatigue tests, average values were not calculated, instead, all the results were plotted in the fatigue curves.

Figure 3.11 – Fatigue life according to ITT: (a) lab specimens and (b) field samples



The results of the laboratory specimens presented a good value of R^2 , which was not observed for the samples extracted from the field. Some hypothesis may arise from these results: (i) there can be a lot of variability among the field samples characteristics; (ii) field compaction might not follow a standard pattern throughout

the entire field layer; and (iii) the extraction of the specimens might produce different sample conditions, especially due to induced micro-cracking that can be formed during the extraction process. It is important to state that in real pavement constructions, the stress amplitudes are normally lower than the ones applied in the test, so the fatigue life for the mix tested should be higher than what is presented in the graphs.

The 4PBB tests were performed in prismatic-shaped 380mm- long × 50mm- thick × 63mm- wide beam specimens. The temperature used was 20°C, the same as the other fatigue tests performed in this dissertation. Seven strain levels were selected (between 200 and 800µε, with increments of 100µε) as the testing system is capable of providing this range for asphaltic materials. During the test, several variables are recorded for each loading cycle (applied loads, beam displacements, maximum tensile stress, maximum tensile strain, phase angle, and stiffness). The flexural beam stiffness (S) is calculated by Equation 3.12.

$$S = \frac{\sigma_t}{\epsilon_t} \quad (3.12)$$

Where: S is the flexural beam stiffness (Pa);
 σ_t is the maximum tensile stress (Pa);
 ϵ_t is the maximum tensile strain (mm/mm).

The results were analyzed in terms of different approaches: classical fatigue life (considering the decrease on stiffness values), peak value of normalized modulus, and fatigue life based on dissipated energy. In terms of decreasing stiffness (Figure 3.12a), there is a general consensus that fatigue occurs at the point of 50% of the initial flexural stiffness (Rowe et al., 2012), but some authors also consider 40% for failure criterion. The normalized modulus, calculated by Equation 3.13, is plotted against the number of cycles and its peak value is obtained by the maximum value of the polynomial-fit curve (Figure 3.12a).

$$E_{norm}^* = \frac{S_n \times N}{S_i \times 50} \quad (3.13)$$

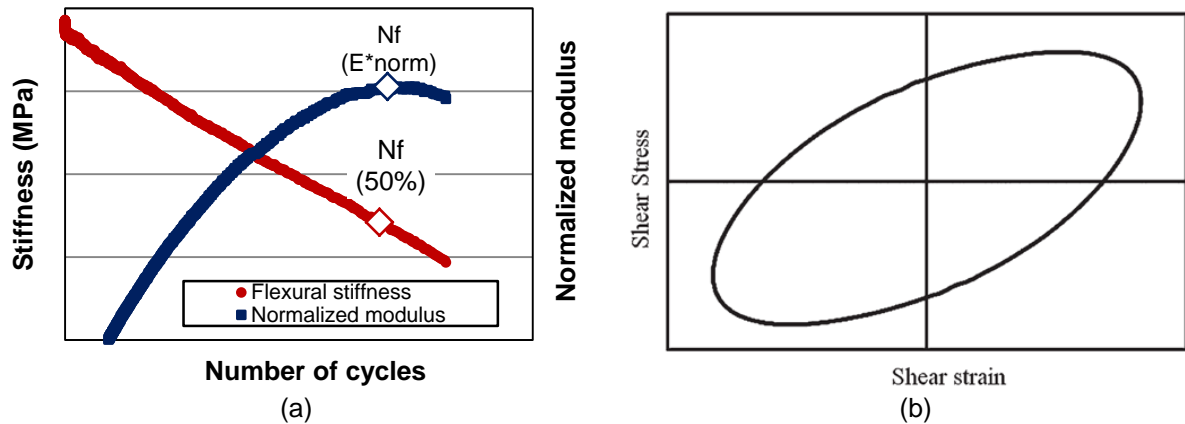
Where: E^*_{norm} is the normalized modulus;
 S_n is the flexural beam stiffness at cycle n (Pa);
 N is the accumulated number of cycles at cycle n;
 S_i is the initial flexural beam stiffness at cycle 50 (Pa).

The dissipated energy theory considers that asphalt mixes, as they behave as a viscoelastic material, dissipate energy during the loading and unloading cycles. Elastic materials recover all the energy stored during those cycles, while viscoelastic materials, such as asphalt mixes, dissipate part of that energy in form of heat. A hysteresis loop (Figure 3.12b) for fatigue testing performed in asphalt mixes can be constructed as a function of the stresses and strains obtained for each cycle of the test. The increasing loading cycles tend to initiate and propagate cracks in the specimen, making the dissipated energy change during the entire process. The dissipated energy (DE) per cycle itself is calculated by Equation 3.14.

$$DE = \pi \sigma_n \varepsilon_n \sin(\phi_n) \quad (3.14)$$

Where: DE is the dissipated energy per cycle;
 σ_n is stress value at cycle n;
 ε_n is the strain value at cycle n;
 ϕ_n is the phase angle at cycle n.

Figure 3.12 – Four point beam bending test: (a) stiffness and normalized modulus evolution and (b) hysteresis loop (Ahmed, 2016)



Ghuzlan and Carpenter (2000) introduced the concept of ratio of dissipated energy change (RDEC). The curve of RDEC versus number of cycles (Figure 3.13) can be divided into three parts. The plateau phase (stage II) can be considered as the part of test in which the percentage of input energy being transformed into damage is constant, until it reaches a point where the RDEC value rapidly increases, providing a true failure of the specimen (stage III). The failure criterion used in this approach takes into consideration the traditional (50% reduction in initial stiffness).

Figure 3.13 – Evolution of ratio dissipated energy change (Shen and Carpenter, 2005)

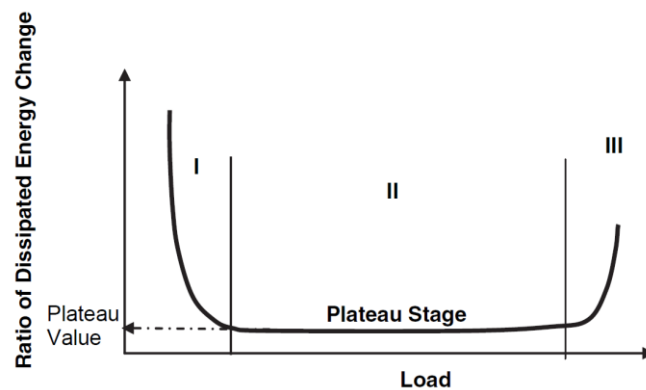
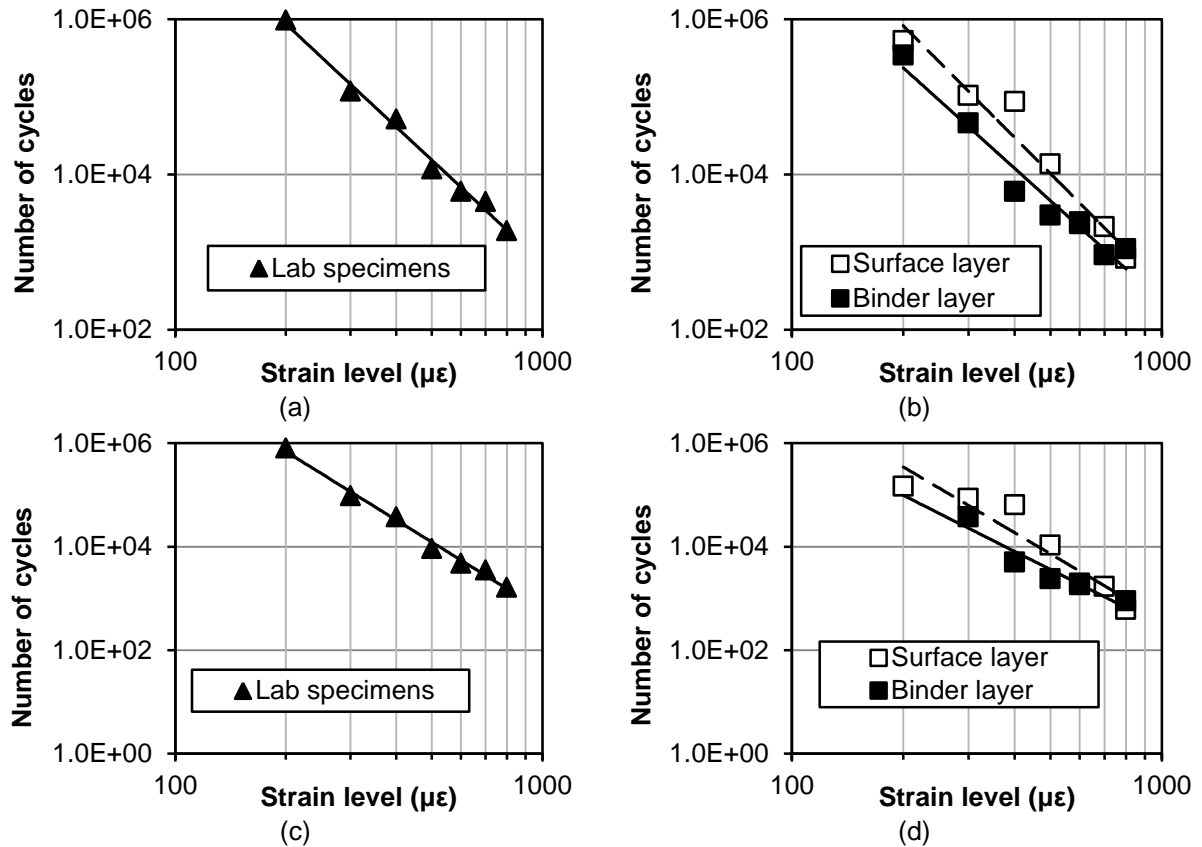


Figure 3.14 shows the results for the laboratory specimens and the field samples in terms of four point bending beam fatigue test using the traditional analysis (number of cycles until decrease in stiffness values). Field samples were divided into surface layer and binder layer, since the construction experimental site was constituted by a 12cm-thick asphalt concrete layer, placed in two layers of 6cm each.

Figure 3.14 – Fatigue life according to 4PBBT: (a) lab specimens and (b) field samples (40% of E^*); (c) lab specimens and (d) field samples (50% of E^*)



One can assume that fatigue tests with only one specimen per condition (in this case, for each strain level) is too risky and would provide results with high variability among them, but for the four point bending beam test, this was not the case. The fatigue curves provided values of R^2 higher than 0.90, which is an indication of good log-log correlation among the data obtained. Field core specimens provided higher variability among the results, which might be explained by several factors that influence the homogeneity of the final mix compacted in the field. Despite having the same composition, fatigue resistance was higher for the samples taken from the surface layer compared to samples from the binder layer. This might be explained by better compaction of the surface layer. Table 3.3 provides the fatigue curve parameters of each condition tested.

Table 3.3 – Fatigue curves parameters for 4PBTT

| Asphalt mix | 40% of E* | | | 50% of E* | | |
|---------------|----------------------|----------------------|----------------|----------------------|----------------------|----------------|
| | A | B | R ² | A | B | R ² |
| Lab specimens | 1.2×10 ¹⁶ | 4.41 | 0.99 | 9.2×10 ¹⁵ | 4.40 | 0.99 |
| Field samples | surface layer | 8.5×10 ¹⁶ | 4.79 | 1.8×10 ¹⁵ | 4.22 | 0.89 |
| | binder layer | 1.3×10 ¹⁵ | 4.24 | 0.96 | 1.9×10 ¹³ | 3.60 |

In general, the fatigue resistance of laboratory samples was higher than what was observed for field specimens (according to the values of the parameter A). This can be explained by the fact that in the laboratory there is more control related to the production of asphalt mixes. The aggregate gradation and the binder content are more similar to the mix design, as well as the compaction procedure, which is better controlled than what normally occurs in field constructions.

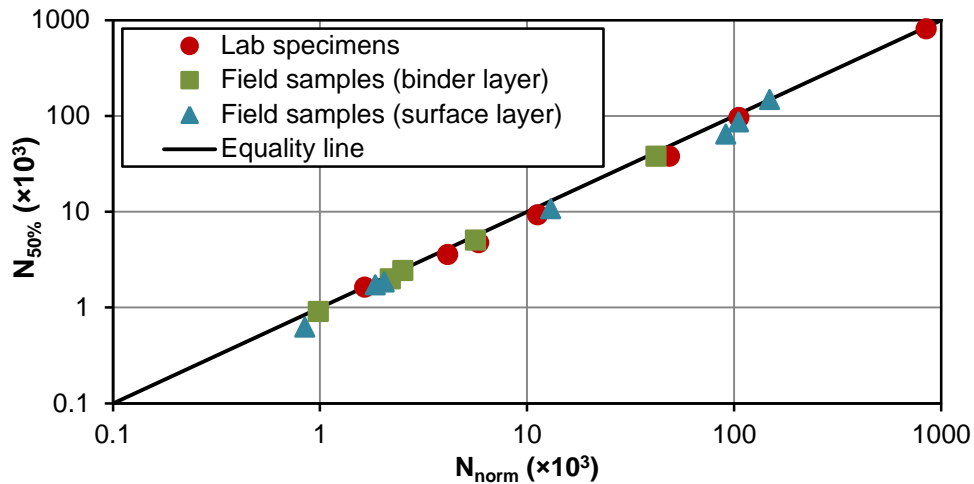
The peak value of the normalized modulus was obtained through the exponential plot of the curve $E^*_{norm} \times$ number of cycles. Equation 3.15 presents the calculation of E^*_{norm} . Figure 3.15 presents the correlation between the results from the traditional fatigue life (50% of E*) and the results from the normalized modulus concept.

$$E^*_{norm} = \frac{S_i \times N_i}{S_0 \times N_0} \quad (3.15)$$

Where:

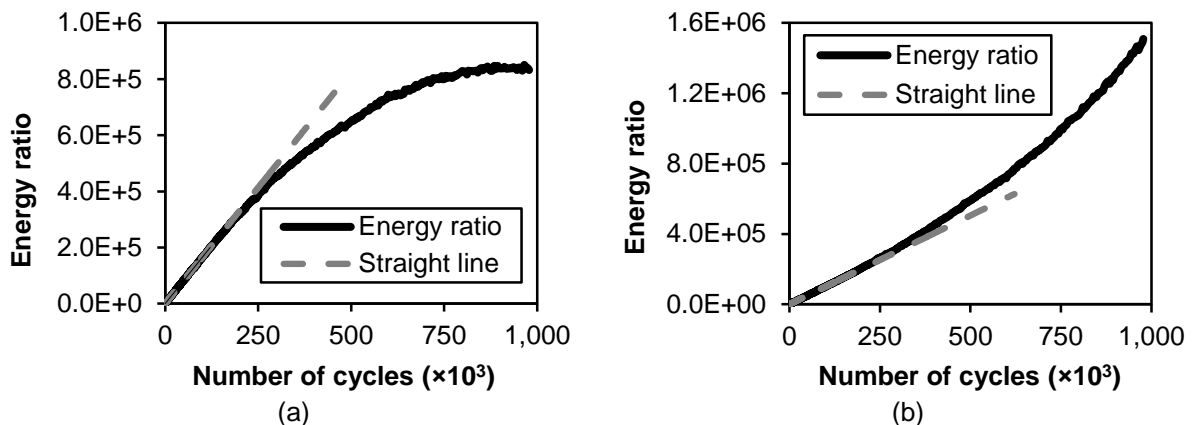
- S_i is the stiffness at cycle n ;
- S_0 is the initial stiffness (50th cycle);
- N_i is the n - number of cycles;
- N_0 is the cycle of the initial stiffness (50th cycle).

Figure 3.15 – Comparison between fatigue life: 50% of stiffness versus peak of normalized modulus



The dissipated energy approach was also studied in this dissertation. The 1990's Pronk and Hopman method (Abojaradeh, 2013) was one of the first fatigue characterization approaches to use the concepts of dissipated energy. This method considered that the transition between micro- and macro-crack formation (fatigue cracking) defines the number of load cycles in which the energy ratio is calculated (Figure 3.16a). Later, in 1997, Pronk suggested another way to calculate the energy ratio for strain controlled tests, by using the ratio of cumulative dissipated energy. The fatigue life was defined as the point in which the curve deviated from a straight line (Figure 3.16b).

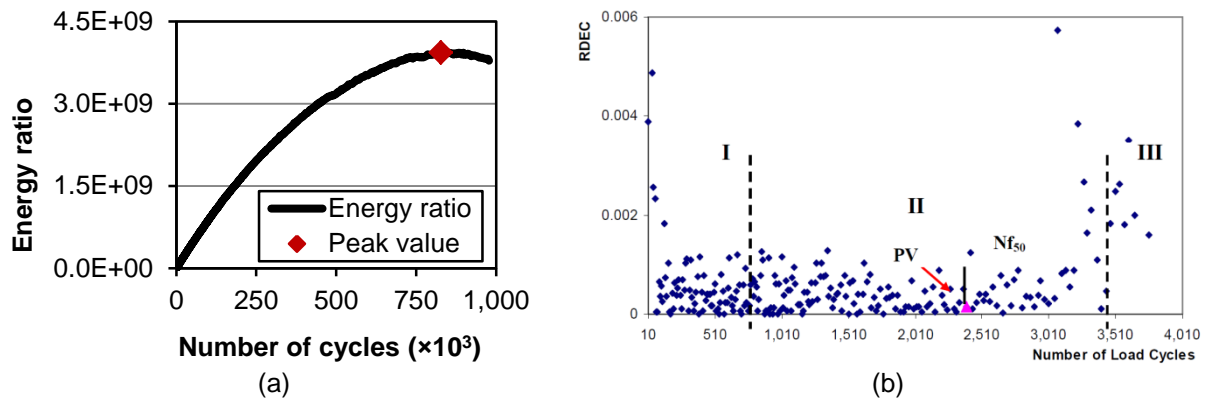
Figure 3.16 – Energy ratio evolution: (a) Pronk's 1990 method and (b) Pronk's 1997 method



The concept of energy ratio was also changed by Rowe and Bouldin (2000), as these authors consider that the peak value of energy ratio plotted against the number of load cycles (Figure 3.17a) represents the macro-crack and formation and

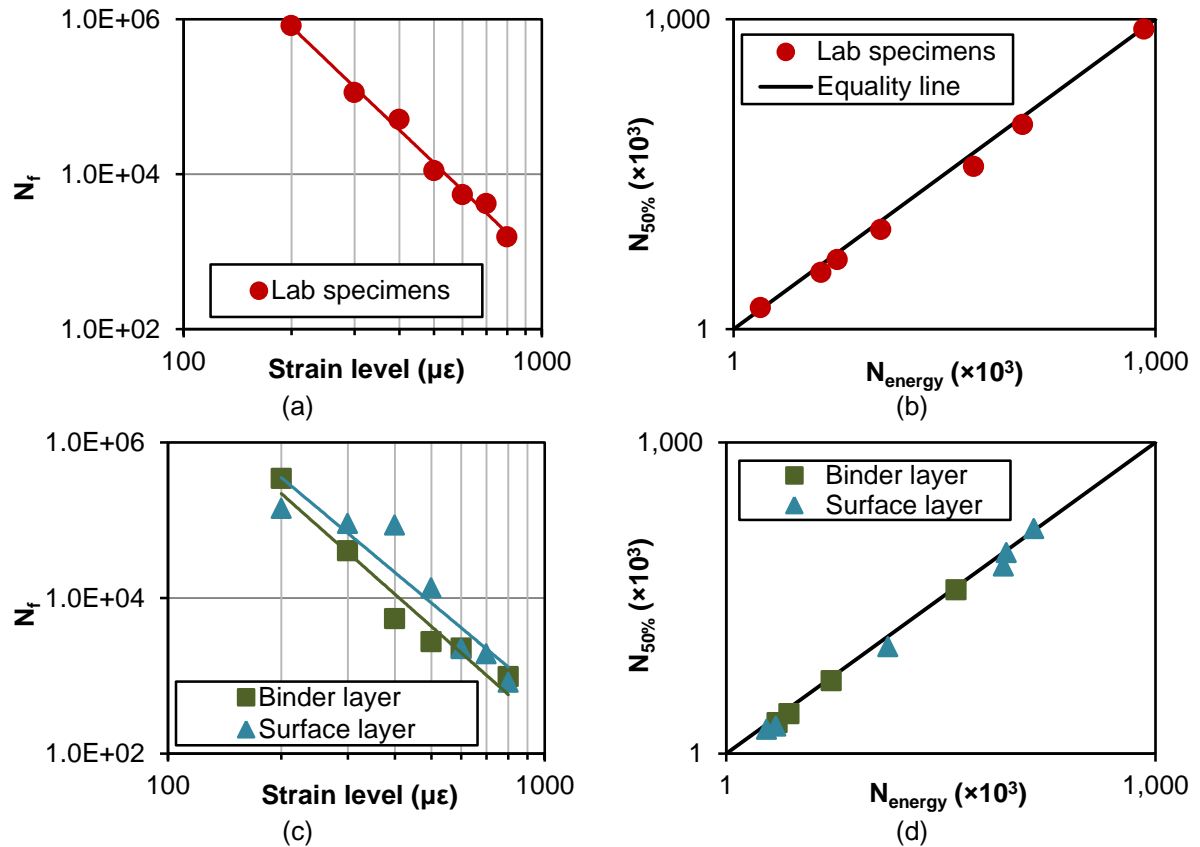
propagation. They concluded that the fatigue cracking by means of the proposed method does not necessarily occur close to the reduction of 50% in the initial stiffness of the asphalt mix. Ghuzlan and Carpenter (2000) proposed a method to provide similar values of fatigue life for any type of loading (constant stress or constant strain). The new failure criterion was defined based on the change in dissipated energy between a cycle divided by the dissipated energy of the previous cycle. The failure point is defined as the number of load cycles at which the change in the energy ratio begins to increase rapidly (Figure 3.17b).

Figure 3.17 – Energy ratio evolution: (a) Rowe and Bouldin method (2000) and (b) Ghuzlan and Carpenter method (2000)



The Ghuzlan and Carpenter (2000) method was not considered in the present dissertation due to the difficulty on finding the failure point among the raw data provided by the test. The fatigue curves are shown in Figure 3.18a and Figure 3.18c, and Figure 3.18b and Figure 3.18d present the correlation between the fatigue life obtained from 50% of stiffness and the fatigue life for the Rowe and Bouldin (2000) method.

Figure 3.18 – Fatigue life according to Rowe and Bouldin method: (a) fatigue life and (b) comparison with 50% of E^* ; (c) field samples and (d) comparison with 50% of E^*



The correlation between the fatigue life obtained by both methods (traditional 50% of stiffness and dissipated energy concept) provided similar results for the three types of samples. Fatigue curves for field specimens are more similar for both binder and surface layers by using the energy method.

Based on Wang et al. (2016), four different statistical parameters were calculated to compare the traditional fatigue life (50% of E^*) to fatigue life proposed by the dissipated energy methods. The parameters used are mean absolute error (MAE), standard error ratio (S_e/S_y), correlation of determination (R^2), and average geometric deviation (AGD) and are described by Equations 3.16 to 3.20. Table 3.4 presents the results for each correlation tested.

$$MAE = \left| \frac{N_{f1} - N_{f2}}{N_{f1}} \right| \times 100\% \quad (3.16)$$

Where: N_{f1} is the fatigue life using failure definition 1;
 N_{f2} is the fatigue life using failure definition 2.

$$S_e = \sqrt{\sum (N_{f1} - N_{f2})^2} \quad (3.17)$$

$$S_y = \sqrt{\sum (N_{f1} - \overline{N_{f1}})^2} \quad (3.18)$$

Where: N_{f1} is the fatigue life using failure definition 1;
 N_{f2} is the fatigue life using failure definition 2;
 $\overline{N_{f1}}$ is the mean value of the identified fatigue lives using fatigue definition 1.

$$R^2 = 1 - \left(\frac{S_e}{S_y}\right)^2 \quad (3.19)$$

Where: S_e is the standard error of estimation;
 S_y is the standard error of deviation.

$$AGD = \left(\prod_{i=1}^n R_i\right) \quad (3.20)$$

Where: R is equal to N_{f1}/N_{f2} for $N_{f1} \geq N_{f2}$;
 R is equal to N_{f2}/N_{f1} for $N_{f1} < N_{f2}$.

Table 3.4 – Results of the statistical parameters studied

| Correlation | Statistical parameter | | | |
|---|-----------------------|-----------|-------|-------|
| | MAE (%) | S_e/S_y | R^2 | AGD |
| $N_{50\%}$ versus Pronk (1990) | 54.5 | 0.510 | 0.62 | 1.534 |
| | 34.3 | 0.182 | 0.96 | |
| $N_{50\%}$ versus Pronk (1997) | 8.8 | 0.023 | 0.99 | 1.044 |
| | 8.8 | 0.033 | 0.99 | |
| $N_{50\%}$ versus Rowe and Bouldin (2000) | 12.8 | 0.038 | 0.99 | 1.104 |
| | 15.4 | 0.075 | 0.99 | |

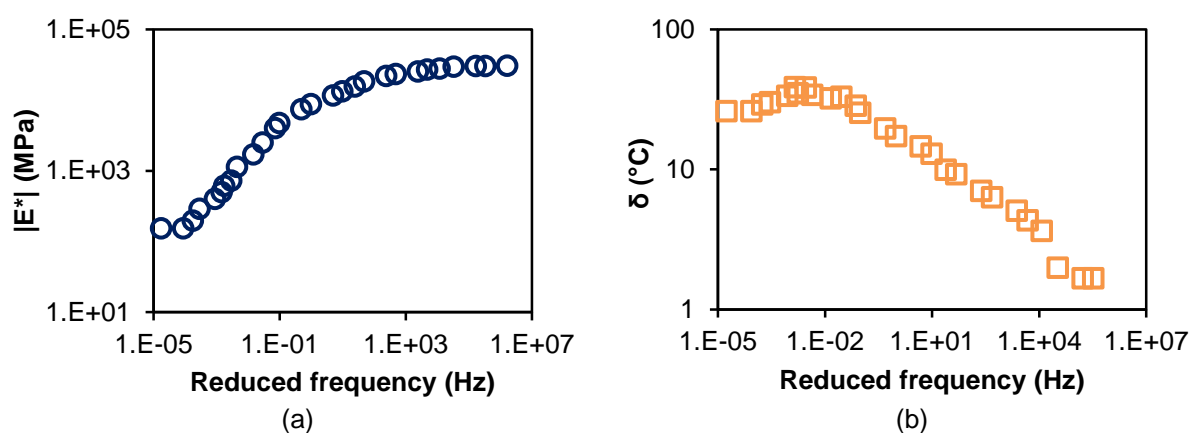
The parameters MAE (%), S_e/S_y , R^2 provide two results because they are different when the order of the variables is changed. In terms of MAE (%), lower values indicate a better agreement between the two failure criteria, so this means that the Rowe/Bouldin definition correlates better with the $N_{50\%}$ definition. For the S_e/S_y

parameter, a lower value is also expected, so in this case, the Pronk (1997) definition has the best fit, but the statistical parameter's values are very similar and very close to 0. In terms of R^2 , a high value (close to 1.0) indicates a better correlation between the failure definitions compare, so Pronk (1997) and Rowe/Bouldin methods provide the better correlations. Finally, a low value of AGD (the minimum is 1.0) means a better agreement between the results, and once again the 1997 and 2000's failure criteria provide the best correlations.

The tension-compression test was performed in order to obtain the results used in the characterization of fatigue life of the asphalt mix in terms of the S-VECD model. The test consists in two steps: characterization of LVE properties and characterization of damage properties by means of dynamic modulus and uniaxial fatigue test, respectively. The dynamic modulus test required three specimens, and four specimens were tested at the temperature of 20°C for the fatigue test.

The dynamic modulus was performed in terms of five temperatures (-10, 4, 20, 40, 54°C) and five frequency amplitudes (0.1, 0.5, 1.0, 5.0 and 10.0Hz). The strain level was in the range of 60 to 65 $\mu\epsilon$. Master curves for dynamic modulus (Figure 3.19a) and phase angle (Figure 3.19b) were plotted using the TTS at the reference temperature of 20°C. The relaxation modulus was then calculated using the theory of viscoelasticity.

Figure 3.19 – Master curves of the asphalt mix: (a) dynamic modulus and (b) phase angle



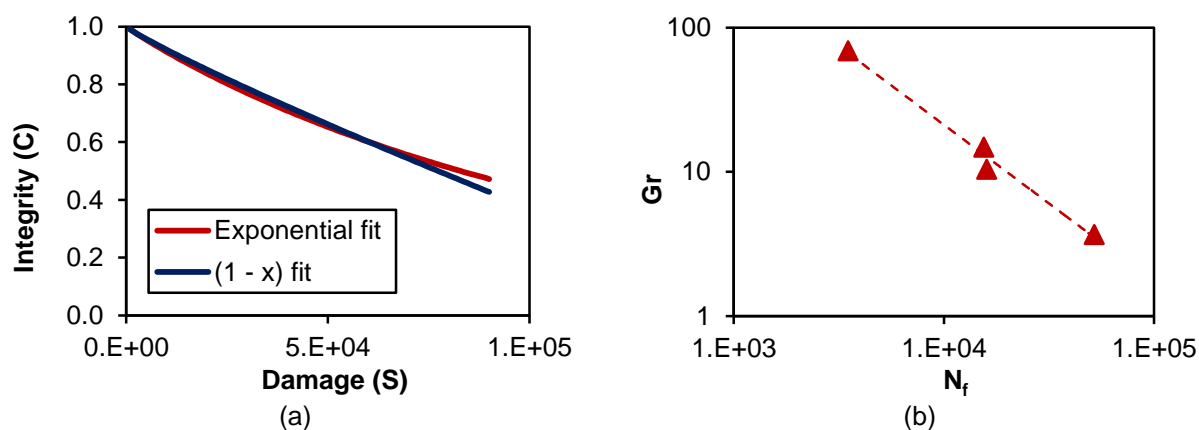
The fatigue damage characterization consisted in submitting the specimens to cyclic sinusoidal constant strain amplitude until drop of the phase angle. The testing system

collected the strain, the loading, the phase angle and the dynamic modulus throughout the test. The results were analyzed by means of the S-VECD model, and the damage characteristic curve ($C \times S$) was plotted (Figure 3.20a) using the coefficients provided by Table 3.5, which also includes the parameters Y and Δ used in the failure envelop ($G_r \times N_f$), shown in Figure 3.20b. The G_r parameter, proposed by Sabouri and Kim (2014), corresponds to the rate of release of the pseudo strain energy at failure and it is independent of mode of loading and temperature considered in the test.

Table 3.5 – S-VECD parameters

| Parameter | Value |
|-----------|-----------------------|
| C_{11} | 2.11×10^{-5} |
| C_{12} | 0.895 |
| Y | 488,229.9 |
| Δ | -1.091 |

Figure 3.20 – S-VECD results: (a) damage characteristics curve fittings and (b) G_r curve

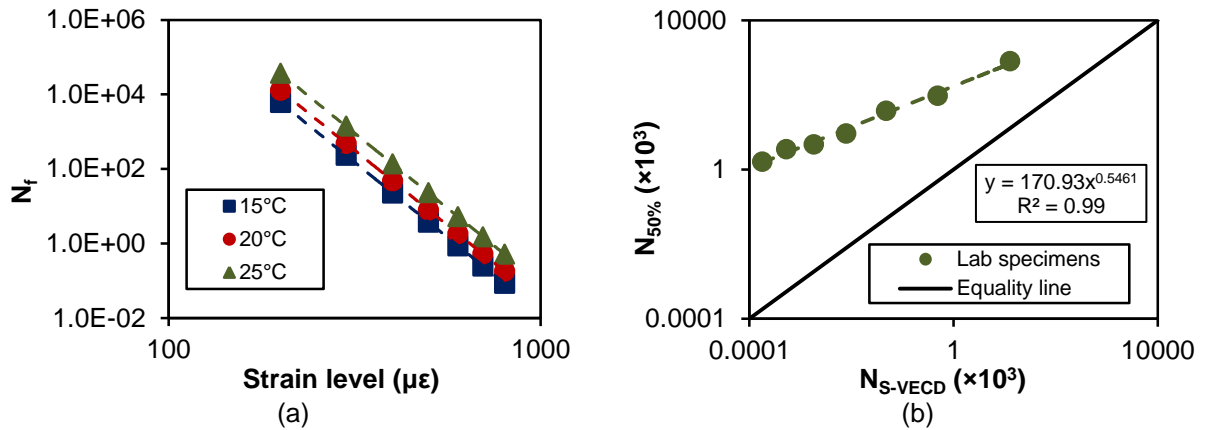


An exponential function and a $(1 - x)$ function fits were considered for the $C \times S$ curve and, since they the data fall very closely, it means that both fits are good for the results. The failure envelop provides a good linear correlation, so this confirms that this parameter is a good failure criterion for different testing conditions (i.e., different strain levels and temperatures).

Using the LVE properties and the parameters provided above, the fatigue life of the asphalt mix was simulated according to the procedure previously presented and the

AI model. Figure 3.21 presents the number of cycles to failure for three typical fatigue cracking temperatures (15, 20 and 25°C) and five strain levels (200, 300, 400, 500, 600, 700 and 800 $\mu\epsilon$), at 10Hz.

Figure 3.21 – S-VECD simulation: fatigue life in different temperatures and (b) comparison with 50% of E* method (20°C)

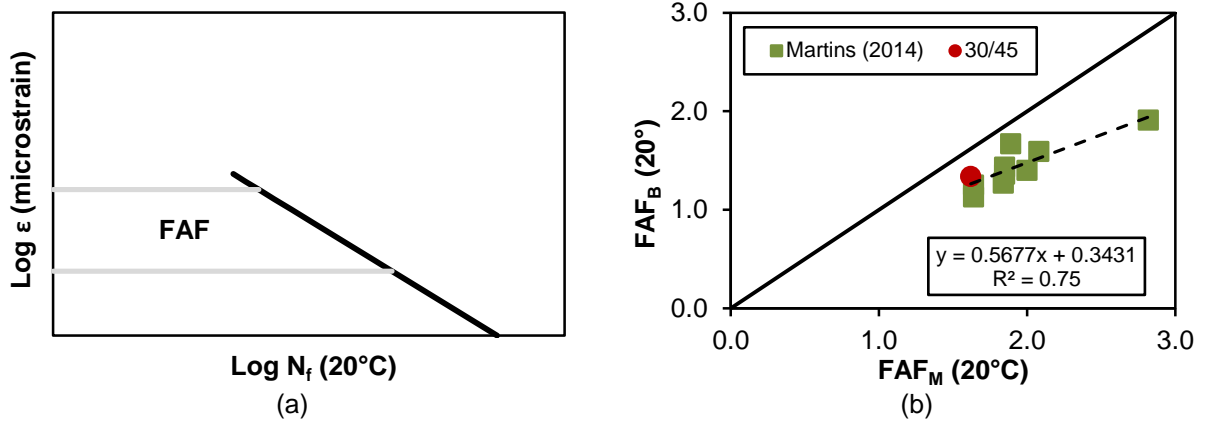


The S-VECD model has been considered as a good method to characterize the fatigue cracking resistance of asphalt mixes. It is important to notice that the fatigue lives curves at different temperatures have the same slope value, i.e., they are parallel. This occurred due to the type of test performed, which includes controlled-on-specimen strain mode-of-loading. For simpler tests, high temperatures might influence the results, especially due to the appearance of plastic strain in the specimens during the test.

Nascimento et al. (2014) proposed a fatigue life criterion obtained from the plot between strain level and number of cycles to failure. Two typical strain amplitudes found on real field constructions are considered (100 and 200 $\mu\epsilon$) and the area under the fatigue curve between those two points is calculated (fatigue area factor, or FAF, presented on Figure 3.22a). The higher the value obtained the better fatigue resistance the asphalt mix is. For asphalt binders, Underwood (2011) proposed the strain levels of 1.25 and 2.50% to be considered in the calculation of the asphalt binders' FAF as he considered that binders normally have a strain value that is about 122 times of the strain level of the mixtures, from previous studies. For the present dissertation, FAF_M and FAF_B , for asphalt mixes (M) and asphalt binders (B), respectively, were calculated in terms of the S-VECD results and the LAS test results. Figure 3.22b presents the correlation between nine binders and nine

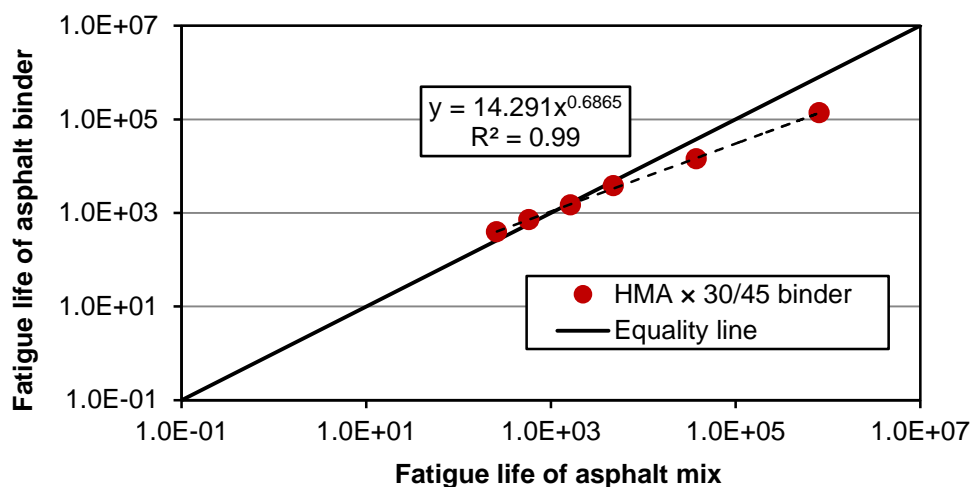
mixtures in terms of FAF_M and FAF_B from Martins (2014) plus the results from the present research.

Figure 3.22 – Fatigue area factor: (a) calculation (Adapted from Nascimento, 2015) and (b) comparison between FAF_B and FAF_M



Following the work done by Saboo and Jumar (2016), there was an attempt of correlating the fatigue results from the LAS binder test to the fatigue life of asphalt mixes tested by means of four point bending beam test (using the failure criterion of 50% of the initial stiffness). These authors assumed that the strain occurring in real pavement binders is about 50 times the strain found in the mixtures. Assuming that this correlation could be valid, Figure 3.23 presents the correlation among the results from each scale and strain amplitude. Strain levels of 2, 4 and 6% were considered for the asphalt binder, so strain levels of 400, 800 and 1,200 $\mu\epsilon$ were considered for the asphalt mix. Note that the value of 1,200 $\mu\epsilon$ was extrapolated from the fatigue curves obtained in the tests.

Figure 3.23 – Comparison between asphalt binder and asphalt mix fatigue lives



3.5 SUMMARY AND FINDINGS

This chapter evaluated one HMA in terms of fatigue cracking resistance by means of different testing and approaches. The asphalt mix was tested by means of stress-controlled ITT, which is a common procedure done in Brazil, strain-controlled 4PBBT and strain-controlled tension-compression test. The results from the different tests were compared among the different methods, and compared to the results obtained for the asphalt binder characterization. The main findings in this chapter are:

- When considering 40 or 50% reduction of the initial stiffness value in the strain-controlled 4PBBT, the fatigue life (N_f) of the asphalt has very similar results;
- The consideration of the normalized modulus (N_{norm}) and the peak energy ration also provide similar results in comparison to the 50% stiffness reduction approach;
- The S-VECD modeling using results from the tension-compression test results in lower fatigue lives, but is capable of providing the fundamental properties of the material tested;
- There is a good agreement between the fatigue life of the asphalt mix and the fatigue life of the asphalt binder studied, considering that the binder is submitted to 50 times the strain found in the mixes.

4 INFLUENCE OF DIFFERENT TYPES OF BASE COURSE ON THE FATIGUE RESISTANCE OF ASPHALT WEARING COURSE

4.1 INTRODUCTION

The increasing volumes of traffic and the heavier wheel and axle loads require asphalt pavement structures with better resistance and higher stiffness to meet a satisfactory performance. The structural design projects should be done in order to prevent excessive horizontal tensile strain at the bottom of the asphalt wearing course, by which fatigue cracking is mostly caused. Normally, unbound base layers provide higher deflections to the pavement structure, which affects the performance of the surface layer in terms of cracking initiation and propagation. For high traffic highways, the use of cement-treated base courses tends to enhance the performance of the asphalt pavement structure, by decreasing the tensile strains at the bottom of the asphalt surface layer.

For pavement road base layers, there is a high variety of soils and aggregate materials that can be used, but sometimes these materials tend to exhibit low bearing capacity and insufficient properties related to the main distresses. The addition of stabilizing materials, e.g., Portland cement, asphalt binder, hydrated lime and others improve the properties of these base layers. The use of Portland cement is a common solution to heavy traffic conditions, because of its hardening due to the curing processes in presence of water (Ismail et al., 2014). In terms of thickness, increasing the stiffness of a base course material with cement requires thinner layers in comparison to unbound base courses (Halsted, Luhr and Adaska, 2006). According to Balbo (2007), a 100mm-thick cement-treated base layer could distribute stress levels equivalent to a 250mm-thick unbound layer. Besides that, perpetual pavements have been proposed in the literature to decrease or eliminate fatigue cracking in the asphalt layers of pavement structures, by minimizing the level of tensile strain at the bottom of the asphalt layer to the point where it reaches the fatigue endurance limit, below which fatigue damage does not accumulate. For this structural solution, there is the increase in the asphalt layers total thickness, by using full-depth asphalt pavements.

This section presents the evaluation of an experimental test road section that includes two different pavement design solutions: one segment constituted by a flexible asphalt pavement, and the other constituted by a semi-rigid structure, with a cement-treated base layer course. This evaluation was done in terms of deflection evolution monitoring, by means of FWD and visual surveys for fatigue cracking evaluation. Fatigue cracking prediction models are compared to field data, obtained in terms of cracked area.

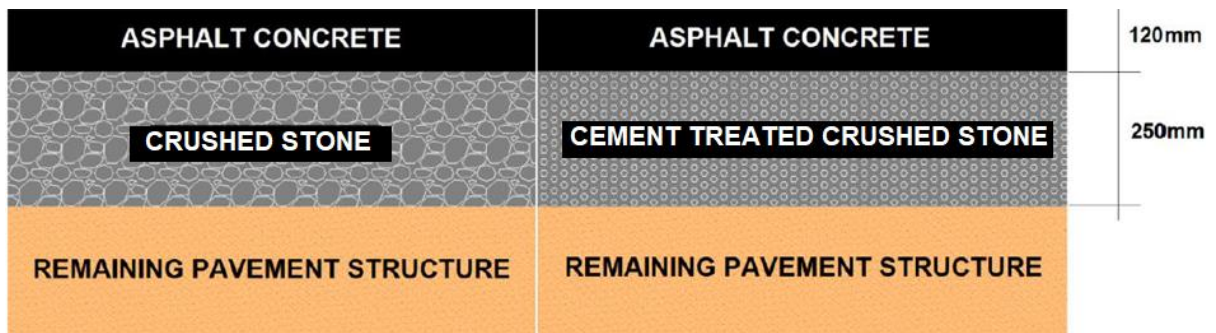
4.2 PROJECT OF THE EXPERIMENTAL PAVEMENT TEST SECTION

The experimental test road section monitored in the present research was constructed in December of 2014 in a high traffic Brazilian federal highway (BR-381) located in the city of Extrema, state of Minas Gerais. This highway runs for a total of 570 kilometers connecting two of the major metropolitan areas in Brazil (São Paulo and Belo Horizonte). Since 2008, this highway has been under concession to a private company for a total of 25 years. The construction was done in the right lane of a two-lane segment of the highway.

Two 100m-length segments were constructed for a project that consisted in the instrumentation of the layers constituting the experimental test site. Both segments have the same asphalt mixture and thickness of 120mm in their wearing course but are constituted by different materials in their base layer: crushed stone, and cement-treated crushed stone. These different types of base course present different responses and damage accumulation due to different responses under loading and damage accumulation due to their different stiffness. The unbound base layer provides a pure flexible pavement, and the cement-treated base layer provides more rigidity to the structure (semi rigid pavement)..

The materials used in each layer of the pavement section were designed in the laboratory. Granitic aggregates composed the unbound and the cement treated (with 5% of cement addition) layers and asphalt surface layer. The asphalt binder used for the HMA composition was an AC 30/45 penetration grade, used in the laboratory characterization. Figure 2.1 presents the pavement structure of the two segments studied in this dissertation: segments 1 and 2, which are the flexible and semi-rigid structures, respectively.

Figure 4.1 – Pavement sections structure



The construction of the experimental test site was finished in two weeks and followed the steps described next. First, the old pavement structure was milled in a 370mm thickness, which corresponded to the existing asphalt surface layer and part of the existing base layer (Figure 4.2a). The milling machine worked in a speed of 100m/h and the width of milling was approximately 1.27m. The RAP material was stocked in piles in the construction surroundings in order to be used for recycled base layers constituting other test sections. The base layers were placed and compacted (Figure 4.2b and Figure 4.2c) with the use of padded, steel and pneumatic drum compactors depending on the type of each material compacted; then finally the asphalt mixture was constructed as the surface layer for the four segments (Figure 4.2d).

Figure 4.2 – Construction of the experimental test site: (a) milling of the old pavement structure, (b) compaction of the crushed stone base layer, (c) placing of the crushed stone with cement, and (d) placing of the asphalt mixture layer



(a)



(b)



(c)



(d)

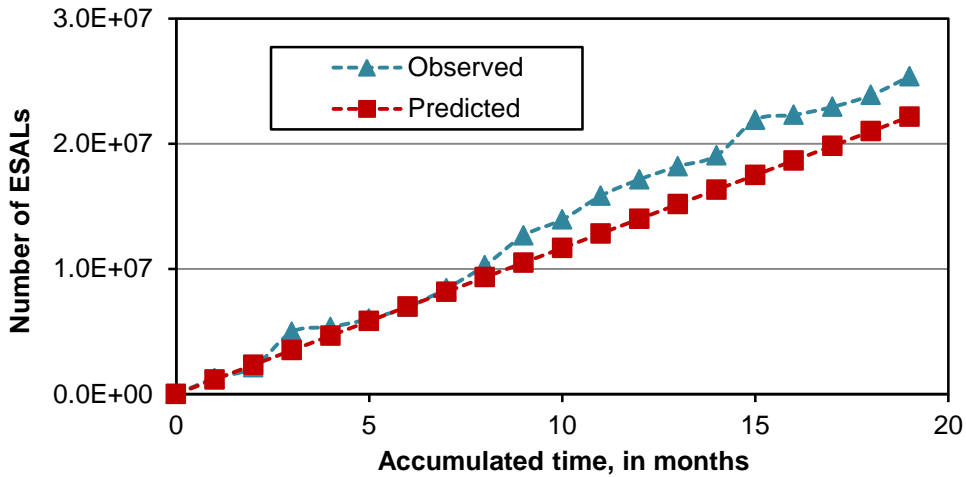
4.3 MONITORING OF THE EXPERIMENTAL TEST SITE

The experimental test site was monitored during 18 months regarding distresses related to rutting (by means of rut depth) and fatigue cracking (by means of cracked area) and also surface conditions, such as micro- and macrotexture. This research focus on the cracking evolution of the surface layer and on the deflection of the structure as the accumulated traffic passed on the segments studied. Also, a WIM device installed 50m from the experimental test site collected information on trucks weights and axles configuration. The data from the WIM system was used to calculate the actual number of accumulated ESALs, based on USACE's equivalent load factors. Despite knowing that AASHTO's equivalent load factors are widely used, the USACE method was used because Brazilian standards still consider these factors.

Although the 18-month period was considered in the present research, but estimates of design traffic for longer periods were done. Figure 4.3 shows the traffic

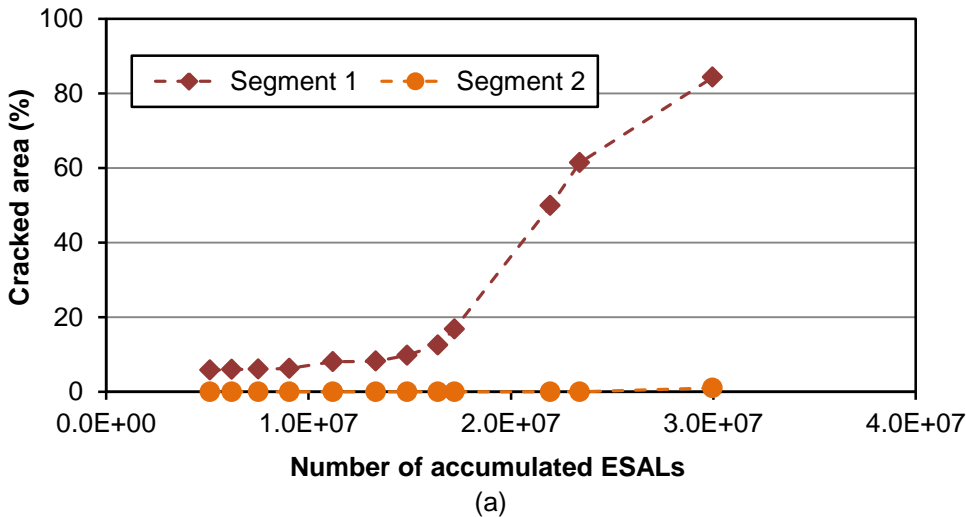
accumulation in terms of ESALs for the period of 18h months considered in this dissertation. The ‘observed’ data relates to the number of ESALs weighted by the WIM system, and the ‘predicted’ data is the number of ESALs predicted by design calculations before the construction.

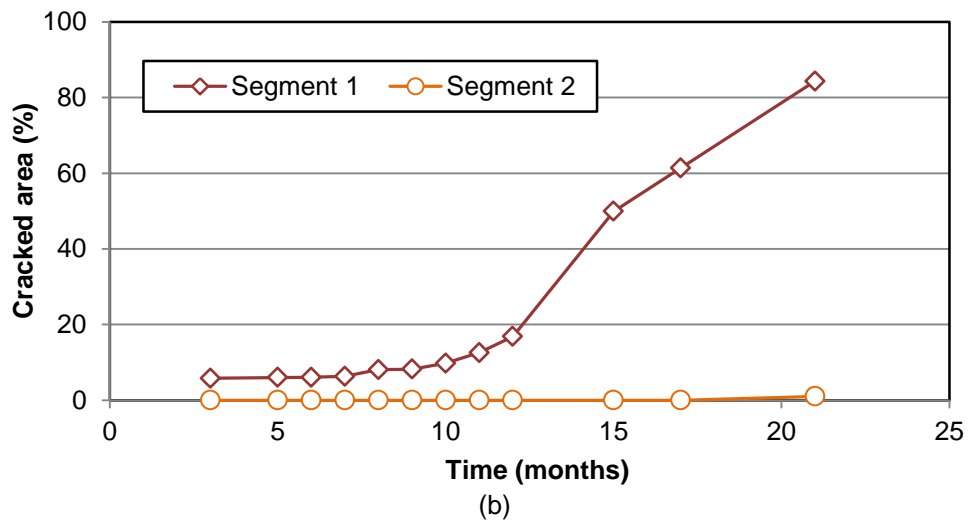
Figure 4.3 – Traffic accumulation throughout the time (ESALs)



The cracking evolution was determined in terms of percentage of cracked area in the surface layer of the pavement structure for both segments studied in the present research. This parameter is calculated by dividing the cracked area by the total surface area of the pavement segment, and the results obtained with accumulated traffic (number of ESALs) and time (in months) are shown in Figure 4.4. An exponential regression curve was fitted to the data collected, with good R² values.

Figure 4.4 – Evolution of cracked area: (a) versus number of ESALs and (b) versus time, in months

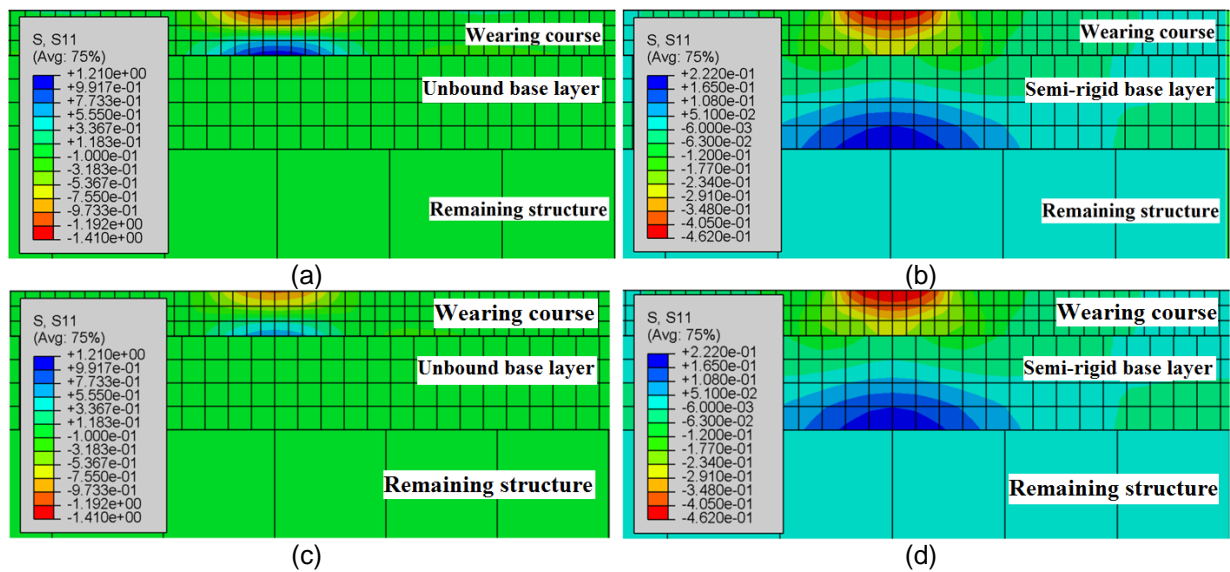




The increase of fatigue cracking in the asphalt surface layer of the experimental test site has different behavior for the different segments. For the flexible pavement section, it is safe to say that the damage accumulation led to high levels of early fatigue cracking, since the cracked area increased very rapidly. This can be explained by the distribution of tensile/compressive stresses occurring in the asphalt surface layer. For semi-rigid asphalt pavements, considering the hypothesis of there is no tensile stress (only compression stresses) at the bottom of the asphalt layer, which is different from what is observed in flexible asphalt pavements. Tensile stresses at the bottom of this layer initiate bottom-up cracks that propagate to the top of the surface layer.

Using the finite element method (FEM), the pavement sections were modeled in three dimensional in the ABAQUS/CAE 6.13 software. The main objective was to obtain the stress/strain values at the different layers of each segment. The model considered a 6.0 × 6.0m squared geometry with a 6.0m-deep subgrade. The modeling was performed in terms of linear elastic characteristics and the Poisson ratios values were 0.35 for the asphalt layer, 0.45 for the unbound base layer, 0.20 for the cement-treated base layer, and 0.45 for the remaining structure. The characteristics of the load to which the molded pavement structure was submitted were based on the FWD equipment: 40kN of load and 150mm of diameter. The initial conditions and the conditions after 15 months were considered in this analysis. Figure 4.5 presents the results in terms of horizontal tensile/compressive stresses for both segments.

Figure 4.5 – Horizontal stresses in the pavement layers: (a) segment 1 at 0 months, (b) segment 2 at 0 months, (c) segment 1 at 15 months, and (d) segment 2 at 15 months (Andrade, 2017)



4.4 NON-DESTRUCTIVE DEFLECTION TESTING

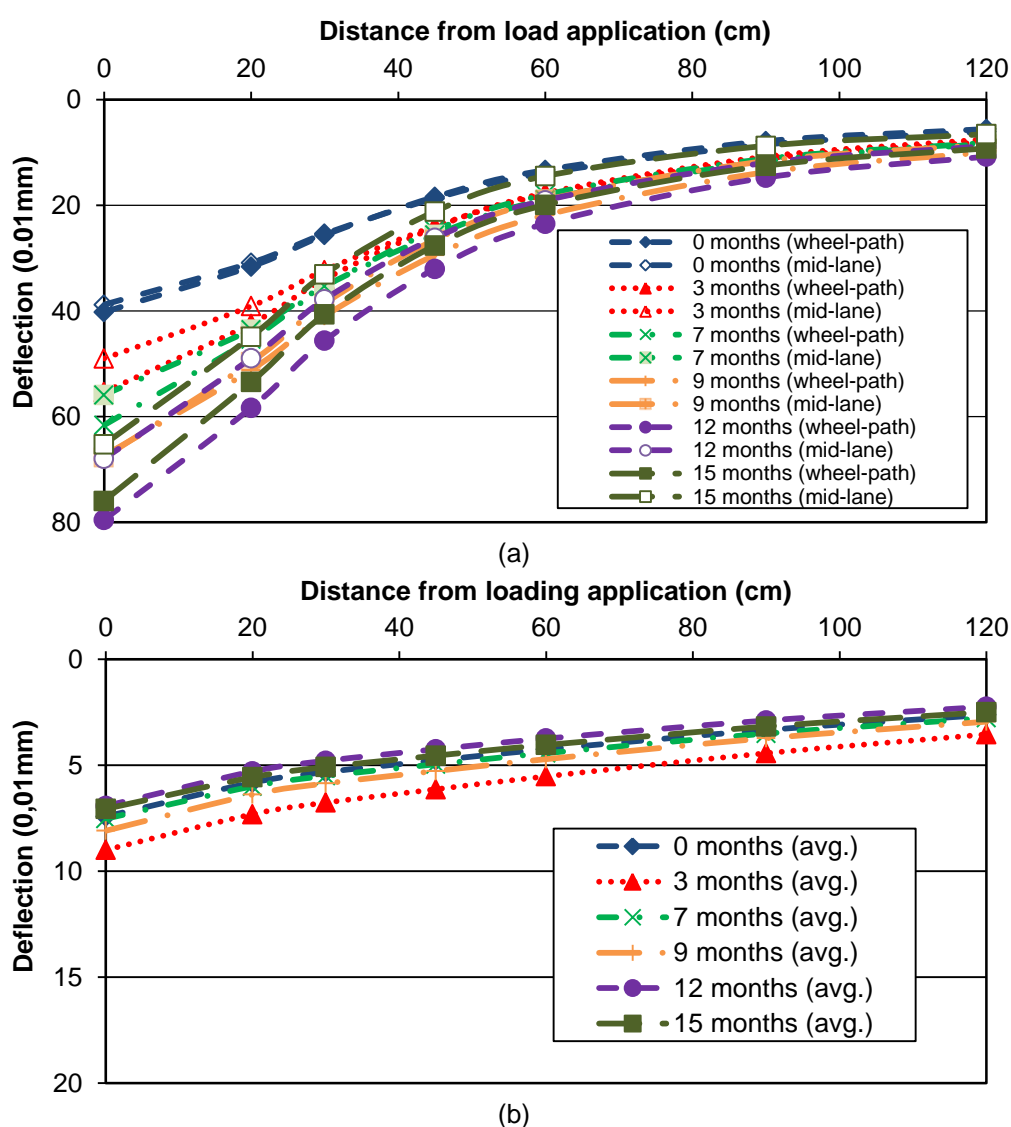
During the period of monitoring the experimental test site, several surveys were conducted in order to characterize the structural performance of the asphalt pavement. Non-destructive deflection tests were done by means of the FWD equipment. The data obtained from these tests were used to plot the deflection basins of the pavement segments and to backcalculate the stiffness of each layer at the time of each survey. For this specific test, surveys were performed until 15 months.

The deflection basins for both segments analyzed were plotted in terms of mid-lane path and right wheel-path. For the flexible pavement segment (segment 1), clear differences were found between the data collected from the two paths tested, except for the first survey performed (0 months). This was not observed for the semi-rigid pavement segment (segment 2). Figure 4.6a and Figure 4.6b present the deflection basins for segments 1 and 2, respectively. The deflections were lower at 15 months in comparison to the previous survey, due to high levels of precipitation observed at the period of 12 months.

It is important to state that there was a correction on the deflection basins in terms of temperature variation, because the surveys were done at different climate conditions. The reference temperature of the pavement structure was chosen as 24°C. First, the

deflection basins were plotted, and then backcalculation was done to obtain the stiffness values of each layer. Then the asphalt layer stiffness values were converted into 24°C, and the new deflections basins were molded using the new stiffness values. As expected, the deflections in segment 1 increased significantly with the traffic accumulation. In general, the deflection basin at the wheel-path lane was higher at the points closer to the load application, due to the traffic loads passing over them.

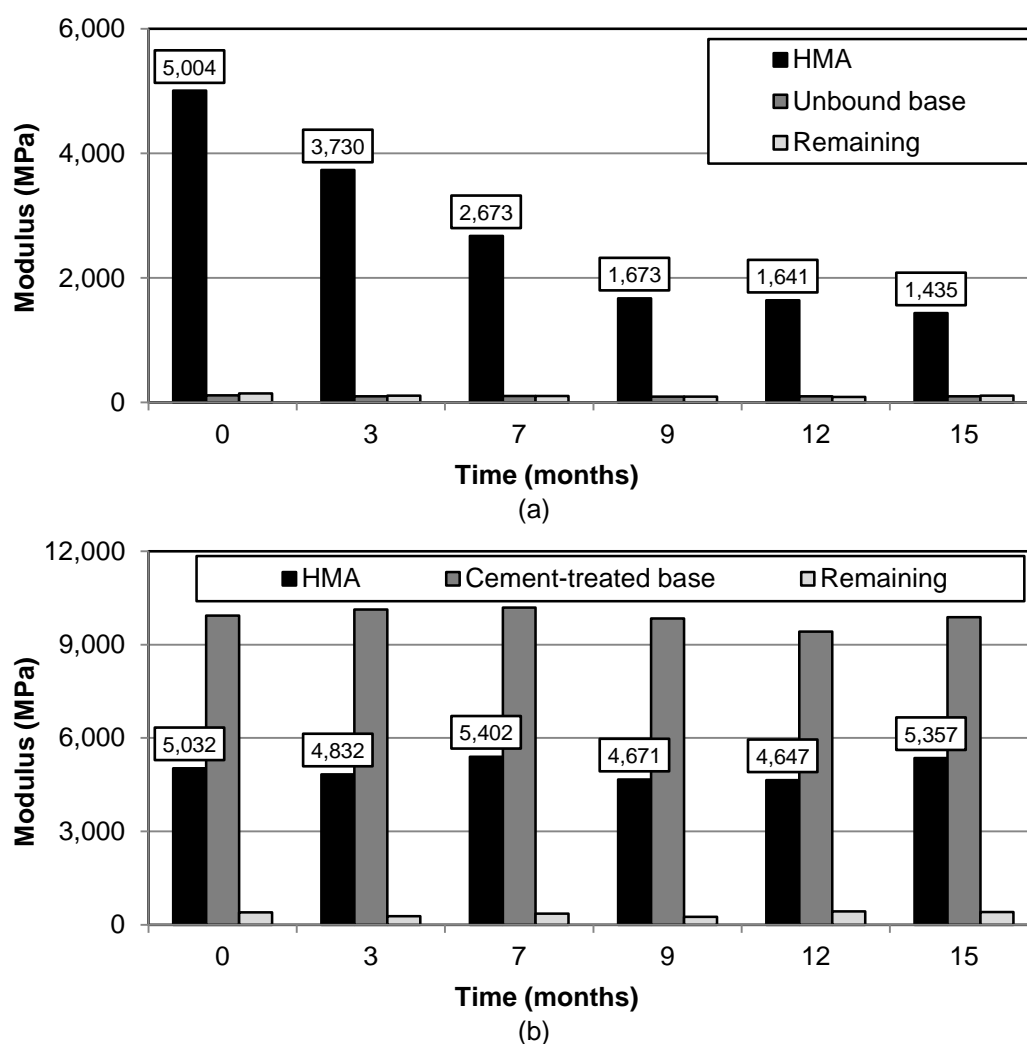
Figure 4.6 – Deflection basins of (a) segment 1 and (b) segment 2



A backcalculation procedure was done in order to evaluate the stiffness changes of each layer due to traffic accumulation, climate effects and crack propagation. Resilient moduli were obtained for each layer with the use of the BAKFAA 2.0 software program. Figure 4.7 presents the results obtained. The drop on the stiffness

values of the HMA layer on segment 1 can be explained by the rapid increase on the cracked area of this particular section. With the increasing cracked area, the water infiltration becomes another major issue, since the high humidity in the base course and in the remaining structure increases their deflection values and reduces their stiffness. The combination of these phenomena accelerates the pavement structure deterioration and the asphalt layer cracking. The stiffness values range of other layers (base course layer and remaining layer) are in accordance with the values obtained by means of the light weight deflectometer equipment during the construction of the experimental test site.

Figure 4.7 – Backcalculated moduli for (a) segment 1 and (b) segment 2



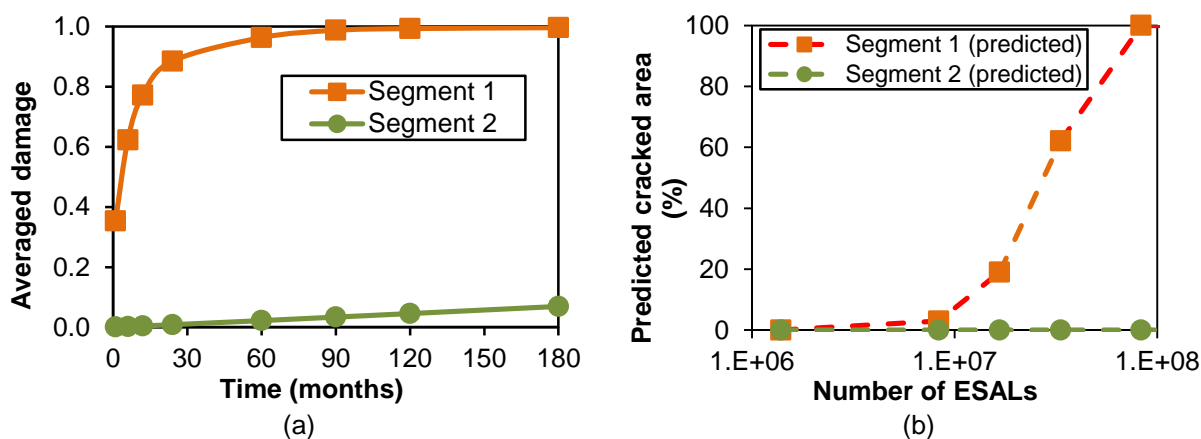
4.5 FATIGUE CRACKING PREDICTION

In this section, the fatigue cracking evolution of the experimental test site is presented in terms of observed cracked area with accumulated traffic. Besides that,

some of the several fatigue cracking prediction models presented in Chapter 1 are tested and compared to the actual data collected from the field.

One of the proposed mechanistic-empirical pavement design methods that consider a fatigue cracking prediction model have been developed using Brazilian road sections (Nascimento, 2015). For the present research, the two segments studied (unbound base layer and cement-treated base layer) were evaluated in terms of fatigue cracking prediction by using the procedure developed by Nascimento (2015). This analysis requires the viscoelastic properties of the asphalt mix in terms of the dynamic modulus parameters and the fatigue curve parameters obtained from the tension-compression test. This method uses the LVECD software for the computational simulations, which uses more detailed data regarding the pavement section to be analyzed: hourly distribution of traffic, traffic average speed and climate conditions (such as temperature and precipitation). Figure 4.8a shows the averaged damage evolution versus time, and Figure 4.8b shows the evolution of cracked area with accumulated traffic.

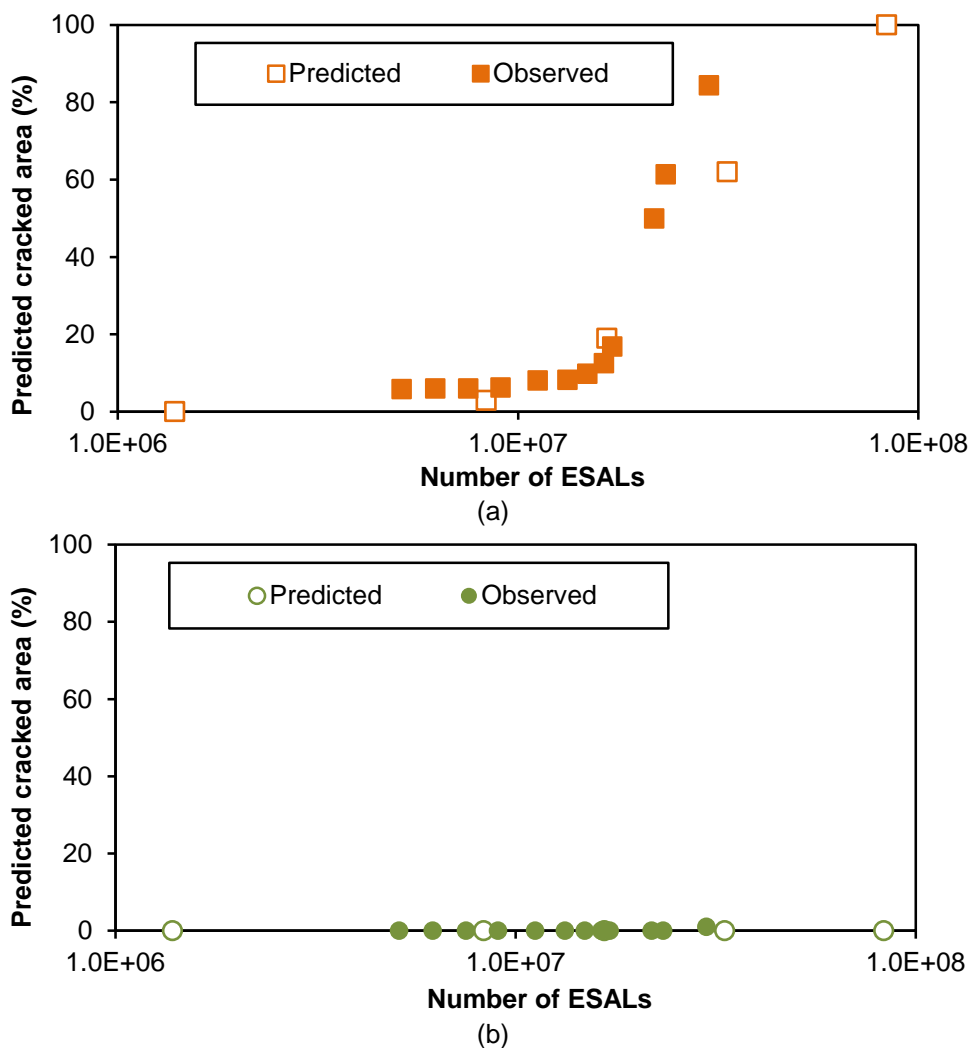
Figure 4.8 – Results from the computer simulations: (a) damage accumulation and (b) predicted cracked area



As expected, the evolution of predicted damage in the surface layer was very different for each segment, despite the same asphalt is used in both segments. The contribution of the base layer is very relevant for the performance of the asphalt mixture layer and the entire pavement structure. The segment with the granular base layer has a faster damage growth, which implicates in an exponential cracked area evolution, reaching 20% at approximately 1.7×10^7 number of ESALs, correspondent

to approximately 12 months. The segment with the cement-treated base layer has low values of averaged damage after 180 months (or 15 years), reaching less than 0.1% of cracked area throughout its entire life cycle. This small percentage of cracking indicates an isolated crack, which probably did not result from fatigue mechanism. Figure 4.9 presents the comparison between the observed cracked area (obtained by the several field evaluation campaigns performed) and the predicted cracked area (from the simulations).

Figure 4.9 – Comparison between observed and predicted cracked area: (a) segment 1 and (b) segment 2



The simulation for both segments analyzed provides good agreement with the values of cracked area obtained in real field evaluation. This is a good indication that the method is well-calibrated for these types of asphalt pavement structures. Besides that, it should be considered that the cement treated base layer might fail due to

fatigue cracking before the asphalt layer. In relation to the evolution of cracked area of segment 1, after 40% the 'observed' data curve deviates from the 'predicted' data curve. This probably happened due to the water entrance into the pavement structure, once the cracked area was already at high levels. This is a difficult phenomenon to predict by any model, and it might be the main reason why the most commonly used fatigue models are used to predict failure at 20% of cracked area. After this point, other factors not considered as input in the models may influence the fatigue cracking, especially the water infiltration into the adjacent layers, causing its weakening and consequences on the strength of the asphalt surface layer.

The simulations performed by means of S-VECD characterization were also compared to the classical fatigue prediction models presented earlier in this research. Since these models are calibrated for 20% of cracked area, the N_f considered here corresponds to the number of accumulated ESALs at this percentage of cracked area, which is commonly used as failure of the asphalt pavement. Segment 2 does not present any cracked area throughout the period considered in the analyses, so only segment 1 was further evaluated.

First, the number of ESALs at failure (N_f) was obtained considering the AASHTO methodology for 20% of cracked area, resulting in 2.78×10^6 . Note that this value is different from what was shown in Figure 7b, once those values were previously calculated in terms of the USACE traffic design method. The prediction models from the classical references, presented in Chapter 1 of the present research, were used to calculate the predicted N_f . The stiffness modulus (9,000MPa, or 1.3×10^6 psi) was obtained during the first 50 cycles of the 4PBBT, which can be considered as the initial stiffness of the material tested. The strain value at the bottom of the asphalt surface layer was obtained at the simulations performed in the ABAQUS software, and the result is $168 \mu\epsilon$. The results of predicted fatigue life (N_f) are shown in Table 1.1.

Table 4.1 – Fatigue life according to classical prediction models

| Reference | N_f |
|--|--------------------|
| Verstraeten, Veverka and Francken (1982) | 4.57×10^4 |
| Powell et al. (1984) | 3.36×10^6 |
| Thompson (1987) | 1.05×10^6 |
| Asphalt Institute (AI) | 1.93×10^6 |
| Shell Oil | 2.62×10^4 |

The values obtained indicate that all the presented models underestimated the pavement structure evaluated. Regarding only the fatigue cracking models that considered the strain level and the stiffness modulus of the asphalt mix as variables on their equations (AI and Shell Oil), the AI model provided a N_f value that was very close to the real failure found on the field (2.78×10^6 versus 1.93×10^6), and this was very different from what resulted from the Shell model (which was more than 100 times lower). The N_f value obtained using the Shell Oil model would lead to cracked area values close to 0%. This means that these methods are not suitable for the asphalt mix studied in the present research. Among the main hypothesis that can explain this behavior is that it does not consider the viscoelasticity of the HMA layer, and most the models presented were not calibrated to the Brazilian scenario in terms of materials and climatic conditions.

4.6 SUMMARY AND FINDINGS

The present research evaluated one HMA in terms of fatigue cracking by means of laboratory testing combined with computer simulations to predict the cracked area of an experimental test site. The dense HMA produced with a neat AC 30/45 penetration grade was evaluated by means of different test methods and analyses. The results from the different tests were compared and used in fatigue cracking prediction models. The main findings are:

- The commonly used fatigue cracking prediction models by Shell Oil and Asphalt Institute (AI) are not well calibrated because they do not consider the base layer

stiffness, the climatic conditions, the viscoelastic characteristics of the asphalt mix, and the asphalt layer thickness (for the AI model);

- The new proposed Brazilian mechanistic-empirical design method provided a good prediction of fatigue cracking evolution for the road test section evaluated. This method considers many factors that are normally not included as input for other prediction models, but still lacks the use of data related to the base layer deterioration, especially due to water infiltration;
- It is possible to predict the fatigue life of an asphalt pavement in terms of crack evolution, by using test methods that are capable of capturing the fundamental properties of the asphalt mix in terms fatigue resistance;
- The prediction of cracked area with time (or number of ESALs) can be a powerful tool to be used in the design process of asphalt pavements, by limiting the maximum value of cracked area as desired.

5 CONCLUSIONS

5.1 FINAL CONSIDERATIONS

The present dissertation studied the fatigue life of asphalt pavements by means of laboratory asphalt binders and mixes characterization, and field evaluation of pavement structures. The importance of studying fatigue cracking of asphalt materials relies on the prediction of pavement service life, which is a difficult task to be done, due to the several coexisting variables during the failure process. As fatigue cracking is one of the major causes of early deterioration in asphalt pavements existing in Brazil, this distress should be addressed more carefully for pavement design purposes. The main conclusions obtained in this research are:

- The rheological characterization of asphalt binders is an important tool for understanding and predicting the behavior of asphalt mixes, but there are no good correlations between the results obtained for both materials using the available techniques;
- The prediction of fatigue failure in asphalt mixes by means of the asphalt binder is mostly important to select the best material to be used in pavement design, but it is important to know that the aggregate skeleton also plays a relevant role regarding mechanical properties;
- Fundamental properties of the asphalt mixes, which are independent of loading mode, specimen geometry and temperature, should be determined for consideration in the prediction of the fatigue performance. Therefore, tests should be enhanced for this purpose;
- The characterization of asphalt mixes in laboratory is generally performed by severe accelerated tests, therefore laboratory-to-field transfer function should be developed, and this depends not only on the type of asphalt mix tested, but also on the pavement structure designed and on field climate conditions ;
- It is possible to predict the fatigue cracking of asphalt pavements, if more realistic test methods that consider the fundamental properties of the asphalt materials are performed, and if field conditions are considered;

- The base layer stiffness, the structural design project, the actual traffic level, the climate conditions, and other aspects are important variables to be considered in the fatigue cracking prediction models;
- In addition, the viscoelastic properties of the asphalt mixes (in terms of behavior related to varying temperature and frequency conditions) provide better results regarding fatigue cracking prediction;
- Classical fatigue prediction models tend to either underestimate or overestimate the fatigue life of an asphalt pavement, mainly because they only consider the initial stiffness of the asphalt mix and the strain value occurring in at the bottom of the asphalt layer;
- Although these well-known models might not be suitable for fatigue cracking prediction, the Asphalt Institute (AI) model seemed to correlate well with field results in terms of cracked area, for flexible pavement sections. This model is more complete than the others due to the consideration of the HMA volumetric properties. Despite that, more comprehensive performance models have to be developed by considering Brazilian traffic and climate conditions for design purposes;
- The Brazilian fatigue cracking model proposed by Nascimento (2015) provides good results in terms of cracked area, therefore this should be an important tool to be used in further asphalt pavement designs;
- Although this new method is a powerful tool for pavement design purposes, it still needs further development regarding the consideration of asphalt pavement structures with other types of materials in their base layers, such as bitumen-stabilized and cement-treated mixes;
- The consideration of the base and other layers deterioration should also be done, especially because asphalt fatigue cracking evolution is influenced by water infiltration and weakening of the other pavement's layers.

5.2 SUGGESTIONS FOR FUTURE WORK

As main suggestions for the continuation of this work, there is the addition of other types of asphalt mixes (with different aggregates characteristics and different asphalt binders) to the study of fatigue cracking prediction. Other pavement structures should also be analyzed in order to validate the presented fatigue cracking model for

Brazilian highways. The influence of the temperature in the asphalt materials fatigue lives should also be considered in the different test methods in order to better assess the temperature that correlates better with field data.

REFERENCES

- AASHTO M 320. **Standard specification for performance graded asphalt binder.** American Association of State Highway and Transportation Officials, Washington, DC, 2009.
- AASHTO T 321. **Standard method of test for determining the fatigue life of compacted asphalt mixtures subjected to repeated flexural bending.** American Association of State Highway and Transportation Officials, Washington, DC, 2007.
- AASHTO TP 101. **Estimating damage tolerance of asphalt binders using the linear amplitude sweep.** American Association of State Highway and Transportation Officials, Washington, DC, 2014.
- ABOJARADEH, M. **Development of fatigue failure criterion for hot-mix asphalt based on dissipated energy and stiffness ratio.** Jordan Journal of Civil Engineering, Vol. 7, No. 1, 2013.
- ADHIKARI, S.; YOU, Z. **Fatigue evaluation of asphalt pavement using beam fatigue apparatus.** The Technology Interface Journal, Vol. 3, No 3, 2010.
- AHMED, T. M. **Fatigue performance of hot mix asphalt tested in controlled stress mode using dynamic shear rheometer.** International Journal of Pavement Engineering, 2016.
- AIREY, G. D.; RAHIMZADEH, B. **Combined bituminous binder and mixture linear rheological properties.** Construction and Building Materials, Vol. 18, p. 535-548, 2004.
- AL-HADDAD, A. H. A. A. **Fatigue evaluation of Iraqi asphalt binders based on the dissipated energy and viscoelastic continuum damage (VECD) properties.** Journal of Civil Engineering and Construction Technology, Vol. 6, Issue 3, p. 27-50, 2015.
- AL-KHATEEB, G. G.; GHUZLAN, K. A. **The combined effect of loading frequency, temperature, and stress level on the fatigue life of asphalt paving mixtures using the IDT test configuration.** International Journal of Fatigue, Vol. 59, p. 254-261, 2014.
- AL-QADI, I. L.; XIE, W.; ELSEIFI, M. **Frequency determination from vehicular loading time pulse to predict appropriate complex modulus in MEPDG.** Journal of the Association of Asphalt Paving Technologists, Vol. 77, p. 739-772, 2008.
- AMERI, M.; JELODAR, Y. A. K.; MONIRI, A. **Relationship between elastic recovery and linear amplitude sweep as asphalt binder fatigue tests.** Journal of Applied Environmental and Biological Sciences, Vol. 5, p. 7-10, 2015.

ANDRADE, L. R. **Comparação do comportamento de pavimentos asfálticos com camadas de base granular, tratada com cimento e com estabilizantes asfálticos para tráfego muito pesado**. M.Sc. thesis, Universidade de São Paulo, São Paulo, 2017. *[In Portuguese]*

ARAO, M. **Análise da vida de fadiga de pavimentos flexíveis em diferentes misturas**. Term paper, Universidade Federal do Rio de Janeiro, Rio de Janeiro, 2014. *[in Portuguese]*

ASADI, H.; LEEK, C.; NIKRAZ, H. **Effect of temperature on fatigue life of asphalt mixture**. AAPA 15th. International Flexible Pavements Conference, Brisbane, 2013.

ASTM D 2872. **Standard test method for effect of heat and air on a moving film of asphalt (rolling thin-film oven test)**. American Society for Testing and Materials, West Conshohocken, PA, 2012.

ASTM D 7175. **Standard test method for determining the rheological properties of asphalt binder using a dynamic shear rheometer**. American Society for Testing and Materials, West Conshohocken, PA, 2008.

ASTM D 7460. **Standard test method for determining fatigue failure of compacted asphalt concrete subjected to repeated flexural bending**. American Society for Testing and Materials, West Conshohocken, PA, 2010.

AWANTI, S. S. **Laboratory evaluation of SMA mixes prepared with SBS modified and neat bitumen**. 2nd Conference of Transportation Research Group of India, Procedia – Social and Behavioral Sciences, Vol. 104, p. 59-68, 2013.

BAHIA, H. U.; HANSON, D. I.; ZENG, M.; ZHAI, H.; KHATRI, M.A.; ANDERSON, R.M. **Characterization of modified asphalt binders in Superpave mix design**. National Cooperative Highway Research Program (NCHRP), Report No. 459, 2001, 117 p.

BAHIA, H.; TABATABAEE, H. A.; MANDAL, T.; FAHEEM, A. **Field evaluation of Wisconsin modified binder selection guidelines – phase II**. Wisconsin Highway Research Program Project No. 0092-13-02, 2013, 89 p.

BALBO, J. T. **Pavimentação asfáltica – materiais, projeto e restauração**. 1st ed.: Oficina de Textos, 2007. *[in Portuguese]*

BARKSDALE, R. G. **Compressive stress pulse times in flexible pavements for use in dynamic testing**. Highway Research Record: Highway Research Board, No. 345, p. 32-44, 1971.

BARRA, B. S. **Avaliação da ação da água no módulo complexo e na fadiga de misturas asfálticas densas**. Ph.D. dissertation, Universidade Federal de Santa Catarina, Florianópolis, Brazil, 2009. *[in Portuguese]*

BERNUCCI, L. L. B.; MOTTA, L. M.; CERATTI, J. A. P.; SOARES, J. B. **Pavimentação asfáltica: formação básica para engenheiros**. 1st ed., Rio de Janeiro: ABEDA, 2006. *[in Portuguese]*

BERTHELOT, C.; LOEWEN, T.; TAYLOR, B. **Mechanistic-empirical load equivalencies using weigh in motion**. 6th International Conference on Heavy Vehicle Weights and Dimensions Proceedings, Saskatoon, p. 135-144, 2000.

BHATTACHARJEE, S.; MALLICK, R. B. **Determining damage development in hot-mix asphalt with use of continuum damage mechanics and small-scale accelerated pavement test**. Transportation Research Record: Journal of the Transportation Research Board, Washington, No. 2296, p. 125-134, 2012.

BODIN, D.; TERRIR, J. P.; PERROTEAU, C.; MARSAC, P. **Effect of temperature on fatigue performance of asphalt mixes**. 11th. International Conference on Asphalt Pavements, Nagoya, 2010.

BOUDABBOUS, M.; MILLIEN, A.; PETIT, C.; NEJI, J. **Energy approach for the fatigue of thermoviscoelastic materials: application to asphalt materials in pavement surface layers**. International Journal of Fatigue, Vol. 47, p. 308-318, 2013.

BROWN, S. F. **Determination of Young's modulus for bituminous materials in pavement design**. Highway Research Record: Highway Research Board, No. 431, p. 38-49, 1974.

CAMARGO, F. F. **Field and laboratory performance evaluation of a field-blended rubber asphalt**. Ph.D. dissertation, Universidade de São Paulo, São Paulo, 2016. *[in Portuguese]*

CERATTI, J. A. P. **Estudo do comportamento a fadiga de solos estabilizados com cimento para utilização em pavimentos**. Ph.D. dissertation, Universidade Federal do Rio de Janeiro, Rio de Janeiro, 1991. *[in Portuguese]*

CHRISTOPHER, B. R.; SCHWARTZ, C.; BOUDREAU, R. **Geotechnical aspects of pavements**. Report No. FHWA NHI05-037, 2006, 598 p.

CLYNE, T. R.; MARASTEANU, M. O. **Inventory of properties of Minnesota certified asphalt binders**. Report No. MN/RC-2004-35, Minnesota Department of Transportation, 2004, 102 p.

COLPO, G. B. **Análise de fadiga de misturas asfálticas através do ensaio de flexão em viga quatro pontos**. M.Sc. thesis, Universidade Federal do Rio Grande do Sul, Porto Alegre, 2014.

COMINSKY, R. J.; HUBER, G. A.; KENNEDY, T. W.; ANDERSON, M. **The Superpave mix design manual for new construction and overlays**. SHRP-A-407, Strategic Highway Research Program, National Research Council, Washington, 1994.

CORTÉ, J. F.; GOUX, M. T. **Design of pavement structures: the French technical guide**. Transportation Research Record: Journal of the Transportation Research Board, Washington, No. 1589, p. 116-24, 1996.

COUTINHO, R. P. **Utilização da parte fina de misturas asfálticas para avaliação do dano por fadiga**. M.Sc. thesis, Universidade Federal do Ceará, Fortaleza, 2012. *[In Portuguese]*

DENNEMAN, E.; ANOCHIE-BOATENG, J.; NKGAPELE, M.; KOMBA, J. **Revision of damage models for asphalt pavements**. Conference on Asphalt Pavements for Southern Africa, 2011.

DI BENEDETTO, H.; LA ROCHE, C.; PRONK, A.; LUNDSTRÖM, R. **Fatigue of bituminous mixtures**. Materials and Structures, Vol. 37, p. 202-216, 2004.

EPPS, J. A.; MONISMITH, C. L. **Fatigue of asphalt concrete mixtures – summary of existing information**. Fatigue of Compacted Bituminous Aggregate Mixtures, ASTM STP 508, American Society for Testing and Materials, p. 19-45, 1972.

FAKHRI, M.; HASSANI, K.; GHANIZADEH, A. R. **Impact of loading frequency on the fatigue behavior of SBS modified asphalt mixtures**. 2nd Conference of Transportation Research Group of India, Procedia – Social and Behavioral Sciences, Vol. 104, p. 69-78, 2013.

FHWA. **Testing for fatigue cracking in the asphalt mixture performance tester**. Federal Highway Transportation, Report No. FHWA-HIF-16-027, 2016.

FINN, F. N.; YAPP, M. T.; COPLANTZ, J. S.; DURRANI, A. Z. **Asphalt properties and relationship to pavement performance**. Summary Report No. SR-ARE-A-003A-89-3, University of California – Berkeley, 1990, 404 p.

FLINTSCH, G. W.; DIEFENDERFER, B. K.; NUNEZ, O. **Composite pavement systems: synthesis of design and construction practices**. Report No. FHWA/VTRC 09-CR2, 2008, 60 p.

FONTES, L. P. T. L. **Optimização do desempenho de misturas betuminosas com betume modificado com borracha para reabilitação de pavimentos**. Ph.D. dissertation, Universidade do Minho, 2009. *[in Portuguese]*

FRANCO, F. A. C. P. **Método de dimensionamento mecanístico-empírico de pavimentos asfálticos – SISPAV**. Ph.D. dissertation, Universidade Federal do Rio de Janeiro, Rio de Janeiro, 2007. *[in Portuguese]*

FRITZEN, M. A. **Desenvolvimento e validação de função de transferência para previsão do dano por fadiga em pavimentos asfálticos**. Ph.D. dissertation, Universidade Federal do Rio de Janeiro, Rio de Janeiro, 2016. *[in Portuguese]*

GAUTHIER, G.; LE HIR, Y.; PLANCHE, J. P. **Fatigue of bituminous binders and mixes: analysis and correlations using a new, intrinsic approach**. 3rd. Eurasphalt & Eurobitume Congress, Vienna, 2004.

GERSHKOFF, D. R.; CARSWELL, J.; NICHOLLS, J. C. **Rheological properties of polymer-modified binders for use in rolled asphalt wearing course**. London: ICE Publishing, 1997.

GHUZLAN, K. A.; CARPENTER, S. H. **Energy-derived, damage-based failure criterion for fatigue testing**. Transportation Research Record: Journal of the Transportation Research Board, Washington, No. 1723, p. 141-149, 2000.

GHUZLAN, K. A.; CARPENTER, S. H. **Energy-derived, damage-based failure criterion for fatigue testing**. Transportation Research Record: Journal of the Transportation Research Board, Washington, No. 1723, p. 141-149, 2000.

GHUZLAN, K. A.; CARPENTER, S. H. **Traditional fatigue analysis of asphalt concrete mixtures**. Transportation Research Board: Annual Meeting, Washington, 2003.

GIBSON, N.; QI, X.; SHENOY, A.; AL-KHATEEB, KUTAY, M. E.; ANDRIESCU, A.; STUART, K.; YOUTCHEFF, J.; HARMAN, T. **Performance testing for Superpave and structural validation**. Report No. FHWA-HRT-11-045, Federal Highway Administration, 2012, 276 p.

HAFEEZ, I.; KAMAL, M. A.; MIRZA, M. W.; BARKATULLAH; BILAL, S. **Laboratory fatigue performance evaluation of different field laid asphalt mixtures**. Construction and Building Materials, Vol. 44, p. 792-797, 2013.

HAFEEZ, I.; KAMAL, M. A.; MIRZA, M.W. **An experimental study to select aggregate gradation for stone mastic asphalt**. Journal of the Chinese Institute of Engineers, Vol. 38, Issue 1, p. 1-8, 2015.

HALSTED, G. E.; LUHR, D. R.; ADASKA, W. S. **Guide to cement-treated base (CTB)**. 1st. ed.: Portland Cement Association, 2006, 26 p.

HARVEY, J. T.; DEACON, J. A.; TSAI, B.; MONISMITH, C. L. **Fatigue performance of asphalt concrete mixes and its relationship to asphalt concrete pavement performance in California**. Report No. RTA-65W485-2, 1995, 137 p.

HARVEY, J. T.; TSAI, B.W. **Effects of asphalt content and air void content on mix fatigue and stiffness**. Transportation Research Record: Journal of the Transportation Research Board, Washington, No. 1543, p. 38-45, 1996.

HINTZ, C. **Understanding mechanisms leading to asphalt binder fatigue**. Ph.D. dissertation, University of Wisconsin-Madison, 2012.

HINTZ, C.; BAHIA, H. **Simplification of linear amplitude sweep test and specification parameter**. Transportation Research Record: Journal of the Transportation Research Board, Washington, No. 2370, p. 10-16, 2013.

HINTZ, C.; VELASQUEZ, R.; JOHNSON, C.; BAHIA, H. **Modification and validation of linear amplitude sweep test for binder fatigue specification.** Transportation Research Record: Journal of the Transportation Research Board, Washington, No. 2207, p. 99-106, 2011.

HUANG, S.; DI BENEDETTO, H. **Advances in asphalt materials: road and pavement construction.** 1st. ed.: Woodhead Publishing, 2015, 492 p.

HUANG, Y. H. S. **Pavement analysis and design.** 2nd. ed.: Pearson, 2003, 792 p.

HUNTER, R. N.; SELF, A.; READ, J. **The Shell bitumen handbook.** 6th ed., London: ICE Publishing, 2015.

ISMAIL, A.; BAGHINI, M. S.; KARIM, M. R. B.; SHOKRI, F.; AL-MANSOBA, R. A.; FIROOZI, A. A.; FIROOZI, A. A. **Laboratory investigation on the strength characteristics of cement-treated Base.** Applied Mechanics and Materials, Vol. 507, p. 353-360, 2014.

JOHNSON, C. M. **Estimating asphalt binder fatigue resistance using an accelerated test method.** Ph.D. dissertation, University of Wisconsin-Madison, 2010.

KHATTAK, M. J.; BALADI, G. Y. **Engineering properties of polymer-modified asphalt mixtures.** Transportation Research Record: Journal of the Transportation Research Board, Washington, No. 1638, p. 12-22, 1998.

KIM, Y. R.; KHOSLA, N. P.; KIM, N. **Effect of temperature and mixture variables on fatigue life predicted by diametral fatigue testing.** Transportation Research Record: Journal of the Transportation Research Board, Washington, No. 1317, p. 128-138, 1991.

KIM, Y. R.; KIM, N.; KHOSLA, N. P. **Effects of aggregate type and gradation on fatigue and permanent deformation of asphalt concrete.** Effects of Aggregates and Mineral Fillers on Asphalt Mixture Performance, ASTM STP 1147, American Society for Testing and Materials, Philadelphia, 1992.

LI, N. **Asphalt mixture fatigue testing: influence of test type and specimen size.** Ph.D. dissertation, Technische Universiteit Delft, Delft, 2013.

LI, Y. **Asphalt pavement fatigue cracking modeling.** Ph.D. dissertation, Louisiana State University and Agricultural and Mechanical College, 1999.

LITTLE, D. N.; CROCKFORD, W. W.; GADDAM, V. K. R. **Resilient modulus of asphalt concrete.** Report No. FHWA/TX-93-1177-1F, Texas Transportation Institute, 1992, 168 p.

LOUREIRO, T. G. **Estudo da evolução do dano por fadiga em misturas asfálticas.** M.Sc. thesis, Universidade Federal do Ceará, Fortaleza, 2003.

LUNDSTROM, R.; DI BENEDETTO, H.; ISACSSON, U. **Influence of asphalt mixture stiffness on fatigue failure**. Journal of Materials in Civil Engineering, Vol. 16, Issue 6, p. 516-525, 2004.

LYNGDAL, E. T. **Critical analysis of PH and PG+ asphalt binder test methods**. M.Sc. thesis, University of Wisconsin-Madison, 2015.

MANGIAFICO, S. **Linear viscoelastic properties and fatigue of bituminous mixtures produced with Reclaimed Asphalt Pavement and corresponding binder blends**. Ph.D. dissertation, l'École Nationale des Travaux Publics de l'État, Lyon, France, 2014.

MANNAN, U. A.; ISLAM, M. R.; TAREFDER, R. A. **Effects of recycled asphalt pavements on the fatigue life of asphalt under different strain levels and loading frequencies**. International Journal of Fatigue, Vol. 78, p. 72-80, 2015.

MARTINS, A. T. **Contribuição para a validação do ensaio de resistência ao dano por fadiga para ligantes asfálticos**. M.Sc. thesis, Universidade Federal do Rio de Janeiro, Rio de Janeiro, 2014. [*in Portuguese*]

MARTONO, W.; BAHIA, H. U. **Developing a surrogate test for fatigue asphalt binders**. Transportation Research Board: Annual Meeting, Washington, 2008.

MASAD, E.; SOMADEVAN, N.; BAHIA, H. U.; KOSE, S. **Modeling and experimental measurements of strain distribution in asphalt mixes**. Journal of Transportation Engineering, Vol. 127, Issue 6, p. 477-485, 2001.

MASHAAN, N. S.; KARIM, M. R.; AZIZ, M. A.; IBRAHIM, M. R.; KATMAN, H. Y.; KOTING, S. **Evaluation of fatigue life of CRM-reinforced SMA and its relationship to dynamic stiffness**. The Scientific World Journal, Vol. 2014, 2014, 11 p.

MAZUMDER, M.; KIM, H.; LEE, S. **Performance properties of polymer modified asphalt binders containing wax additives**. International Journal of Pavement Research and Technology, Vol. 9, p. 128-139, 2016.

MEDINA, J.; MOTTA, L. M. G. **Análise do pulso de carga em pavimentos**. Anais da XXIX Reunião Anual da ABPV, Cuiabá, 1995. [*in Portuguese*]

MEDINA, J.; MOTTA, L. M. G. **Mecânica dos pavimentos**. 3rd ed.: Editora Interciência, 2015. [*in Portuguese*]

MEJLUN, L.; JUDYCKI, J.; DOLZYCKI, B. **Comparison of elastic and viscoelastic analysis of asphalt pavement at high temperature**. Modern Building Materials, Structures and Techniques, Vol. 172, p. 746-753, 2017.

METCALF, J. B. **Application of full-scale accelerated pavement testing**. Transportation Research Board, National Research Council, 1996, 117 p.

MOTTA, L. M. G. **Método de dimensionamento de pavimentos flexíveis: critério de confiabilidade e ensaios de cargas repetidas**. Ph.D. dissertation, Universidade Federal do Rio de Janeiro, Rio de Janeiro, 1991. *[in Portuguese]*

NASCIMENTO, L. A. H. **Implementation and validation of the viscoelastic continuum damage theory for asphalt mixture and pavement analysis in Brazil**. Ph.D. dissertation, North Caroline State University, Raleigh, 2015.

NASCIMENTO, L. A. H.; ROCHA, S. M. N.; NASCIMENTO, C. E. H.; KIM, Y. R.; CHACUR, M.; MARTINS, A. T. **Uso da mecânica do dano contínuo na caracterização de misturas asfálticas brasileiras**. 21o. Encontro de Asfalto, Rio de Janeiro, 2014. *[in Portuguese]*

NCHRP, National Cooperative Highway **Research Program. Guide for mechanistic-empirical design of new and rehabilitated structures**. Report No.01-37A. Transportation Research Board, Washington, DC, 2004.

NEGRÃO, D. P. **Contribuição para calibração de curva de evolução de afundamentos em trilha de roda de revestimentos asfálticos com utilização de resultados obtidos de simulador de tráfego em escala real**. Ph.D. dissertation, Universidade de São Paulo, São Paulo, 2012. *[in Portuguese]*

NEJAD, F. M.; AFLAKI, E.; MOHAMMADI, M. A. **Fatigue behavior of SMA and HMA mixtures**. Construction and Building Materials, Vol. 24, Issue 7, p. 1158-1165, 2010.

NGUEN, Q. T.; DI BENEDETTO, H.; SAUZÉAT, C. **Determination of thermal properties of asphalt mixtures as another output from cyclic tension-compression test**. Road Materials and Pavement Design, Vol. 13, Issue 1, p. 85-103, 2012.

NGUYEN, M. T.; LEE, H. J.; BAEK, J. **Fatigue analysis of asphalt concrete under indirect tensile mode of loading using crack images**. Journal of Testing and Evaluation, Vol. 41, Issue No. 1, 2013.

NUNES, L. C. **Fadiga de misturas asfálticas descontínuas com asfalto-borracha de 4a. geração**. M.Sc. thesis, Universidade de Brasília, Brasília, 2017. *[in Portuguese]*

NUÑEZ, J. Y. **Caracterização à fadiga de ligantes asfálticos modificados envelhecidos a curto e longo**. M.Sc. thesis, Universidade de São Paulo, São Carlos, 2013. *[in Portuguese]*

ONGEL, A.; HARVEY, J. **Analysis of 30 years of pavement temperatures using the enhanced integrated climate model (EICM)**. Draft Report, California Department of Transportation, 2004, 81 p.

OTTO, G. G.; MOMM, L.; VALENTE, A. M. **Dano em rodovias devido a carga dinâmica com sistemas MS/WIM**. 8o. Congresso Brasileiro de Rodovias e Concessões, CBR&C, Santos, 2013. *[in Portuguese]*

PAMPLONA, T. F. **Efeito da adição de ácido polifosfórico em ligantes asfálticos de diferentes fontes**. M.Sc. thesis, Universidade de São Paulo, São Carlos, 2013. *[in Portuguese]*

PARK, D.; BUCH, N.; SUH, Y. **Development of fatigue cracking model for flexible pavements**. KSCE Journal of Civil Engineering, Vol. 5, No. 4, p. 397-402, 2001.

PARK, H. J.; KIM, Y. R. **Investigation into top-down cracking of asphalt pavements in North Carolina**. Transportation Research Record: Journal of the Transportation Research Board, Washington, No. 2368, p. 45-55, 2013.

PÉREZ-JIMÉNEZ, F.; BOTELLA, R.; MIRÓ, R. **Damage and thixotropy in asphalt mixture and binder fatigue tests**. Transportation Research Record: Journal of the Transportation Research Board, Washington, No. 2293, p. 8-17, 2012.

PETERSEN, J. C.; ROBERTSON, R. E.; BRANTHAVER, J. F.; HARNSBERGER, P. M.; DUVALL, J. J.; KIM, S. S.; ANDERSON, D. A.; CHRISTIANSEN, D. W.; BAHIA, H. U. **Binder characterization and evaluation – volume 1**. SHRP-A-367, Strategic Highway Research Program, National Research Council, Washington, 1994.

PINTO, S. **Estudo do comportamento à fadiga de misturas betuminosas e aplicação na avaliação estrutural de pavimentos**. Ph.D. dissertation, Universidade Federal do Rio de Janeiro, Rio de Janeiro, 1991. *[in Portuguese]*

PINTO, S.; PREUSSLER, E. **Pavimentação rodoviária: conceitos fundamentais sobre pavimentos flexíveis**. Rio de Janeiro: Copiadora e Artes, 2002. *[in Portuguese]*

PLANCHE, J. P.; ANDERSON, D. A.; GAUTHIER, G.; LE HIR, Y. M.; MARTIN, D. **Evaluation of fatigue properties of bituminous binders**. Materials and Structures, Vol. 37, p. 356-359, 2004.

PMSP, PREFEITURA MUNICIPAL DE SÃO PAULO. **Instrução de Projeto – Projeto de pavimentação**. São Paulo: Secretaria de Infraestrutura Urbana, 2006.

PMSP, PREFEITURA MUNICIPAL DE SÃO PAULO. **Instrução de Projeto 08 – Análise mecanicista à fadiga de estruturas do pavimento**. São Paulo: Secretaria de Infraestrutura Urbana, 2004.

PORTER, B. W.; KENNEDY, T. W. **Comparison of fatigue test methods for asphalt materials**. Report No. 3-9-72-183, The Texas Highway Department, 1975, 132 p.

POWELL, W. D.; POTTER, J. F.; MAYHEW, H. C.; NUNN, M. E. **The structural design of bituminous pavements**. TRRL Laboratory Report, Issue No. 1115, Transport and Road Research Laboratory, 1984.

PRAMESTI, F. P.; MOLENAAR, A. A. A.; VAN DE VEN, M. F. C. **The prediction of fatigue life based on four point bending test**. The 2nd International Conference on Rehabilitation and Maintenance in Civil Engineering, Procedia Engineering, Vol. 54, p. 851-862, 2013.

PREFEITURA DO MUNICÍPIO DE SÃO PAULO. **Instrução de projeto 08 (IP-08/2004): análise mecanicista à fadiga de estruturas do pavimento**. São Paulo: Secretaria de Infraestrutura Urbana, 2004. *[in Portuguese]*

PREUSSLER, E. S. **Estudo da deformação resiliente de pavimentos flexíveis e aplicação ao projeto de camadas de reforço**. Ph.D. dissertation, Universidade Federal do Rio de Janeiro, Rio de Janeiro, 1983. *[in Portuguese]*

PRIEST, A. I. **Calibration of fatigue transfer functions for mechanistic-empirical flexible pavement design**. M.Sc. thesis, Auburn University, Auburn, 2005.

PRIEST, A. L.; TIMM, D. H. **Methodology and calibration of fatigue transfer functions for mechanistic-empirical flexible pavement design**. NCAT Report No. 06-03, 2006, 102 p.

QIAN, G.; LIU, H.; ZHENG, J.; JIANG, L. **Experiment of tension-compression fatigue and damage for asphalt mixtures**. Journal of Highway and Transportation Research and Development, Vol. 7, Issue 2, p. 15-21, 2013.

RAJBONGSHI, P. **A critical discussion on mechanistic-empirical fatigue evaluation of asphalt pavements**. International Journal of Pavement Research and Technology, Vol. 2, Issue No. 5, p. 223-226, 2009.

RODRIGUES, R. M. **Projeto de reforço de pavimentos rodoviários e aeroportuários pelo método da resiliência: uma nova versão do programa TECNAPAV**. Ph.D. dissertation, Universidade Federal do Rio de Janeiro, Rio de Janeiro, 1987. *[in Portuguese]*

ROWE, G. M. **Performance of asphalt mixtures in the trapezoidal fatigue test**. Journal of the Association of the Asphalt Paving Technologists, Vol. 62, p. 344-384, 1993.

ROWE, G. M.; BLANKENSHIP, P.; SHARROCK, M. J.; BENNERT, T. **The fatigue performance of asphalt mixtures in the four point bending beam fatigue test in accordance with AASHTO and ASTM analysis methods**. 5th. Eurasphalt & Eurobitume Congress, 2012.

ROWE, G. M.; BOULDIN, M. G. **Improved techniques to evaluate the fatigue resistance of asphalt mixtures**. 2nd. Eurasphalt & Eurobitume Congress, Barcelona, 2000.

SABOO, N.; KUMAR, P. **Performance characterization of polymer modified asphalt binders and mixes**. Advances in Civil Engineering, Vol. 2016, 2016.

SABOURI, M.; KIM, Y. R. **Development of a failure criterion for asphalt mixtures under different modes of fatigue loading**. Transportation Research Record: Journal of the Transportation Research Board, Washington, No. 2447, p. 117-125, 2014.

SAFAEI, F.; CASTORENA, C. **Temperature effects of linear amplitude sweep testing and analysis**. Transportation Research Record: Journal of the Transportation Research Board, Washington, No. 2574, p. 92-100, 2015.

SAFAEI, F.; LEE, J.; NASCIMENTO, L. A. H.; HINTZ, C.; KIM, Y. R. **Implications of warm-mix asphalt on long-term oxidative ageing and fatigue performance of asphalt binders and mixtures**. Road Materials and Pavement Design, Vol. 15, p. 45-61, 2014.

SALEH, M. **Calibration and validation of the Shell fatigue model using AC10 and AC14 dense grade hot mix asphalt fatigue laboratory data**. Engineering Journal, Vol. 15, Issue No. 5, 2012.

SCHAPERLY, R. A. **A theory of crack growth in viscoelastic media**. Technical Report, Texas A&M University, 1973, 131 p.

SHAN, L.; ZHANG, H.; TAN, Y.; XU, Y. **Effect of load control mode on the fatigue performance of asphalt binder**. Materials and Structures, Vol. 49, p. 1391-1402, 2016.

SHEN, S.; CARPENTER, S. H. **Application of the dissipated energy concept in fatigue endurance limit testing**. Transportation Research Record: Journal of the Transportation Research Board, Washington, No. 1929, p. 165-173, 2005.

SHRP-A-404. **Fatigue response of asphalt-aggregate mixes**. Asphalt Research Program, Institute of Transportation Studies, 1994.

SKOK, E.; JOHNSON, E.; TURK, A. **Asphalt pavement analyzer (APA) evaluation**. Report No. MN/RC 2003-02, Minnesota Department of Transportation, 2003, 85 p.

SOUSA, J. B.; PAIS, J. C.; PRATES, M.; BARROS, R.; LANGLOIS, P.; LECLERC, A. **Effect of aggregate gradation on fatigue life of asphalt concrete mixes**. Transportation Research Record: Journal of the Transportation Research Board, Washington, No. 1630, p. 62-68, 1998.

STUBBS, A.; SALEH, M.; JEFFERY-WRIGHT; H. **Investigation into the validation of the Shell fatigue transfer function**. IPENZ Transportation Conference, Christchurch, 2010.

SUGANDH, R.; ZEA, M.; TANDON, V.; SMIT, A.; PROZZI, J. **Performance evaluation of HMA consisting of modified asphalt binder**. Report No. FHWA/TX-07/04824-2, 2007, 120 p.

TABATABAEE, N.; TABATABAEE, H. A. **Multiple stress creep and recovery and time sweep fatigue tests: crumb rubber modified binder and mixture performance.** Transportation Research Record: Journal of the Transportation Research Board, Washington, No. 2180, p. 67-74, 2010.

THOMPSON, M. R. **ILLI-PAVE based full-depth asphalt concrete pavement design procedure.** Proceedings, Sixth International Conference on Structural Design of Asphalt Pavements, Vol. 1, p. 13-22, 1987.

TIMOSHENKO, S. P. **History of strength of materials.** 1st ed.: McGraw-Hill Book Company, 1953.

UNDERWOOD, B. S. **Multiscale constitutive modeling of asphalt concrete.** Ph.D. dissertation, North Carolina State University, Raleigh, 2011.

VERSTRAETEN, J.; VEVERKA, V.; FRANCKEN, L. **Rational and practical designs of asphalt pavements to avoid cracking and rutting.** Proceedings, Fifth International Conference on the Structural Design of Asphalt Pavements, 1982.

WANG, C.; CASTORENA, C.; ZHANG, J.; KIM, Y. R. **Unified failure criterion for asphalt binder under cyclic fatigue loading.** Road Materials and Pavement Design, Vol. 16, Issue 2, 2015.

WANG, C.; ZHANG, H.; CASTORENA, C.; ZHANG, J.; KIM, Y. R. **Identifying fatigue failure in asphalt binder time sweep tests.** Construction and Building Materials, Vol. 121, p. 535-546, 2016.

WEN, H.; LI, X. **Development of a damage-based phenomenological fatigue model for asphalt pavements.** Journal of Materials in Civil Engineering, Vol. 25, No. 8, 2013.

WILLIS, J. R.; TURNER, P.; JULIAN, G.; TAYLOR, A. J.; TRAN, N.; PADULA, F. G. **Effects of changing virgin binder grade and content on RAP mixture properties.** NCAT Report No. 12-03, 2012, 47 p.

WITCZAK, M. W.; KALOUSH, K.; PELLINEN, T.; EL-BASYOUNY, M.; QUINTUS, H. V. **Simple performance test for Superpave mix design.** NCHRP Report 465, 2002, 114 p.

YEO, I.; SUH, Y.; MUN, S. **Development of a remaining fatigue life model for asphalt black base through accelerated pavement testing.** Construction and Building Materials, Vol. 22, p. 1881-1886, 2008.

ZHAO, Y.; ALAE, M.; FU, G. **Investigation of mechanisms of top-down fatigue cracking of asphalt pavement.** Road Materials and Pavement Design, p. 1-12, 2017.